Graphene Based Membranes for High Salinity, Produced Water Treatment by Pervaporation Separation

by

Khalfan Almarzooqi

A thesis

presented to the University of Waterloo

in fulfillment of the

thesis requirement for the degree of

Doctor of Philosophy

in

Chemical Engineering

Waterloo, Ontario, Canada, 2023

Examining Committee Membership

The following served on the Examining Committee for this thesis. The decision of the Examining Committee is by majority vote.

External Examiner   MADHUMITA RAY

                                       Professor

Supervisors   MICHAEL A. POPE

                                       Associate Professor

                                       ALI ELKAMEL

                                       Professor

Internal Members   TING TSUI

                                       Associate Professor

                                       AIPING YU

                                       Professor

Internal-external Member   WILLIAM MELEK

                                       Professor

Author's Declaration

This thesis consists of material all of which I authored or co-authored: see Statement of Contributions included in the thesis. This is a true copy of the thesis, including any required final revisions, as accepted by my examiners.

I understand that my thesis may be made electronically available to the public.

Statement of Contributions

This thesis consists in part of manuscripts written for publication. The main work is divided into two manuscripts which are published, or ready for submission, as follows:

- Chapter 3 is adopted from:

K. Almarzooqi, M. Ashrafi, T. Kanthan, A. Elkamel, and M. A. Pope, "Graphene Oxide Membranes for High Salinity, Produced Water Separation by Pervaporation," Membranes (Basel), vol. 11, no. 7, p. 475, Jun. 2021, doi: 10.3390/membranes11070475

Author contributions:

Conceptualization: K. Almarzooqi, M. Ashrafi, and M. A. Pope.

Methodology: K. Almarzooqi, M. Ashrafi, and T. Kanthan.

Validation: M. A. Pope.

Formal analysis: K. Almarzooqi, M. Ashrafi, and T. Kanthan.

Investigation: K. Almarzooqi, M. Ashrafi, and T. Kanthan.

Resources, M. A. Pope.

Writing—original draft preparation: K. Almarzooqi, and M. Ashrafi.

writing—review and editing: T. Kanthan, and M. A. Pope

Supervision: A. Elkamel, and M. A. Pope

Project administration: A. Elkamel, and M. A. Pope

Funding acquisition: M. A. Pope

- Chapter 4 is adopted from:

K. Almarzooqi, T. Tsui, A. Elkamel, and M. A. Pope, "Highly stable, metal cation-crosslinked partially reduced graphene oxide membrane for high salinity and produced water treatment by pervaporative separation," [Ready for submission]

Abstract

Petroleum industries generate huge volumes of wastewater that is associated with oil and gas during extraction, known as produced water. It accounts for 98% of the amount extracted, and comprises diverse pollutants of salts, suspended solids, dissolved organic solutes, and dispersed oils; that require to be safely treated before being disposed to the environment, or reused for various beneficial applications. Nowadays, graphene-based membranes have shown potential as a membrane material due to their high performance and stability features. This research demonstrated the use of graphene oxide membranes supported on polyethersulfone films (GO/PES) for high salinity water, simulated produced water model (PWM), and PWM with simulated foulants treatment via the pervaporation separation technology. The membranes showed the highest water flux of 47.8 L m^{-2} h^{-1} for NaCl solutions in pervaporation testing operated at 60 $^{\circ}$C, and salt and organic rejections of 99.9% and 56%, respectively. In addition, the membranes were tested for long-term pervaporation for 72 hours and showed a decline of 50–60% from the initial flux in the worst-case-scenario. Moreover, in-depth investigation of the Zn^{2+} crosslinker showed a hydrolysis reaction to $Zn(OH)_2$, with the progress of the long-term pervaporation, in which much of it is being leached out. Consequently, since GO membranes are not stable in water, it remains challenging to be utilized in the industry. A more stable GO membrane in aqueous phase was proposed. The membrane's stability was enhanced by divalent and trivalent metal cations of Zn^{2+} and Fe^{3+} crosslinkers, respectively, and partial reduction under vacuum. Two orders of fabrications were investigated of either crosslinking rGO (method I) or reducing M^+–rGO (method II). The prepared membranes were examined for their characterization and performance. Fe^{3+}–rGO prepared by method II showed the best organic solute rejection of 69%. Moreover, long-term pervaporation experiment was performed for 12 hours for Zn^{2+}–rGO membranes, and revealed a drop in flux of 6% only, while Zn^{2+}–GO membrane had a drop in flux of 24%.

Additionally, the stability of the membranes was tested via an abrasion method using a rotary wheel abrader. The conducted experiments revealed that Fe^{3+}–rGO membranes had the maximum mechanical integrity with an abrasion resistance of 95% compared to the initial control (non-reduced and non-crosslinked) GO/PES membrane.

Acknowledgements

Table of Contents

List of Figures

xii

List of Tables

Chapter 1
Introduction

1.1 Background and Motivation

Nowadays, there is a huge continuous demand for oil and gas products, in order to meet the increasing energy demand globally. Therefore, oil and gas industries are continuously exploring and expanding the number of petroleum wells and their production around the world. During the extraction of the oil and gas, produced water is generated in huge quantities from the petroleum fields, accounting for 98% of the volume extracted. The produced water possesses a high concentration of salts, suspended solids, organic solutes, and oily wastes that are harmful to the ecosystem when disposed directly to the environment. Petroleum industries manage this water effluent by reinjecting it back to the oil formation or purifying it for useful uses. In past years, studies carried out on produced water separation technologies emphasized the need of efficient purifying methods that are cost effective since the current technologies do not comply with the strict environmental regulations. As a result, petroleum processing plants had shifted from the conventional separation methods to the membrane separation technologies for higher separation performances. Nevertheless, there is still a need for a novel membrane in order to increase the separation process efficiency, lower the operational energy demand and cost, and meet the environmental legislations. The current membrane separation technologies have limited capabilities in term of separation permeability, salt and organic rejections, and antifouling properties, and require high operational cost, maintenance, and long shut down period for cleaning and regeneration.

In this research, a newly produced water membrane is proposed. The pervaporation technique is suggested using graphene oxide/polyethersulfone (GO/PES). Graphene oxide membranes were chosen due to their high flux and selectivity performances, fouling resistivity and lifetime. Furthermore, the

pervaporation technique has been used for salts/water and organic/water separations, like NaCl and $MgCl_2$ salts solution; and organic solutions like ethanol, methanol, and acetone. However, it has not been intensively investigated for produced water purification which contains mostly salts and organics; because the pervaporation technique has not been significantly improved yet, although it is an old separation method. Besides, the pervaporation could be significantly more economical substitute separation method to the conventional azeotropic processes (water/organic, and organic/organic), and conventional salt/water separation processes; and it utilizes less energy. Therefore, this project illustrates the first feasibility study of produced water treatment using graphene-based membranes by pervaporative separation technology.

In addition, graphene oxide membranes have inherited properties that limit its capabilities and utilization, illustrated by the huge trade-off between its water permeation flux, molecular sieving, and stability upon hydration. Graphene oxide membranes consist of ample number of oxygen-containing functional groups that are distributed asymmetrically on the edges and on the basal plan. Upon hydration of GO membranes, these negatively charged oxygen groups start to repel each other by electrostatic repulsion forces leading to an increase in the interlayer d-spacing. This results in lowering the separation efficiency, as well as GO swelling and disintegration in water.

Therefore, to address this concern, this project presents a treatment method aiming for increasing the stability and rejection of GO membranes by the method of crosslinking and partially reducing the GO nanosheets.

1.2 Research Objectives

This objective of the first research project is to improve oil field produced water treatment membrane technology by studying the feasibility of purifying it using GO membranes supported on polyethersulfone (GO/PES) via pervaporation separation technique.

The scope of the first project is as following:

- Study the changes occur to the synthesized GO/PES membranes characterization before and after the pervaporation separation.

- Assess the membranes permeation and rejection performances for: saline water, single organic solute component in water (phenol, cresol, naphthenic acid), produced water model (mix of salt and organic solutes).

- Investigate the synthesized membranes performance stability over long period of time using pure water, saline water, produced water, and oily foulants.

- Study the impact of long-term pervaporation testing on the degradation of Zn^{2+}–GO crosslinker.

The second study of this project concentrated on improving the performance and stability of GO/PES membranes using metal cation crosslinker, and physical reduction. Two metal cation candidates of divalent Zn^{2+} and trivalent Fe^{3+} are utilized for the nanosheets crosslinking treatments, as the following:

- First method: partially reduce GO/PES membranes for different period of time, then crosslinking the rGO/PES in the crosslinker solution.

- Second method: crosslinking GO/PES membranes by different crosslinker solution concentration, then partially reduce the M^+–GO under vacuum.

Further, different examination for the prepared M^+– rGO membranes by the two methods were performed to study the following aspects:

- Chemical and physical characterization.

- Pervaporation performance, using saline water, produced water model, and produced water model with added foulants.

- Stability resistance testing utilizing controlled rotating wheel abrasion test.

The obtained results from this research will shed light on the promising graphene-based membrane material for pervaporative separation as a more economical and environmental technique.

1.3 Dissertation Outline

In this dissertation, **Chapter 2** illustrates the background and literature review on produced water, its amount and significance, constituents, and industrial managements. Further, it shows the different separation technologies utilized for produced water purification including the conventional techniques and membrane separation techniques. Additionally, the literature focuses on different types of membrane separation technologies, module configuration, membrane materials, and fabrication methods. Then, it focusses more details on graphene oxide as a membrane material. In addition, the latest produced water separation by graphene

oxide membrane up-to-date progress is shown along with the challenges faced in membrane separations, and treatment methods to improve it.

Chapter 3 shows the first study conducted that examined the feasibility of using graphene oxide membranes for high salinity, produced water separation via pervaporation technology. It illustrates the performances of GO/PES membranes examined and their salt, organic solutes, and foulants rejections for short- and long-term pervaporation technique. Also, it highlights the compositional change for the GO membranes after testing.

Chapter 4 portrays the second study conducted to improve the performance and stability of GO/PES membranes in the pervaporation separation. The study discusses the partial reduction treatment of GO and the incorporation of metal ion cations into the GO lamellar structure that were utilized for highly saline water, produced water model, and produced water model with foulants purification by pervaporation separation. Also, it highlighted the effect of membranes treatment orders on their characterizations, performances, and stabilities.

Chapter 5 of this dissertation draws general conclusions of this project, stating the remarkable findings in the research. It further provides future work and suggestions for moving forward steps for interested researchers in this project.

Chapter 2
Literature Review

2.1 Produced Water Source and Amount

Petroleum industries produce significant volumes of wastewater resulted from the oil and gas extraction and production in the petroleum fields. This wastewater that is associated with the oil and gas from the hydrocarbon reservoir formation, is known as the produced water. The produced water is considered the highest single wastewater stream generated in the petroleum fields, accounting for 80% of the total wastewater amount [1]. Produced water chemical and physical properties and volume rely significantly on the geographic location and depth of the reservoir, its geologic formation and structure, additive chemical injections to the reservoir like biocides and corrosion inhibitors, and its age [2], [3]. In addition, the water injections to the deep oil wells to maintain its pressure or raise the oil level up, ultimately transform into part of the produced water [4]. Moreover, these properties can vary throughout the life span of the reservoir itself, and no two reservoirs are alike in their properties; therefore, regional specific studies are needed [5].

The content of water in oil varies depending on the nature of the petroleum well that is been extracted from, and can range up to 98% of the total volume extracted in the nearly depleted reservoirs [1]. In a recent report by the Produced Water Society in 2019, the total volume of produced water was estimated to be around 300 MMB/D [6]. According to U.S. Department of Energy, the amount of produced water is three times of the oil volume [7]. Additionally, the amount of produced water is projected to increase to twelve times the oil volume due to the aging of oil reservoirs [1], [8]. The volumes of produced water generated are successively growing as the market demand on petroleum products is continuously increasing.

6

2.2 Produced Water Composition

Generally, produced water consists of complex compositions that include [2], [5], [9], [10]:

- Dispersed oil - This is the most dangerous contaminant for the process; droplets of dispersed oil of 2–30 microns.

- Dissolved organic compounds - This includes organic acids, polycyclic aromatic hydrocarbons (PAHs) and other volatile compounds.

- Treatment chemicals - This includes all chemicals that were added during petroleum extraction or enhanced oil recovery (EOR) process such as: corrosion inhibitors, biocides and emulsion breakers.

- Produced solids - This includes all organic and inorganic scales, silts, carbonates, and solids from well bore operations.

- Bacteria - Anaerobic bacteria present in oil.

- Light and heavy metals - Metals typically have lower toxicity compared to organic contaminations, however these metals can form secondary products and precipitate during treatment processes. Common dissolved metals include zinc, lead, manganese, iron, and barium.

2.3 Produced Water Management

Produced water treatment is carried out with the objective of meeting the environmental regulation for discharge, or the quality standards for reusage in various applications. Produced water can be reused for several alternatives such as the following:

- Discharge to the environment after meeting the allowable limits of disposal legislation and compliance so as to lower the ecosystem degradation [11].

7

- Petroleum industries reuse the treated water for the rest of the processes in the operational plant; or reinject it back to the oil well in order to maintain the pressure inside the petroleum reservoirs or enhance the oil extraction. Reinjection of the produced water is predominantly used to lower the cost of treatment for disposal requirement [12]. In China, produced water reusage in petroleum industries has gained much consideration, since it reduces the burden of disposing it to the environment, and lowers the demand on freshwater resources [13].

- In territories where the water is scarce, produced water can form a beneficial source for potable water, livestock watering and agriculture irrigation [12], [14].

- As global attention is seeking towards greener sources of energy, there is a growing demand of biofuels which are produced from water-intensive processes. Produced water was successfully used for irrigating the biofuel corps to lower the demand on freshwater resources [15].

2.4 Produced Water Separation Technologies

Several separation technologies have been developed for produced water treatment sine it consists of complex mixture of impurities with various concentrations. The processes of separation involve different techniques and equipment. Mostly, conventional technologies which are either mechanical (physical) or chemical are utilized [4], [7], [16]. In general, produced water treatment of the onshore fields is relatively easier than the offshore fields, because of the lack of sufficient space or weight constraints of the offshore platform.

2.4.1 Floatation and Settling by Separators

Separators divide extracts into singular streams to make further treatment and management easier. These processes take advantage of gravity and differences in buoyancy using either horizontal or

vertical separators depending on the contents to be separated. The use of the separators was the option before the membrane separation technology was developed, yet it has still been used till today. Separators can be utilized at ambient temperature or with the supply of heat [17], [18].

Some separators are two-phase involving oil and water while others are three-phase for gas, oil, and water separation. With the presence of water, the first stage of separation is conventionally three-phase; with the subsequent stages being either two-phase or three-phase.

In gravity separation, the well stream is fed to a horizontal separation vessel, in which the liquid feed mixture will be retained inside the vessel for a certain period of time to allow the gas to fizz out, and the water and gas settle separately. The oil will flow out along the middle part of the vessel, and the water will settle below it and flow out from the bottom outlet. This technique requires several post-treatment stages and pressure reduction often takes place at different stages to enhance control over separation of volatile components [17].

2.4.2 Filtration Treatment

Filtration technique is one of the relatively easier methods to treat produced water by the mean of a porous media that allow the penetration of the water only and excluding the contaminants. Different porous filtration beds are used such as sand, grains, gravels, walnut shell, and stones. Industries widely use sand filters to remove metals from formation water [19], [20]. This method is a multistage and works along with pre-purification phases like pH adjustment, aeration, and solid separation, with 90% treatment efficiency [2], [21]. However, the downside of this technique is that it is considered a costly method, takes long time to settle, does not separate salts in water, contaminants build-up often clogs the system which requires further chemical and mechanical cleaning [20], [22].

2.4.3 Adsorption Treatment

Adsorption technique uses more economical adsorbent media for treating produced water in a packed bed vessel that include activated carbon, organoclays, copolymers, activated aluminum and zeolite [23]. The adsorbents used can retain different pollutants like heavy metals, organic and inorganic compounds. Industries generally use activated carbon due to its relatively cheaper price, high surface area, and high adsorption rate and reactivity [24]. This method is utilized as a post-treatment step in a multi-stage separation technique since the adsorbent materials can not handle the overload of contaminants. Moreover, this method requires frequent regeneration after few batches to backwash the system and regain its performance. Also, adsorbents suffer from short life span of the active filtration element, as well as the high cost of installation [17], [25].

2.4.4 Chemical Oxidation Treatment

This treatment technique is commonly utilized for purifying produced water from organic and inorganic compounds as well as color and odour removal. Industries widely use oxygen, ozone, peroxide, and permanganate as treatment oxidants. It depends on the activity of oxidation and reduction reactions that occurs in produced water, and separation is achieved by mixing it with the oxidants for a specific contact time to break down the pollutants [26], [27]. In addition, this technique requires an extensive post-treatment stage in order to remove the oxidized constituents. Also, it has a high energy consumption rate (around 18% of the total operational and maintenance rate), as well as a high cost of the chemical oxidants.

2.4.5 Hydrocyclones Technique

Hydrocyclone separators are one of the efficient physical separation techniques used for removing solid particles that is commonly used in offshore petroleum fields, since it occupies smaller space than other

separation equipment. This technique depends on the difference in density of the suspended solid particulates in the feed stream. Hydrocyclone units have a cylindrical top with a reduced area towards the base in a conical shape as shown in Figure 2-1. Produced water is fed to the top of the equipment and the purified water is collected at the overhead outlet, while the solid particulates settle at the lower chamber and drain out. This method requires a post-treatment in multi-stage separation unit in order to remove the dissolved organics from the produced water. While this technique has a long life span, and does not involve an extensive maintenance or cleaning, the main disadvantage is that it generates a large volume of concentrated solid waste slurry [28], [29].
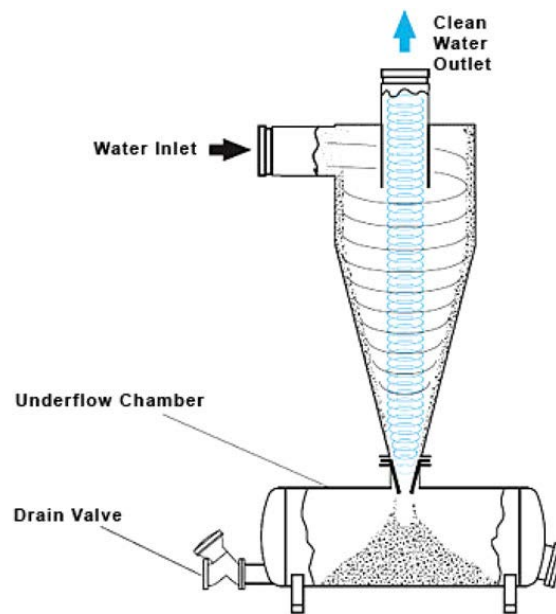
Figure 2-1: Hydrocyclone separation equipment (adopted from [4]**).**

2.4.6 Gas Flotation Separation

The gas flotation method utilizes air, nitrogen, or other inert gas fine bubbles that are injected through the produced water in a vessel in opposite flow directions of each other. Industries uses this technique commonly in order to remove solid suspended particles and oil droplets that are difficult to be removed

11

by gravity sedimentation. Solids and oil contaminants are attached to the air bubbles as it rises up in the vessel towards the top surface of the water. It eventually creates a foam which can be skimmed off as froth [26], [30].

2.4.7 Membrane Separations

Membrane separation technologies are one of the efficient techniques for produced water treatment that draw attention in the last decade. It depends on utilizing microscopic filters to selectively separate salts and solutes from solutions using specific pore ratings [31]. Membrane technologies have started replacing azeotic distillation processes. Industries continuously upgrade or modify their membrane technologies for more advanced performance. Major technologies and methods include microfiltration (MF), ultrafiltration (UF), nanofiltration (NF) and reverse osmosis (RO), which will be discussed in more details in the next section.

Furthermore, produced water treatment technologies are used in different combinations, and there is no single technique that can be employed to acquire the desired effluent properties [32]. Currently, two or more stages of treatment techniques are implemented in series. The choice of the precise techniques between the available alternatives is based on assessing the amount of produced water, solutes constituents and concentrations, available space, environmental legislation, and the ultimate reusage target of the produced water.

2.5 Membrane Separation Technology

2.5.1 Positive and Negative Aspects of Membrane Technology

Membrane separation technology has many advantages over conventional techniques that include occupation of small space, relatively easier operation which is also less time consuming, little or no use of chemical, easier to automate, relatively less costly than other conventional techniques, low maintenance requirements, and low consumption of energy during continuous operation [16], [31], [33], [34].

However, membrane separation has some disadvantages. The process is likely to face solutes deposition on the membrane surface which eventually leads to pore plugging and reduce the membrane's permeability and its overall functionality. There are two classifications of fouling formation on the membrane: hydraulically reversible and irreversible. In the hydraulic reversible type, foulants are attached to the membrane loosely and they could be easily detached through applying backwashing. Whereas, in irreversible type, foulants could only be detached by chemical treatment as they are tightly attached to the membrane. However, both types of fouling leads to an increase in operational cost, yet the irreversible type reduces the life span of the membrane on the long run due to its effect on the membranes' active sites [35], [36]. Additionally, in some membrane separation techniques which require high pressure supply by the use of pumps like reverse osmosis (RO), forward osmosis (FO), and nanofiltration (NF), it might require high energy consumption and operational cost which limit their applications [37].

2.5.2 Types of Membrane Technologies

2.5.2.1 Microfiltration (MF), Ultrafiltration (UF), and Nanofiltration (NF)

These types of filtration treatment are pressure-driven membrane processes (PDMP) which work simply by passing a stream through filtration membranes unit. They depend primarily on separating suspended colloidal particles by size exclusion, permitting smaller particulates permeate through membrane pores while retaining bigger ones [38]. **Table 2-1** below illustrates the major differences between these membranes in terms of their separation mechanism, typical fabrication materials, and purpose of usage [2], [32], [39].

Table 2-1: Differences between filtration process membranes.

Process	Separation mechanism	Typical material	Purpose
Microfiltration (MF)	• Macropores sieving • pore size: 0.1–10 mm	• Polymeric • Inorganic	Separate large solids and organics.
Ultrafiltration (UF)	• Mesopores sieving • Pore size: 2-100 nm	• Polymeric • Inorganic	Separate large, dissolved solutes and solids.
Nanofiltration (NF)	• Micropores sieving • Pore size: <2 nm • Charge rejection	• Polymeric	Separate multivalent ions and charged molecules.

While MF and UF require less energy demand and can be operated around 1–2 bars, their effluents require post-treatment stages mainly with reverse osmosis (RO) or NF, in order to separate the salts and total dissolved solids (TDS). In addition, NF has lower operational cost in which industries use it for high TDS concentrations (35,000 ppm) like sea water, at a moderate operating pressure of around 8 bar. However, the drawback of NF is that it cannot remove dispersed oil in produced water treatment [4], [40].

2.5.2.2 Reverse Osmosis (RO)

Osmosis is a natural process in which a solvent (water) tends to move from a region of low to high solute concentration through a semi-permeable membrane to attain chemical potential equilibrium. Therefore, RO separation mechanism takes an advantage of this phenomena by forcing a solvent from a region of high to low solute concentration by exerting a pressure to overcome the natural osmotic pressure [41].

RO is highly efficient and effective as it operates through the least nominal pore sizes. The method is capable of achieving faster rate of separating divalent ions such as magnesium, calcium, iron, arsenic, and sulphate from water, as well as monovalent ions such as chloride and sodium [42].

However, RO is very sensitive for organic solutes in water. Also, it requires high operation pressure which largely limits its membrane's productivity due to the energy needed to provide the necessary pressure. In this technology, different types of membrane materials are used for produced water purification such as: polyethersulfone, polyamide, zeolite, and polyvinylidene fluoride (PVDF).

2.5.2.3 Forward Osmosis (FO)

This technology uses salt concentration gradient as a driving osmotic pressure through membrane. The process does not necessarily need the application of an external pressure, as water naturally move from a region of low solute concentration through the membrane to the draw solution (high concentration region), an advantage that makes them more energy-efficient than RO membranes. Low concentrated solution solvent diffuses through membrane to a highly concentrated draw solution by its natural osmotic pressure rejecting all dissolved and suspended particles. The high concentrated draw solution is initially prepared with a known concentration to create the initial osmotic pressure using special salts like $NH_4HCO_{3(aq)}$, $(NH_4)_2CO_{3(aq)}$, and $NH_4COONH_{2(aq)}$ with concentration of around 10 M. These

15

special salts are easily removed and recovered from obtained fresh water by simple methods like heating or another step of membrane separation [41], [43]. Figure 2-2 demonstrates FO process coupled with brine reconcentration system. Forward osmosis membranes are commercial membranes. Most commonly used are cellulose triacetate and polyamides with different packaging configuration modules like spiral wound, tubular as will be discussed later.
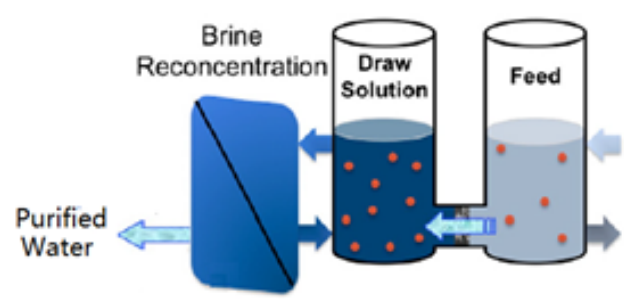
Figure 2-2: Forword osmosis process coupled with brine reconcentration

unit (reproduced from [43]**).**

2.5.2.4 Membrane Distillation (MD)

Membrane distillation is a thermally driven separation technique to induce vapor pressure difference across the two sides of a hydrophobic microporous membrane. It was widely studied for water desalination treatment [44]–[46]. It is considered one of the economical techniques for water treatment from organic and heavy metals since it uses low operating temperatures. Moreover, solar energy can be used as an alternative source for heating purposes in this technique [47]. Moreover, microfiltration membranes are used in MD and therefore, it is less prone to fouling issues [44], [48]. Figure 2-3 shows the basic mechanism [49], [50]. In membrane distillation, the feed solution enters the membrane module at high temperature across the membrane surface, and the permeate is collected at colder temperature

in a counter-current flow on the other side of the membrane. The water evaporation occurs at the membrane surface and the vapor permeate through the membrane due to the pressure difference that is induced because of temperature difference between the feed and permeate streams.
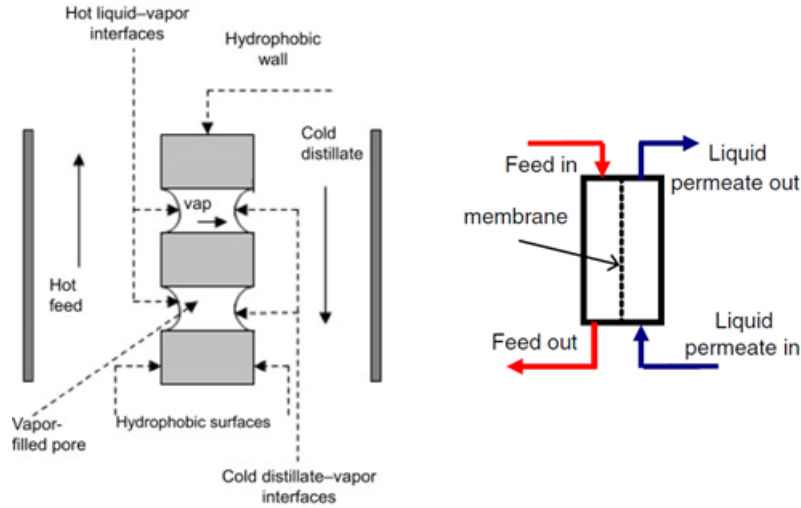
Figure 2-3: Membrane distillation module outline (reproduced from [49], [50])**.**

2.5.2.5 Pervaporation (PV)

Liquid mixture stream is fed to the membrane module and the recovery of the permeate takes place in the form of vapor at the downstream side of the membrane in which it is liquified by cooling using a condenser. The pervaporation process is driven by vacuum using pumps. The pervaporation is ideal for separating liquids with different volatilities, i.e., different partial pressure of components, unlike distillation which depends on differences in boiling point of the components in the mixture [41], [51], [52].

In pervaporation treatment, achieving separation is controlled by factors like membranes' chemical nature and physical structure, solutions' physiochemical features, and interactions between the permeant and membrane [41], [51]. There are three important factors to be highlighted in pervaporation

17

membranes which are: permeability, selectivity, and stability, and there is a huge trade-off between them.

2.5.3 Membrane Module Configuration

Membranes can be manufactured in different configurations to accommodate high fluid flow through their modules. A modules' requirement is to have easy installation, maintenance, and replacement. The size of a module is engineered with several parameters taken into consideration like required capacity, probability of defects occurrence, physical handling, and transportation of a unit [38]. There are two main membrane configurations as described below.

2.5.3.1 Spiral Wound:

This membrane configuration is easier to fabricate compared to capillary tubes. Also, it provides an easy replacement of membranes in the unit. Spiral wound configuration provides multi stages for fluid to pass through. Figure 2-4 shows a schematic diagram of a spiral wound membrane [53]. It consists of flat sheet membranes enveloped around a hollow cylinder. Feed fluid travels across the membrane length tangentially and through it towards the hollow cylinder where the permeate is collected [38], [54].
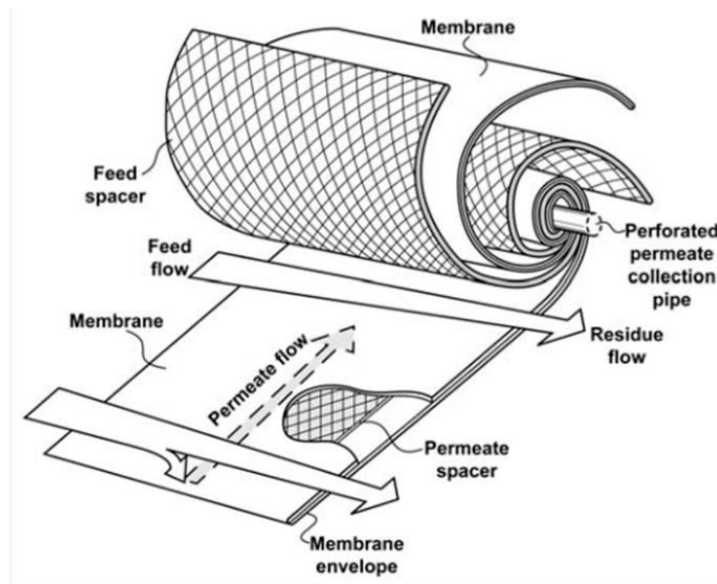
Figure 2-4: Spiral wound membrane configuration (reproduced from [53]**).**

2.5.3.2 Capillary

It is also known as hollow fibers configuration. This configuration has its difficulties in manufacturing but has its advantage of high packing density due to its small strand diameter. Membranes are manufactured in cylindrical tubes all packed in a shell. In this configuration, feed fluid travels across individual membranes along its length, and permeate is collected at the other side of the shell [38], [55].

2.5.4 Membranes Materials

Membrane material has a significant importance for the pervaporation separation compared to other membrane treatment techniques. In some separation methods, membranes are exposed to extreme aggressive feed streams with high temperatures, severe pH values, oxidizing chemicals, and erosive materials [41]. Membranes can be categorized depending on their structure type and general morphology. Two major categories of membranes are symmetric and asymmetric. Different categories of symmetric membranes are microscopic, non-porous, dense, isotropic, and sometimes electrically charged membranes.

On the other hand, there are two categories of asymmetric membranes, anisotropic (thin-film compound anisotropic) and liquid supported membranes [39]. Membrane classification can also be based on the nature of the material such as ceramic, inorganic, or composite membranes.

2.5.4.1 Polymeric Membranes

Common produced water polymeric membranes are made from polyacrylonitrile (PAN) and polyvinylidene difluoride (PVDF). These membranes are relatively cheaper. They can separate solid particles and emulsions efficiently than ceramic membranes [39].

Major disadvantages of polymeric membranes include the fact that they have low capacity to separate volatile and low molecular weight compounds. They also have fouling challenges resulting from oil or sulfides, which require regular cleaning. These membranes can also hardly operate at very high temperatures [31], [56].

2.5.4.2 Inorganic Membranes

Despite the fact that organic membranes form the largest majority of membranes used in industry, inorganic membranes are increasingly utilized as a membrane material for separations. Inorganic membranes are thermally and chemically stable compared to polymeric membranes [41]. There are four types of inorganic membranes commonly used which are ceramic, metallic, glass, and zeolitic. Additionally, only ceramic membranes have achieved the commercial scale between other inorganic membranes.

2.5.4.3 Metallic Membranes

Metallic membranes are manufactured using metallic powder such as tungsten, stainless steel, or molybdenum. For highly corrosive solutions separation applications, stainless steel is utilized as the

basic material. However, this type of membrane material has limited usage due to its high cost of fabrication for commercial large-scale applications [41], [57].

2.5.4.4 Ceramic Membranes

Ceramic membranes are prepared by using a combination of aluminum, silicon, zirconium, or titanium with non-metals such as carbides, oxides, or nitrides. Common materials for ceramic membranes include aluminum oxide and zirconium oxide. Ceramic membranes are in the form of tubular modules along which the feed flows. The membrane has porous support layers with decreasing pore radius and an active layer that forms the active sites for separation [56], [58].

Ceramic membrane can effectively separate organic matter, oil, and other metal oxides. They cannot, however, separate dissolved ions and organic materials. Industries can utilize pre-treatment and purification mechanisms such as cartridge filtration.

These membranes have the advantages of higher flux as they are highly porous with more hydrophilic surfaces, good pore distribution, improved performance recovery because of their chemical and thermal resistance compared to other organic membranes [59]. In addition, although membrane fouling is one of the major challenges when using membranes for water treatment, the high thermal and chemical stability associated with ceramic membranes makes cleaning relatively possible and easier than in the case of polymeric membranes [60].

However, ceramic membranes have significant disadvantages that include leakage and sealing problems after installation since ceramic materials expand easily. Besides, the material is relatively brittle; hence, it needs careful handling [60]. They also require higher operational costs than polymeric membranes due to energy needed to push permeates through their thick membranes [31].

2.5.4.5 Zeolite and Composite Membranes

These membranes are applicable with reverse osmosis to separate ions from aqueous solutions. Zeolite or ceramic membranes are applicable with MF techniques to separate water from oil-water emulsions [58]. Zeolite membranes are stable against oil fouling, with considerable manageable caustic solutions. They also have higher oil rejection and flux efficiency above 99% for water solutions with 100 ppm of oil content.

2.5.4.6 Carbon Membranes

Graphite molecular sieves are used to synthesize membranes for nanofiltrations with a pore diameter size of 1 – 4 nm. These membranes are generally utilized for gas treatments. Despite its outstanding separation properties, it has a downside of fabrication complexities in producing a defect-free membranes for commercial large-scale applications [41]. Carbon membranes include carbon nanotubes, and graphene-based membranes will be discussed in the next section.

2.5.5 Graphene Oxide (GO) Membranes

Graphene Oxide and its derivative has drawn much attention, and intensive number of research have been done to develop it for different applications. It is currently an exciting membrane material for water treatment due to its ultra-two-dimensional structure as well as its multi-functional outer membrane chemistry which provide it with high mass transfer and molecular sieving features [61]–[63]. Basically, GO is a flat hexagonal atomic thick layer structured lattice of sp^2 hybridized carbon. There has been a debate on the GO structure for decades often focusing on the distribution of function chemical groups on the membrane's basal plane. Lerf–Klinowski proposed a generic model which is been widely accepted in the recent past as shown in Figure 2-5.
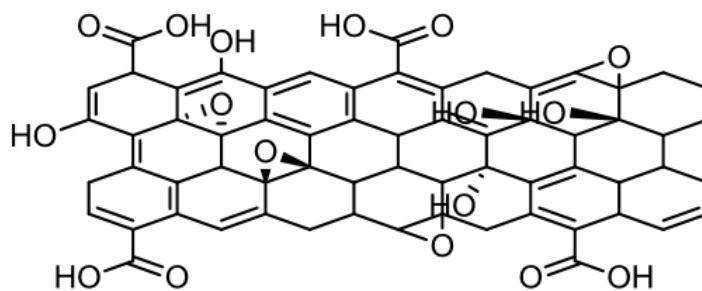
Figure 2-5: Left-Klinowski GO model [64]**.**

The surface possesses a large amount of oxygen containing functional groups like carboxylic acid, hydroxyl, and epoxy that are distributed asymmetrically, allowing large amounts of oxygen on the basal plane and the edges of the membrane, conventionally gives a two to three C/O ratio [65], or in some reports two to four [66].

The high concentration of functional groups on the basal plane of GO membrane surface creates nanoscale wrinkles which lead to vacancy assembly defects and amorphous areas when they are stacked. Surface features as such give water molecules access points of selective entry into the GO membranes. Figure 2-6 shows an electron micrograph cross section image of a GO membrane illustrating wrinkles in the structure [67].
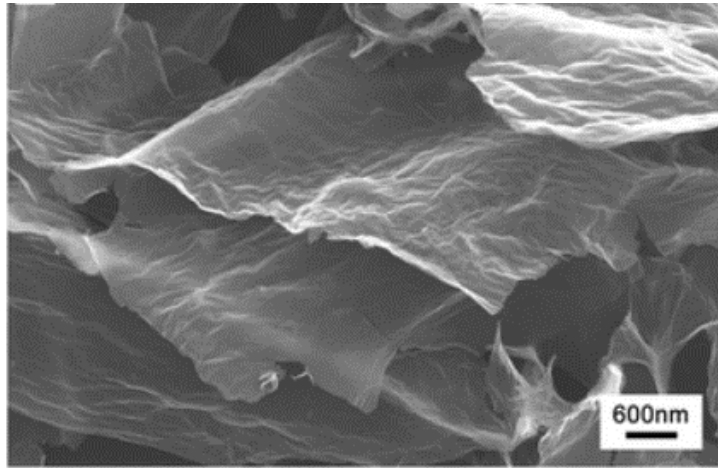
Figure 2-6: Electron micrograph cross section image of a GO membrane showing wrinkles formed in the structure (reproduced from [67]**).**

Figure 2-7 demonstrates the selective movement of permeants travel across a GO membrane through the interlayer, inter-edge spaces, wrinkles, as well as pores, using atomistic simulations of water flowing through interlayer gallery and pores of GO sheets. Interlamellar spaces are of interest in membrane separation since water separation is effectively happening through it [68].
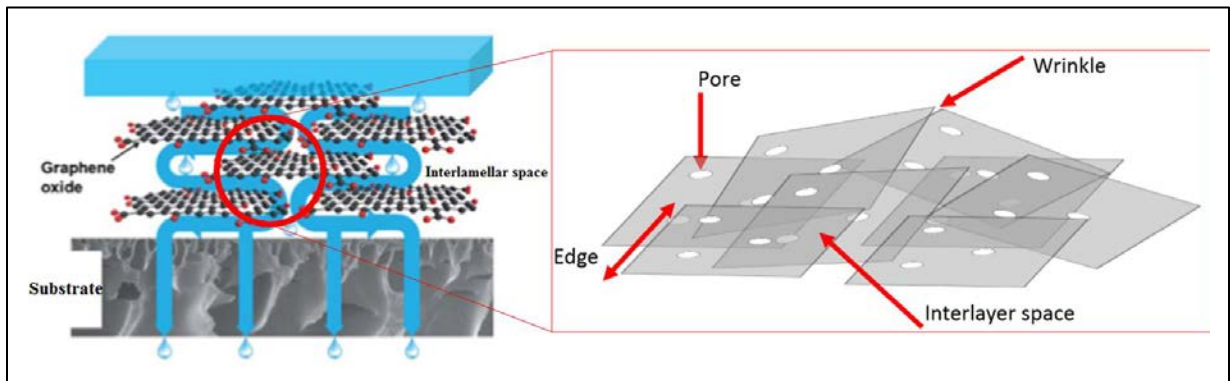
Figure 2-7: GO membrane lamellar stacking and water entrance

routes (Reproduced from [67]**).**

The performance of the pervaporation using GO membranes is thought to be dependent on several factors which are: the supporting substrate material, morphology, and porosity; GO thickness layer and

24

spacing between interlayer sheets; and functional groups of GO in the membrane. A study investigated the effect of GO membrane thickness on its performance and concluded that membranes with a thinner thickness have higher flux. Reducing membrane thickness results in a decreased pathway for water to go through (tortuosity), and thus increasing flux [69]. Another study showed that when thickness of GO layer is less than optimal, support layer surface was not covered thoroughly [70].

GO membranes were first introduced by Nair et al. [71] in 2012 for filtration application. It illustrated fast permeation flux through the membrane and retention of organic liquids of ethanol, propanol, hexane, acetone, and decane, and gas molecules of H_2, N_2, Ar and He. Moreover, water permeation flux through GO membranes is 1–2 order of magnitude greater in pervaporation, because of the huge capillary pressure generated by evaporation in the interlayer of GO nanosheets[72], [73].

2.5.5.1 Mechanism of Water Transport in GO Membranes by Pervaporation

Water permeation through GO lamellar membranes is still not well defined particularly in pervaporation, which involve selective phase change for molecules from liquid to vapor at the membrane surface. Consequently, it is not clear where the liquid phase turns to vapor in GO membrane nanochannels. There are two models been proposed in the literature without confirming their certainties, solution-diffusion model, pore-flow model.

In solution-diffusion model (also known as adsorption-diffusion model), preferential adsorption and diffusion of the water molecules continuously taking place through the dense layer of the membrane [74], [75]. There are three key steps of water permeation in this model as shown in Figure 2-8:

- Selective adsorption of liquid mixture at the surface of the membrane.
- Diffusion of the adsorbed molecules through the membrane driven by pressure difference.

25

- Desorption of the permeated molecules at the downstream side of the membrane as water vapor.
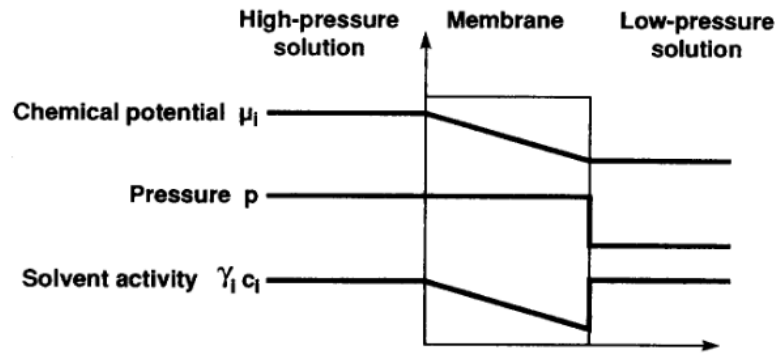
Figure 2-8: Solution-diffusion model (reproduced from [74]**).**

The first two steps are the rate determining steps of the water transport in this model, while the rate of third step of desorption strongly depends on the rate of the first step of adsorption, and it is directly proportional to it [76].

Generally, the solution-diffusion model is used to explain the liquid transport mechanism throughout the membrane. However, this model does not explain the fast and high water flux through the long tortuous and low friction graphitic domains. Therefore, a new study has proposed a new model to explain the pervaporative water transport mechanism through the multilayer GO membranes by a pore-flow model based on membrane distillation simulations [72].

In pore-flow model, the water form 1 – 3 layers of bulk flow through the interlayer space of the GO bulk. Unlike the solution-diffusion model that depends on the concentration gradient, the driving force of the pervaporation separation is much higher and caused by the large pressure difference between the two phases of vapor and liquid water. First, water molecules enter through the surface pores due to the

hydrophilicity of GO, in which they flow afterwards through the pathways by the capillary pressure caused by the water meniscus inside the nanochannels.

Water molecules flow in the entire nanochannels of the dense membrane as a liquid phase, and eventually evaporates at the end of the pore, rather than inside the nanochannel; since the pressure at the vapor permeate side is less than the feed side, hence the nanochannel is filled with liquid water as shown in Figure 2-9 [72].
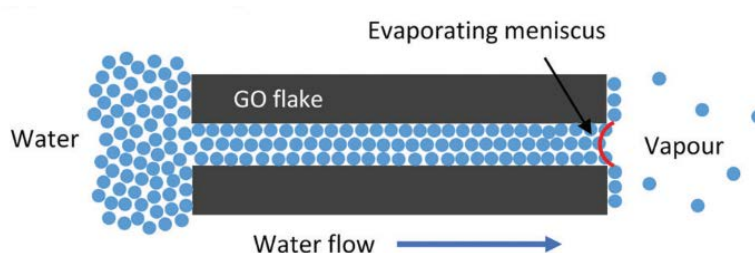
Figure 2-9: Pore-flow model (reproduced from [72]**).**

Additionally, because of the hydrogen bond interactions between water molecules and hydroxyl groups on GO surface, the evaporation energy requirement from the membrane is similar to the evaporation energy needed from bulk water.

2.6 Produced Water Separation Progress To-Date in Membrane Separation

Saline wastewater purification has been intensively studied for salt and dye removal by graphene-base membrane, however, very limited studies have been done for produced water treatment. In addition, performances of graphene-based membranes to-date are still under the theoretical limit. Additionally, produced water purification has not broadly been investigated by the pervaporation technique.

Table 2-2 describes the highest performance GO membranes to date in terms of permeate flux and removal efficiencies, used for different produced water membrane separation techniques.

Table 2-2: Highest performance produced water separation GO membrane till now.

Membrane technology	Membrane type/ material	Removal efficiency (%)	Produced water content	Flux $(L\ h^{-1}m^{-2})$
Microfiltration (MF)	GO/ Al_2O_3 on commercial ceramic base [77]	Oil: 98.7%	Oil: 1000 mg L^{-1}	667
Nanofiltration (NF)	amine-GO/PSF [78]	Salt: 60%-95% Organic: 47%	---	49.30
	GO/β-cyclodextrin/PSF [79]	Salt: 74%-89% Oil: 100%	Salt: 1000 ppm Oil: 1000 ppm	Salt/water: 107 Oil/water: 103.5
	GO/PES & TiO_2 nanoribbons/PES [80]	Salt: 81% Oil: 88%	Salt: 10,220 ppm	85
Air gap membrane distillation (AGMD)	G/PVDF [81]	Salt: 99.99%	---	20.5

GO modified Al_2O_3 deposited on commercial ceramic membranes were utilized in a microfiltration crossflow membrane separation model [77]. The modification portrayed 27.8% higher permeation flux of 667 L $h^{-1}m^{-2}$ using a pressure of 0.1 MPa. It also showed an improved oil rejection of 98.7%.

Nevertheless, no examination was done for salt rejection as microfiltration is not ideal for salt rejection [32], [39]. In addition, air gap membrane distillation technique (AGMD) was used for produced water treatment using a composite flat-film membrane of graphene/polyvinylidene difluoride (G/PVDF). The phase inverted membrane was used to purify the effluent of coal seam gas produced water brine after treatment with RO. The AGMD module resulted in high salt rejection of 99.99% of flux of 20.5 L m^{-2} h^{-1}, yet it was not ideal for organic solutes purification. This process was used as a post-treatment for RO system, and therefore, it is a multi-stage system which demands higher energy consumption.

Additionally, in a current research, shale gas produced water was purified using a modified polysulfone (PSF) nanofiltration technique by amine-GO deposited on the PSF substrate [78]. The membrane that was prepared by interfacial polymerization illustrated salt rejections of 60% to 95 %, and organic solute rejection of 47%; under a pressure of 0.1 MPa to 0.5 MPa. Moreover, GO/β-cyclodextrin deposited on porous PSF base membrane was also used for high pressure-driven nanofiltration technique [79], with applied pressure of 0.6 MPa. The best optimized membrane was used for oil in water nanofiltration separation and had a permeation flux and organic solute rejection of 103.5 L m^{-2} h^{-1}, and 100% respectively. Additionally, despite the high organic solutes' rejection, the membrane had only 89% and 74% of salt rejection for monovalent and divalent salts in the low concentrated saline solution, respectively; with a permeation flux of 107 L m^{-2} h^{-1}.

Furthermore, in a current similar study to our examined membrane, a phase inverted GO/PES and TiO$_2$ nanoribbons/PES was tested for a real produced water from a petroleum industry [80]. The membrane was examined at a pressure of 0.3 MPa in nanofiltration module. Their best optimal membrane showed a very low salt rejection of maximum of 81% only for a low concentration of chloride ion solution of 10,220 ppm. Also, it showed a good oil rejection of 88% with a permeation flux performance of 85 L m^{-2} h^{-1}.

2.7 Challenges of GO Membranes Using Pervaporation

2.7.1 Swelling and Deformation

Stability of GO lamellar structured membranes is the most significant issue faced during the membrane separation since GO sheets swell upon hydration in water. GO has an ample amount of oxygen containing groups that are distributed between its nanosheets. These oxygen containing groups become more negatively charged when hydrated and therefore the nanosheets repel each other by electrostatic forces. Hence, the interlayer d-spacing in the GO lamellar structure increases causing it to swell, which consequently, affects its integrity and selectivity performance [82]–[85]. Moreover, during the pervaporation test, the interaction forces between water molecules with hydrogen bonds and π-π interactions of GO sheets results in decreasing the permeate flux performance [70].

2.7.2 GO Fouling and Concentration Polarization.

Different materials have different tendencies for fouling aggravation based on factors such as: hydrophobicity, surface morphology, and pore size. Moreover, pressure driven separation techniques are more prone for fouling formation. Membranes with high antifouling properties are important for maintaining a steady separation performance [86], [87]. In a study examining fouling resistivity of different polymeric membranes used for wastewater ultrafiltration from extracellular polymeric substances (EPS), which are high molecular weight natural polymers that secrete microorganisms [58]. Based on the membranes tested, the study concluded that polyacrylonitrile (PAN) has the highest fouling residence, followed by polyvinylidene fluoride (PVDF), then polyethersulfone (PES).

In another study experimenting membrane fouling by measuring adsorption capacity, the study revealed that GO membranes have an increased affinity towards organic foulants four to five times higher than polymeric membranes [84]. However, this did not aggravate the fouling problem because adsorption

of organic foulants happens primarily on the basal plane of the GO sheets; and therefore, GO is found to be a promising anti-fouling material for produced water treatment. Additionally, in a study by [88], it is highlighted that GO is providing more negative charges to the surface of the membrane facing water; these negatively charges provide electrostatic repulsive forces towards the microorganisms. Further, the study proved that with the increase of GO content in GO/PSF matrix, the thickness of the microorganism formed at the membrane surface decreased.

Generally, there are very few studies done on fouling related to produced water separation. Such studies are important in determining cleaning applications [89]. Reports show that chemical cleaning is still necessary by a backwash with acidic surfactants, and it is required after several days of operation in order to sustain its performance [60], [90]. In a study by [89], acid solutions of nitric acid (1.0 wt%), and NaOH (0.2 wt%) were used for chemical cleaning; yet it was ineffective and resulted in no recovery of the flux. Further, the study showed no effect of varying the operational conditions on fouling mechanism. Furthermore, inorganic membranes were also tested for MF, but they exhibited low efficiencies than ceramic based MF membranes.

Also, there is no direct relation between temperature and fouling occurrence, but as a general rule, fouling resistivity increases as temperature increases due to the increase of solute solubility.

Furthermore, as the membrane separation progresses, the concentration of the solute in the bulk of the feed mixture is increasing, because more of the solvent is drawn to the permeate side. The retained solute concentration gradually increases and accumulates near the membrane surface. This build- up of the solutes can be reduced by different approaches of optimizing the membrane module design, feed flow rate, and operating temperature [38].

2.8 GO Membranes Fabrication:

There are several methods for making GO-incorporated membranes that have been proposed in the literature. The following are the typical techniques for preparing GO membranes:

2.8.1 GO Coatings

Coating of GO or GO-composite dispersion on a porous support was applied by some techniques, like spray coating, spin coating, or doctor blade casting on a wide sheet of polymeric substrate or inorganic substrates. The role of GO is to provide a selective layer, as well as a protecting layer to the membrane from contacting objects in the liquid feed, and therefore reducing foulants and bacterial impacts [62], [68].

A post treatment of phase inversion in air or liquid might follow this step, in order to create the required pores in the membrane. In phase inversion, when the casted film is submerged in the solvent, migration of the solvent out and non-solvent in is occurring between the two phases. Optimization for the GO content, time of inversion, miscibility of non-solvent with the solvent, a scheme of tertiary solvent and additives.

According to [88], the increase of GO content in polymeric solutions increases its viscosity; and therefore, during phase inversion, there is a possibility for a delay of the creep relaxation of the membrane which is responsible for relieving the stresses. Consequently, smaller pores are created. This indicates that GO content should be optimized for achieving higher water fluxes.

2.8.2 Mix Matrix Membrane (MMM)

GO can be incorporated to polymeric membranes to form a GO/polymer mixed matrix membrane (MMM). GO functions as an additive to provide the desired characteristics to the membrane matrix, like adjusting hydrophilicity, increasing permeability and selectivity, antifouling resistivity, and mechanical integrity [68], [91]. In research conducted by [88], a small amount of GO (around 1 wt%)

was added to the polysulfone (PSF) polymer and was used for water treatment using a membrane bioreactor (MBR). It resulted in a dramatic increase of the antifouling property of the membrane according to surface zeta potential measurements conducted to analyze the mobility of particles inducing membrane's surface charge. In another study by [92], GO/polyvinyl difluoride (PVDF) composite membrane was fabricated and used for microfiltration. According to this study, mixing GO in the PVDF polymeric membrane didn't only increase the antifouling properties, but also increased its mechanical strength based on tensile strength measurements that amplified the strength around 55%.

2.8.3 Pressure Assisted Filtration

Deposition of GO sheets to create a lamellar arrangement carried out by a pressure assisted (or vacuum) filtration on a porous substrate. Permeation in this structure occurs in the interlayer pathways of the nanochannels between GO sheets. Recently, many researchers are focusing on developing GO surface properties and tuning the interlayer nanochannels between GO sheets. Pressure assisted filtration deposition yields highly ordered lamellar stacked structure, while vacuum assisted filtration deposition results in less ordered structure because the initial vacuum drain the GO dispersed solution of directly very easily. Therefore, a highly dense and aligned stack of GO is formed at the bottom side that slows down the drainage of the top side. Nevertheless, GO membranes that are prepared by pressure assisted deposition technique are unstable in water, due to the increase of the interlayer spaces upon hydration [93], [94]. Figure 2-10 illustrates the difference between the pressure and vacuum assisted filtration deposition [70], [95].
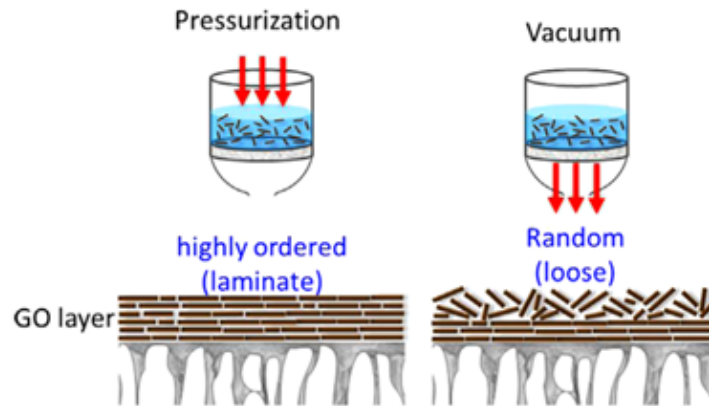
Figure 2-10: Pressure- (or vacuum-) assisted deposition (reproduced from [95]**).**

2.8.4 Langmuir-Blodgett (LB) Deposition

The Langmuir-Blodgett (LB) method has been significantly developed in the past recent years since it is capable of fabricating large sheets of ultrathin 2D materials [96]. This technique generally works by immersing a substrate in water environment; GO suspension is dissolved in a volatile organic solvent like 1,2-dichloroethane (DCE) and deposited at the water surface where the volatile solvent evaporates and GO sheets spread along the surface forming a monolayer thin film at the interface above the substrate. Deposition of GO suspension is done slowly by a syringe pump in order to allow the solvent to evaporate and prevent coagulation of GO sheets. An optimum amount of GO depending on size of trough used, is deposited so as to ensure the surface of air-water is covered with a thin layer of GO. Afterwards, a usual step is followed to compress the GO nanosheets at the interface together by moving barriers to ensure the interface is completely covered and free of gaps that might eventually form a defect. Subsequently, the water medium is drawn out slowly by reversing the syringe pump or using vacuum and the floating GO flakes are eventually packed on the surface of the substrate. Figure 2-11 illustrates the scheme of the setup and deposition technique.

34
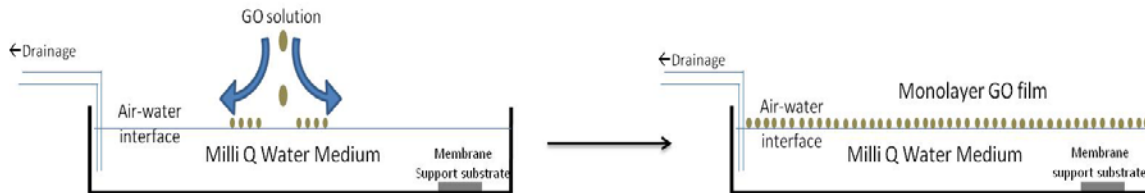
Figure 2-11: Assemble of trough used for GO deposition at air-water interface.

Generally, an ideal GO membrane would be constructed from a single layer of GO sheet containing desirable defect sizes and rich in oxygen containing groups to allow preferred selectivity, and highly porous to achieve high permeability. Currently, due to a lack of a consistent reliable way of producing single layer GO membranes, and tuning nanochannels in between sheets make it challenging for commercial large-scale industries.

2.9 GO Membranes Stability Enhancement

The stability and structural integrity of GO in aqueous solutions is crucial in water treatment by GO membrane separation techniques. Several efforts were introduced to improve the GO membranes stability such as creating strong attraction forces between the nanosheets like crosslinking and reduce the repulsive forces by GO reduction.

2.9.1 GO crosslinking

GO nanosheets crosslinking is achieved by utilizing crosslinkers to hold the adjacent GO nanosheets together and inhibiting the interlamellar d-spacing increase upon hydration. Different crosslinkers are employed like: organic molecules [97], low molecular weight molecules [98], short polymer chains [99], and ions [100], by covalent and non-covalent bonding. In addition, crosslinking treatment is also

used to adjust and control the lamellar distance of the GO membrane structure so as to attain a certain molecular sieving specification [101], [102].

Moreover, in a study conducted using K^+ as a crosslinker, metal cation crosslinkers had shown a better control of the interlayer d-spacing than organic molecules and polymeric crosslinkers, and they can reject other ions that have larger hydrated size [100]. The study also revealed a surprising finding that crosslinked K–GO membrane was rejecting K^+ ions itself when tested for filtration of KCl solution, due to the lower d-spacing attained after crosslinking [100]. Additionally, utilizing a polymer crosslinker of high molecular weight might lead to create a disturbance to the GO structure. Nevertheless, the presence of competing ions to the crosslinker in the solution that have stronger cation–π interactions with GO, can cause the crosslinker to leach out of the structure, which eventually affect the membranes' stability and selectivity [103].

Additionally, different metal cations result in different interlayer spacing. Two trivalent metal cations, Al^{3+} and Fe^{3+}, were incorporated in GO and the resulted membrane was compared for their interlamellar distance [104]. Fe–GO membranes portrayed larger interlayer d-spacing than Al–GO, because Fe^{3+} can form 6 coordination bonding with the hydroxyl groups in GO, while Al^{3+} can form 4 and 6 bonding. Consequently, there are more attraction forces that hold and compress the GO layers together.

Metal cation–GO (M^+–GO) crosslinking can be created unintentionally like through GO synthesis during Mn_2O_3 processing which releases Mn^{2+} ions; or through GO filtration by Al_2O_3 disc that releases Al^{3+} [85]. M^+ ions are inserted into the GO lattice at the sites of the oxide groups and aromatic rings [100], as shown in Figure 2-12 (modified from [105]).
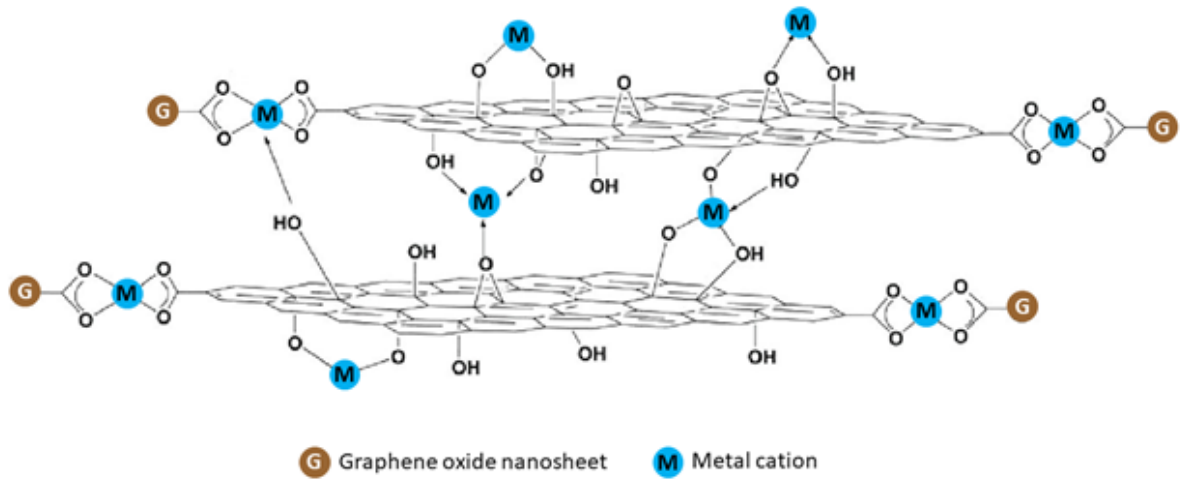
Figure 2-12: Metal cation–GO crosslinked structure (modified from [105]**).**

Generally, metal-GO crosslinking can be synthesized in three methods depending on the treatment sequences of metal insertion [106]:

- Pre-crosslinking method:

In this method, GO and metal cations are mixed and dispersed together to form small tangled GO nanosheet stacks, and then the membrane is fabricated by vacuum filtering the dispersion on a substrate. However, the disadvantage of this method is that the formed GO membrane is not sufficiently strong for long-term separation and disintegrate after several hours [107].

- Post-crosslinking method:

In this method, stacking of GO membranes will be fabricated before being crosslinked. Afterwards, the as prepared GO membranes are either immersed in the crosslinker solution, or the solution is vacuum filtered through the membrane. This method is producing a highly stable GO membranes; but, the crosslinker dispersion has to overcome the high mass transfer resistance with the GO stack to ensure a good distribution of the ions throughout the membrane. [107], [108].

- In-situ crosslinking method [106]:

In this method, metal-GO membranes are fabricated either by vacuum filtration or natural deposition method. In vacuum filtration, a metal containing substrate is prepared in advance, and then it is used to pass the GO dispersion through. Afterwards, the metal ions will leach out of the substrate to the GO layer and crosslink the nanosheets together.

In natural deposition method, a metal foil is positioned under the substrate, and the GO solution is poured above it. The acidity of the GO solution will etch the metal foil releasing metal ions that penetrate the porous substrate by concentration gradient and crosslink the GO nanosheets that gradually deposit on the substrate forming an ordered GO stacking.

The disadvantage of in-situ crosslinking method is that it produces different degrees of crosslinking throughout the membrane. GO layer that is close to the substrate is highly crosslinked compared to the upper layer of GO.

2.9.2 GO reduction

Reducing GO nanosheets enhance the membranes' stability by lowering the amount of oxygen containing groups that repel each other when hydrated, and largely increase the π–π interaction forces between the rGO nanosheets [109]. In a study investigated the effect of GO membrane reduction degree rate on its structure and performance, it was revealed that weak reductions maintain the good dispersion and hydrophilicity of GO [110]. Additionally, weak reductions provide the GO with both important properties of expanding the number of pristine sp^2 graphene regions and preserving the interlayer d-spacing between the GO nanosheets at the same time. Consequently, the resultant membranes had 4 times higher water permeation flux than GO, and over 10^4 times higher flux than completely reduced rGO. However, they achieved lower dye rejection of 95% for different used dyes in the feed solution.

In addition, a higher stability for GO membranes was achieved by partial reduction of GO. Also, other studies showed that water permeation flux in higher C/O ratio GO membranes is ten times higher than those with low C/O ratio [111]–[113].

Water permeation through the pristine graphitic sp^2 regions of the GO structure has lower flux friction than highly functionalized GO structure, since water molecules tend to form hydrogen bond interactions with the oxygen containing functional groups in GO [71], [72]. Therefore, water flows in rGO at a higher rate than GO.

Nevertheless, since oxygen containing groups are lost in the GO reduction treatment, the interlayer d-spacing between the GO nanosheets is decreased, and therefore, there is a trade-off of that the water transportation pathway volume is reduced resulting in low permeation flux rate [112]. Generally, rGO membranes are hydrophobic, even in the presence of few oxygen functional groups [114].

GO reduction can be achieved by chemical or thermal treatment techniques [113], [115], [116]. In chemical reduction, a reductant solution like hydrazine, and hydroiodic acid are employed to reduce the oxygen containing groups in GO. In thermal reduction treatment, high temperature environments used to reduce GO either under inert gas, air; or vacuum using a controlled environment oven.

2.10 References

[1]   P. J. McCabe, "Oil and Natural Gas: Global Resources," in Fossil Energy, New York, NY: Springer New York, 2013, pp. 7–23. doi: 10.1007/978-1-4614-5722-0_2.

[2]   R. T. Duraisamy, A. H. Beni, A. Henni, R. T. Duraisamy, A. H. Beni, and A. Henni, "State of the Art Treatment of Produced Water," Water Treatment, Jan. 2013, doi: 10.5772/53478.

[3]   L. W. Dillon Completions Manager, C. J. Donald Drazan, M. B. Dusseault Professor of Geological, and C. P. Foerster, "MANAGEMENT OF PRODUCED WATER FROM OIL AND GAS WELLS," npc.org, 2011, Accessed: Nov. 02, 2022. [Online]. Available: https://www.npc.org/Prudent_Development-Topic_Papers/2-17_Management_of_Produced_Water_Paper.pdf

[4]   E. Igunnu, G. C.-I. journal of low-carbon, and undefined 2014, "Produced water treatment technologies," academic.oup.com, Accessed: Oct. 04, 2022. [Online]. Available: https://academic.oup.com/ijlct/article-abstract/9/3/157/807670

[5]   J. Neff, K. Lee, and E. M. DeBlois, "Produced Water: Overview of Composition, Fates, and Effects," Produced Water, pp. 3–54, 2011, doi: 10.1007/978-1-4614-0046-2_1.

[6]   N. Sönnichsen, "Daily demand for crude oil worldwide from 2006 to 2020." 2020.

[7]   C. Clark and J. Veil, "Produced water volumes and management practices in the United States.," 2009, Accessed: Sep. 29, 2022. [Online]. Available: https://www.osti.gov/biblio/1007397

[8]   J. M. Dickhout, J. Moreno, P. M. Biesheuvel, L. Boels, R. G. H. Lammertink, and W. M. de Vos, "Produced water treatment by membranes: A review from a colloidal perspective," J Colloid Interface Sci, vol. 487, pp. 523–534, Feb. 2017, doi: 10.1016/J.JCIS.2016.10.013.

[9]   H. Ozgun et al., "Effects of the pre-treatment alternatives on the treatment of oil-gas field produced water by nanofiltration and reverse osmosis membranes," Journal of Chemical Technology & Biotechnology, vol. 88, no. 8, pp. 1576–1583, Aug. 2013, doi: 10.1002/JCTB.4007.

[10]   P. J. C. Tibbetts, I. T. Buchanan, L. J. Gawel, and R. Large, "A Comprehensive Determination of Produced Water Composition," Produced Water, pp. 97–112, 1992, doi: 10.1007/978-1-4615-2902-6_9.

[11]   I. Schifter, C. González-Macías, L. Salazar-Coria, G. Sánchez-Reyna, and C. González-Lozano, "Long-term effects of discharges of produced water the marine environment from petroleum-related activities at Sonda de Campeche, Gulf of México," Environ Monit Assess, vol. 187, no. 11, pp. 1–24, Nov. 2015, doi: 10.1007/S10661-015-4944-1/TABLES/8.

[12]   J. D. Arthur, B. G. Langhus, and C. Patel, "Technical summary of oil & gas produced water treatment technologies," All Consulting, LLC, Tulsa, OK, 2005.

[13]   M. A. Al-Ghouti, M. A. Al-Kaabi, M. Y. Ashfaq, and D. A. Da'na, "Produced water characteristics, treatment and reuse: A review," Journal of Water Process Engineering, vol. 28, pp. 222–239, Apr. 2019, doi: 10.1016/J.JWPE.2019.02.001.

[14]   A. Echchelh, T. Hess, and R. Sakrabani, "Reusing oil and gas produced water for irrigation of food crops in drylands," Agric Water Manag, vol. 206, pp. 124–134, Jul. 2018, doi: 10.1016/J.AGWAT.2018.05.006.

[15]   N. E. Pica, K. Carlson, J. J. Steiner, and R. Waskom, "Produced water reuse for irrigation of non-food biofuel crops: Effects on switchgrass and rapeseed germination, physiology and

biomass yield," Ind Crops Prod, vol. 100, pp. 65–76, Jun. 2017, doi: 10.1016/J.INDCROP.2017.02.011.

[16]   A. Fakhru'l-Razi, A. Pendashteh, L. C. Abdullah, D. R. A. Biak, S. S. Madaeni, and Z. Z. Abidin, "Review of technologies for oil and gas produced water treatment," J Hazard Mater, vol. 170, no. 2–3, pp. 530–551, 2009.

[17]   U. E. N. C. for E. Assessment, "An integrated framework for treatment and management of produced water - Technical assessment of produced water treatment technologies," Mar. 2009.

[18]   O. H.-2004 B. Conference and undefined 2004, "Evolutionary developments of thermal desalination plants in the Arab Gulf region," researchgate.net, Accessed: Nov. 03, 2022. [Online]. Available: https://www.researchgate.net/profile/Osman-Hamed-2/publication/228945604_Evolutionary_developments_of_thermal_desalination_plants_in_the_Arab_Gulf_region/links/554edf3008ae12808b365304/Evolutionary-developments-of-thermal-desalination-plants-in-the-Arab-Gulf-region.pdf

[19]   M. Scholz, "Slow Filtration," Wetlands for Water Pollution Control, pp. 61–68, Jan. 2016, doi: 10.1016/B978-0-444-63607-2.00010-1.

[20]   Z. Cha, C. F. Lin, C. J. Cheng, and P. K. Andy Hong, "Removal of oil and oil sheen from produced water by pressure-assisted ozonation and sand filtration," Chemosphere, vol. 78, no. 5, pp. 583–590, Jan. 2010, doi: 10.1016/J.CHEMOSPHERE.2009.10.051.

[21]   M. A. Adewumi, J. E. Erb, and R. W. Watson, "Initial Design Considerations for a Cost Effective Treatment of Stripper Oil Well Produced Water," Produced Water, pp. 511–522, 1992, doi: 10.1007/978-1-4615-2902-6_40.

[22]   L. M. Multon and T. Viraraghavan, "Removal of Oil from Produced Water by Coalescence/Filtration in a Granular Bed," http://dx.doi.org/10.1080/09593332808618665, vol. 27, no. 5, pp. 529–544, 2010, doi: 10.1080/09593332808618665.

[23]   T. P. Daigle and L. D. Cox, "Ultra deep water discharge of produced water and/or solids at the seabed," Research Partnership to Secure Energy for America (RPSEA), 2012.

[24]   A. Bhatnagar, W. Hogland, M. Marques, and M. Sillanpää, "An overview of the modification methods of activated carbon for its water treatment applications," Chemical Engineering Journal, vol. 219, pp. 499–511, Mar. 2013, doi: 10.1016/J.CEJ.2012.12.038.

[25]   K. Konieczny, M. Bodzek, M. R.- Desalination, and undefined 2006, "A coagulation–MF system for water treatment using ceramic membranes," Elsevier, Accessed: Nov. 04, 2022. [Online]. Available: https://www.sciencedirect.com/science/article/pii/S0011916406011179

[26]   A. L. L. Consulting, "Handbook on coal bed methane produced water: Management and beneficial use alternatives," Prepared for: Groundwater Protection Research Foundation, US Department of Energy, National Petroleum Technology Ofce, Bureau of Land Management, July, 2003.

[27]   K. Yasuda et al., "Oil emulsions and the different recent demulsification techniques in the petroleum industry - A review," IOP Conf Ser Mater Sci Eng, vol. 702, no. 1, p. 012060, Nov. 2019, doi: 10.1088/1757-899X/702/1/012060.

[28]   M. Antunes, R. A. Medronho, L. Svarovsky, and M. T. Thew, "Hydrocyclones: Analysis and Applications." Svarovsky, L., Thew, MT, Eds, 1992.

[29]   M. Bagheri, R. Roshandel, and J. Shayegan, "Optimal selection of an integrated produced water treatment system in the upstream of oil industry," Process Safety and Environmental Protection, vol. 117, pp. 67–81, Jul. 2018, doi: 10.1016/J.PSEP.2018.04.010.

[30]   M. Çakmakce, N. Kayaalp, I. K.- Desalination, and undefined 2008, "Desalination of produced water from oil production fields by membrane processes," Elsevier, Accessed: Nov. 04, 2022. [Online]. Available: https://www.sciencedirect.com/science/article/pii/S0011916407007679

[31]   M. Padaki et al., "Membrane technology enhancement in oil–water separation. A review," Desalination, vol. 357, pp. 197–207, Feb. 2015, doi: 10.1016/J.DESAL.2014.11.023.

[32]   K. Amakiri, A. Canon, M. Molinari, A. A.-D.- Chemosphere, and undefined 2022, "Review of oilfield produced water treatment technologies," Elsevier, Accessed: Nov. 05, 2022. [Online]. Available: https://www.sciencedirect.com/science/article/pii/S0045653522005574

[33]   S. Alzahrani and A. W. Mohammad, "Challenges and trends in membrane technology implementation for produced water treatment: A review," Journal of Water Process Engineering, vol. 4, pp. 107–133, 2014.

[34]   H. Abdelrazeq et al., "Sustainable innovation in membrane technologies for produced water treatment: Challenges and limitations," mdpi.com, 2021, doi: 10.3390/su13126759.

[35]   S. Zinadini, A. Zinatizadeh, … M. R.-J. of M., and undefined 2014, "Preparation of a novel antifouling mixed matrix PES membrane by embedding graphene oxide nanoplates," Elsevier, Accessed: Nov. 04, 2022. [Online]. Available: https://www.sciencedirect.com/science/article/pii/S037673881300882X

[36]   L. Tijing, Y. Woo, J. Choi, S. Lee, … S. K.-J. of M., and undefined 2015, "Fouling and its control in membrane distillation—A review," Elsevier, Accessed: Nov. 04, 2022. [Online]. Available: https://www.sciencedirect.com/science/article/pii/S0376738814007443

[37]   M. Elimelech and W. A. Phillip, "The future of seawater desalination: Energy, technology, and the environment," Science (1979), vol. 333, no. 6043, pp. 712–717, Aug. 2011, doi: 10.1126/SCIENCE.1200488.

[38]   R. Noble and S. Stern, Membrane separations technology: principles and applications. 1995. Accessed: Nov. 05, 2022. [Online]. Available: https://books.google.com/books?hl=en&lr=&id=-AfNV215sPAC&oi=fnd&pg=PR2&dq=Noble,+R.+D.,+%26+Stern,+S.+A.+(Eds.).+(1995).+Membrane+separations+technology:+principles+and+applications+(Vol.+2).+Elsevier&ots=IWYBI17AZr&sig=ZpCFnHxAETxMYYPGhYK9NVrPB2w

[39]   R. W. Baker, Membrane technology and applications. 2012. Accessed: Nov. 05, 2022. [Online].   Available: https://books.google.com/books?hl=en&lr=&id=FhtBKUq4rL8C&oi=fnd&pg=PR11&dq=Baker+R.+W.+(2004)+Membrane+Technology+and+Applications,+Second+Edition.+England:+John+Wiley+%26+Sons,+Ltd.+&ots=afu63FzKgW&sig=lI8yZIG5bZ12elBdjqDoUT0DP3U

[40]   A. Lidén, K. P.-J. of W. S. R. and, and undefined 2016, "Comparison between ultrafiltration and nanofiltration hollow-fiber membranes for removal of natural organic matter: a pilot study," iwaponline.com, Accessed: Nov. 05, 2022. [Online]. Available: https://iwaponline.com/aqua/article-abstract/65/1/43/29324

[41]   B. Freeman, "Introduction to Membrane Science and Technology. By Heinrich Strathmann.,"
Angewandte Chemie International Edition, vol. 51, no. 38, pp. 9485–9485, Sep. 2012, doi:
10.1002/ANIE.201205786.

[42]   A. Subramani and J. G. Jacangelo, "Emerging desalination technologies for water treatment:
A critical review," Water Res, vol. 75, pp. 164–187, May 2015, doi:
10.1016/J.WATRES.2015.02.032.

[43]   B. Coday, P. Xu, E. Beaudry, J. Herron, K. L.- Desalination, and undefined 2014, "The sweet
spot of forward osmosis: Treatment of produced water, drilling wastewater, and other complex
and difficult liquid streams," Elsevier, Accessed: Nov. 05, 2022. [Online]. Available:
https://www.sciencedirect.com/science/article/pii/S0011916413005390

[44]   A. Alkhudhiri, N. Darwish, and N. Hilal, "Membrane distillation: A comprehensive review,"
Desalination, vol. 287, pp. 2–18, Feb. 2012, doi: 10.1016/J.DESAL.2011.08.027.

[45]   P. D. Dongare et al., "Nanophotonics-enabled solar membrane distillation for off-grid water
purification," Proc Natl Acad Sci U S A, vol. 114, no. 27, pp. 6936–6941, Jul. 2017, doi:
10.1073/PNAS.1701835114/SUPPL_FILE/PNAS.201701835SI.PDF.

[46]   I. A. Said, T. R. Chomiak, Z. He, and Q. Li, "Low-cost high-efficiency solar membrane
distillation for treatment of oil produced waters," Sep Purif Technol, vol. 250, p. 117170, Nov.
2020, doi: 10.1016/J.SEPPUR.2020.117170.

[47]   M. C. García-Payo, M. A. Izquierdo-Gil, and C. Fernández-Pineda, "Air gap membrane
distillation of aqueous alcohol solutions," J Memb Sci, vol. 169, no. 1, pp. 61–80, Apr. 2000,
doi: 10.1016/S0376-7388(99)00326-9.

[48]   J. Blanco Gálvez, L. García-Rodríguez, and I. Martín-Mateos, "Seawater desalination by an innovative solar-powered membrane distillation system: the MEDESOL project," Desalination, vol. 246, no. 1–3, pp. 567–576, Sep. 2009, doi: 10.1016/J.DESAL.2008.12.005.

[49]   P. Pal, "Arsenic Removal by Membrane Distillation," Groundwater Arsenic Remediation, pp. 179–270, Jan. 2015, doi: 10.1016/B978-0-12-801281-9.00005-9.

[50]   M. R. Qtaishat and F. Banat, "Desalination by solar powered membrane distillation systems," Desalination, vol. 308, pp. 186–197, Jan. 2013, doi: 10.1016/J.DESAL.2012.01.021.

[51]   X. Feng and R. Y. M. Huang, "Liquid separation by membrane pervaporation: a review," Ind Eng Chem Res, vol. 36, no. 4, pp. 1048–1066, 1997.

[52]   Q. Liu, R. D. Noble, J. L. Falconer, and H. H. Funke, "Organics/water separation by pervaporation with a zeolite membrane," J Memb Sci, vol. 117, no. 1–2, pp. 163–174, Aug. 1996, doi: 10.1016/0376-7388(96)00058-0.

[53]   R. W. Baker, "Future directions of membrane gas separation technology," Ind Eng Chem Res, vol. 41, no. 6, pp. 1393–1411, Mar. 2002, doi: 10.1021/IE0108088/ASSET/IMAGES/LARGE/IE0108088F00024.JPEG.

[54]   "Spiral Wound Membranes." https://synderfiltration.com/learning-center/articles/module-configurations-process/spiral-wound-membranes/ (accessed Nov. 05, 2022).

[55]   "Hollow Fiber Membranes." https://synderfiltration.com/learning-center/articles/module-configurations-process/hollow-fiber-membranes/ (accessed Nov. 05, 2022).

[56]   K. S. Ashaghi, … M. E.-O. E., and undefined 2007, "Ceramic ultra-and nanofiltration membranes for oilfield produced water treatment: A mini review," benthamopen.com, vol. 1,

pp. 1–8, 2007, Accessed: Nov. 04, 2022. [Online]. Available: https://benthamopen.com/ABSTRACT/TOENVIRJ-1-1

[57] M. Mulder and J. Mulder, Basic principles of membrane technology. 1996. Accessed: Nov. 05, 2022. [Online]. Available: https://books.google.com/books?hl=en&lr=&id=SP2_GYvL384C&oi=fnd&pg=PA1&dq=M ulder+M.+(1996).+Basic+Principles+of+Membrane+Technology,+second+edition&ots=GtE 96mV722&sig=H9Vk_Erl2N-nfpCz7LgJwpQUl5U

[58] J. Cui, X. Zhang, H. Liu, S. Liu, K. Y.-J. of M. Science, and undefined 2008, "Preparation and application of zeolite/ceramic microfiltration membranes for treatment of oil contaminated water," Elsevier, Accessed: Nov. 05, 2022. [Online]. Available: https://www.sciencedirect.com/science/article/pii/S037673880800759X

[59] M. Abbasi, M. Sebzari, … A. S.-C. E., and undefined 2012, "Modeling of membrane fouling and flux decline in microfiltration of oily wastewater using ceramic membranes," Taylor & Francis, vol. 199, no. 1, pp. 78–93, Jan. 2012, doi: 10.1080/00986445.2011.570391.

[60] M. Ebrahimi, D. Willershausen, K. Ashaghi, L. E.- Desalination, and undefined 2010, "Investigations on the use of different ceramic membranes for efficient oil-field produced water treatment," Elsevier, Accessed: Nov. 05, 2022. [Online]. Available: https://www.sciencedirect.com/science/article/pii/S0011916409011205

[61] R. K. Joshi et al., "Precise and ultrafast molecular sieving through graphene oxide membranes," Science (1979), vol. 343, no. 6172, pp. 752–754, 2014, doi: 10.1126/SCIENCE.1245711.

[62] M. Paulauskas, "Pervaporation using graphene oxide membranes," 2015.

[63]   Y. You, V. Sahajwalla, M. Yoshimura, and R. K. Joshi, "Graphene and graphene oxide for desalination," Nanoscale, vol. 8, no. 1, pp. 117–119, Dec. 2015, doi: 10.1039/C5NR06154G.

[64]   A. M. Dimiev, L. B. Alemany, and J. M. Tour, "Graphene oxide. Origin of acidity, its instability in water, and a new dynamic structural model," ACS Nano, vol. 7, no. 1, pp. 576–588, 2013.

[65]   T. Szabó et al., "Evolution of surface functional groups in a series of progressively oxidized graphite oxides," Chemistry of materials, vol. 18, no. 11, pp. 2740–2749, 2006.

[66]   D. An, L. Yang, T. J. Wang, and B. Liu, "Separation performance of graphene oxide membrane in aqueous solution," Ind Eng Chem Res, vol. 55, no. 17, pp. 4803–4810, May 2016, doi: 10.1021/ACS.IECR.6B00620.

[67]   B. Liang et al., "High performance graphene oxide/polyacrylonitrile composite pervaporation membranes for desalination applications," pubs.rsc.org, vol. 00, pp. 1–3, 2013, doi: 10.1039/x0xx00000x.

[68]   N. Wei, X. Peng, and Z. Xu, "Understanding water permeation in graphene oxide membranes," ACS Appl Mater Interfaces, vol. 6, no. 8, pp. 5877–5883, 2014.

[69]   J. Yin, G. Zhu, and B. Deng, "Graphene oxide (GO) enhanced polyamide (PA) thin-film nanocomposite (TFN) membrane for water purification," Desalination, vol. 379, pp. 93–101, Feb. 2016, doi: 10.1016/J.DESAL.2015.11.001.

[70]   W. S. Hung et al., "Pressure-assisted self-assembly technique for fabricating composite membranes consisting of highly ordered selective laminate layers of amphiphilic graphene oxide," Carbon N Y, vol. 68, pp. 670–677, Mar. 2014, doi: 10.1016/J.CARBON.2013.11.048.

[71]   R. Nair, H. Wu, P. Jayaram, I. Grigorieva, A. G.- Science, and undefined 2012, "Unimpeded permeation of water through helium-leak–tight graphene-based membranes," science.org,

Accessed: Nov. 06, 2022. [Online]. Available: https://www.science.org/doi/abs/10.1126/science.1211694

[72] J. Y. Chong, B. Wang, and K. Li, "Water transport through graphene oxide membranes: the roles of driving forces," Chemical Communications, vol. 54, no. 20, pp. 2554–2557, Mar. 2018, doi: 10.1039/C7CC09120F.

[73] C. Wang, Z. Li, J. Chen, Y. Yin, and H. Wu, "Structurally stable graphene oxide-based nanofiltration membranes with bioadhesive polydopamine coating," Appl Surf Sci, vol. 427, pp. 1092–1098, Jan. 2018, doi: 10.1016/J.APSUSC.2017.08.124.

[74] J. G. Wijmans and R. W. Baker, "The solution-diffusion model: a review," J Memb Sci, vol. 107, no. 1–2, pp. 1–21, Nov. 1995, doi: 10.1016/0376-7388(95)00102-I.

[75] D. R. Paul, "The Solution-Diffusion Model for Swollen Membranes," http://dx.doi.org/10.1080/03602547608066047, vol. 5, no. 1, pp. 33–50, Jan. 2006, doi: 10.1080/03602547608066047.

[76] A. Pabby, S. Rizvi, and A. Requena, Handbook of membrane separations: chemical, pharmaceutical, food, and biotechnological applications. 2008. doi: 10.1201/b18319-35.

[77] X. Hu et al., "The improved oil/water separation performance of graphene oxide modified Al2O3 microfiltration membrane," J Memb Sci, vol. 476, pp. 200–204, Feb. 2015, doi: 10.1016/J.MEMSCI.2014.11.043.

[78] F. xin Kong, Z. Y. Yang, L. P. Yue, J. fu Chen, and C. mei Guo, "Nanofiltration membrane with substrate incorporated amine-functionalized graphene oxide for enhanced petrochemical wastewater and shale gas produced water desalination," Desalination, vol. 517, p. 115246, Dec. 2021, doi: 10.1016/J.DESAL.2021.115246.

[79]   A. Q. Al-Gamal, T. A. Saleh, and F. I. Alghunaimi, "Nanofiltration membrane with high flux and oil rejection using graphene oxide/β-cyclodextrin for produced water reuse," Mater Today Commun, vol. 31, p. 103438, Jun. 2022, doi: 10.1016/J.MTCOMM.2022.103438.

[80]   T. Ashraf, N. Alfryyan, M. Nasr, S. A. Ahmed, and M. Shaban, "Removal of Scale-Forming Ions and Oil Traces from Oil Field Produced Water Using Graphene Oxide/Polyethersulfone and TiO2 Nanoribbons/Polyethersulfone Nanofiltration Membranes," Polymers 2022, Vol. 14, Page 2572, vol. 14, no. 13, p. 2572, Jun. 2022, doi: 10.3390/POLYM14132572.

[81]   Y. C. Woo et al., "Graphene/PVDF flat-sheet membrane for the treatment of RO brine from coal seam gas produced water by air gap membrane distillation," J Memb Sci, vol. 513, pp. 74–84, Sep. 2016, doi: 10.1016/J.MEMSCI.2016.04.014.

[82]   S. Zheng, Q. Tu, J. J. Urban, S. Li, and B. Mi, "Swelling of Graphene Oxide Membranes in Aqueous Solution: Characterization of Interlayer Spacing and Insight into Water Transport Mechanisms," ACS Nano, vol. 11, p. 52, 2017, doi: 10.1021/acsnano.7b02999.

[83]   J. Ma, Y. He, H. Shi, Y. Fan, H. Yu, and Y. Li, "Stable graphene oxide-based composite membranes intercalated with montmorillonite nanoplatelets for water purification," J Mater Sci, vol. 54, no. 3, pp. 2241–2255, Feb. 2019, doi: 10.1007/S10853-018-2997-6.

[84]   Y.-H. Xi et al., "Graphene oxide membranes with strong stability in aqueous solutions and controllable lamellar spacing," ACS Publications, vol. 8, no. 24, pp. 15557–15566, Jun. 2016, doi: 10.1021/acsami.6b00928.

[85]   C.-N. Yeh, K. Raidongia, J. Shao, Q.-H. Yang, and J. Huang, "On the origin of the stability of graphene oxide membranes in water," Nat Chem, vol. 7, no. 2, pp. 166–170, 2015.

[86]   M. Hu, S. Zheng, and B. Mi, "Organic Fouling of Graphene Oxide Membranes and Its Implications for Membrane Fouling Control in Engineered Osmosis," Environ Sci Technol, vol. 50, no. 2, pp. 685–693, Jan. 2016, doi: 10.1021/ACS.EST.5B03916/ASSET/IMAGES/LARGE/ES-2015-03916X_0007.JPEG.

[87]   F. Meng, S. R. Chae, A. Drews, M. Kraume, H. S. Shin, and F. Yang, "Recent advances in membrane bioreactors (MBRs): Membrane fouling and membrane material," Water Res, vol. 43, no. 6, pp. 1489–1512, Apr. 2009, doi: 10.1016/J.WATRES.2008.12.044.

[88]   J. Lee et al., "Graphene oxide nanoplatelets composite membrane with hydrophilic and antifouling properties for wastewater treatment," J Memb Sci, vol. 448, pp. 223–230, 2013, doi: 10.1016/j.memsci.2013.08.017.

[89]   J. Mueller, Y. Cen, and R. H. Davis, "Crossflow microfiltration of oily water," J Memb Sci, vol. 129, no. 2, pp. 221–235, Jul. 1997, doi: 10.1016/S0376-7388(96)00344-4.

[90]   A. Salahi, M. Abbasi, and T. Mohammadi, "Permeate flux decline during UF of oily wastewater: Experimental and modeling," Desalination, vol. 251, no. 1–3, pp. 153–160, Feb. 2010, doi: 10.1016/J.DESAL.2009.08.006.

[91]   X. Qu, P. J. J. Alvarez, and Q. Li, "Applications of nanotechnology in water and wastewater treatment," Water Res, vol. 47, no. 12, pp. 3931–3946, Aug. 2013, doi: 10.1016/J.WATRES.2012.09.058.

[92]   J. Zhang et al., "Synergetic effects of oxidized carbon nanotubes and graphene oxide on fouling control and anti-fouling mechanism of polyvinylidene fluoride ultrafiltration membranes," J Memb Sci, vol. 448, pp. 81–92, Dec. 2013, doi: 10.1016/J.MEMSCI.2013.07.064.

[93]   C. Cheng et al., "Nanotechnology: Ion transport in complex layered Graphene-Based membranes with tuneable interlayer spacing," Sci Adv, vol. 2, no. 2, Feb. 2016, doi: 10.1126/SCIADV.1501272/SUPPL_FILE/1501272_SM.PDF.

[94]   D. R. Dreyer, S. Park, C. W. Bielawski, and R. S. Ruoff, "The chemistry of graphene oxide," Chem Soc Rev, vol. 39, no. 1, pp. 228–240, Dec. 2009, doi: 10.1039/B917103G.

[95]   C. Tsou, Q. An, S. Lo, … M. D. G.-J. of M., and undefined 2015, "Effect of microstructure of graphene oxide fabricated through different self-assembly techniques on 1-butanol dehydration," Elsevier, Accessed: Oct. 11, 2022. [Online]. Available: https://www.sciencedirect.com/science/article/pii/S0376738814009429

[96]   O. N. Oliveira, L. Caseli, and K. Ariga, "The Past and the Future of Langmuir and Langmuir-Blodgett Films," Chem Rev, vol. 122, no. 6, pp. 6459–6513, Mar. 2022, doi: 10.1021/ACS.CHEMREV.1C00754/ASSET/IMAGES/LARGE/CR1C00754_0038.JPEG.

[97]   W. S. Hung et al., "Cross-linking with diamine monomers to prepare composite graphene oxide-framework membranes with varying d-spacing," Chemistry of Materials, vol. 26, no. 9, pp. 2983–2990, May 2014, doi: 10.1021/CM5007873.

[98]   K. H. Thebo, X. Qian, Q. Zhang, L. Chen, H. M. Cheng, and W. Ren, "Highly stable graphene-oxide-based membranes with superior permeability," Nature Communications 2018 9:1, vol. 9, no. 1, pp. 1–8, Apr. 2018, doi: 10.1038/s41467-018-03919-0.

[99]   M. L. Liu et al., "One-step enhancement of solvent transport, stability and photocatalytic properties of graphene oxide/polyimide membranes with multifunctional cross-linkers," J Mater Chem A Mater, vol. 7, no. 7, pp. 3170–3178, Feb. 2019, doi: 10.1039/C8TA11372F.

[100] L. Chen et al., "Ion sieving in graphene oxide membranes via cationic control of interlayer spacing," Nature 2017 550:7676, vol. 550, no. 7676, pp. 380–383, Oct. 2017, doi: 10.1038/nature24044.

[101] J. Abraham et al., "Tunable sieving of ions using graphene oxide membranes," Nature Nanotechnology 2017 12:6, vol. 12, no. 6, pp. 546–550, Apr. 2017, doi: 10.1038/nnano.2017.21.

[102] S. Xia, M. Ni, T. Zhu, Y. Zhao, N. L.- Desalination, and undefined 2015, "Ultrathin graphene oxide nanosheet membranes with various d-spacing assembled using the pressure-assisted filtration method for removing natural organic," Elsevier, Accessed: Oct. 10, 2022. [Online]. Available: https://www.sciencedirect.com/science/article/pii/S001191641500363X

[103] Y. Ying et al., "Development of a stable cation modified graphene oxide membrane for water treatment," 2d Mater, vol. 4, no. 4, p. 045006, Aug. 2017, doi: 10.1088/2053-1583/AA814C.

[104] T. Liu, B. Yang, N. Graham, W. Yu, and K. Sun, "Trivalent metal cation cross-linked graphene oxide membranes for NOM removal in water treatment," J Memb Sci, vol. 542, pp. 31–40, Nov. 2017, doi: 10.1016/J.MEMSCI.2017.07.061.

[105] S. Park, K. S. Lee, G. Bozoklu, W. Cai, S. B. T. Nguyen, and R. S. Ruoff, "Graphene oxide papers modified by divalent ions - Enhancing mechanical properties via chemical cross-linking," ACS Nano, vol. 2, no. 3, pp. 572–578, Mar. 2008, doi: 10.1021/NN700349A/SUPPL_FILE/NN700349A_SI.PDF.

[106] X. bin Lv et al., "A Novel Strategy to Fabricate Cation-Cross-linked Graphene Oxide Membrane with High Aqueous Stability and High Separation Performance," ACS Appl Mater

Interfaces, vol. 12, no. 50, pp. 56269–56280, Dec. 2020, doi: 10.1021/ACSAMI.0C15178/ASSET/IMAGES/LARGE/AM0C15178_0012.JPEG.

[107] A. Li, K. Han, Y. Zhou, H. Ye, G. Liu, and H. H. Kung, "Incorporating multivalent metal cations into graphene oxide: Towards highly-aqueous-stable free-standing membrane via vacuum filtration with polymeric filters," Mater Today Commun, vol. 11, pp. 139–146, Jun. 2017, doi: 10.1016/J.MTCOMM.2017.04.002.

[108] A. Ghaffar, L. Zhang, X. Zhu, and B. Chen, "Scalable graphene oxide membranes with tunable water channels and stability for ion rejection," Environ Sci Nano, vol. 6, no. 3, pp. 904–915, Mar. 2019, doi: 10.1039/C8EN01273C.

[109] K. Goh, W. Jiang, H. Karahan, … S. Z.-A. F., and undefined 2015, "All-carbon nanoarchitectures as high-performance separation membranes with superior stability," Wiley Online Library, vol. 25, no. 47, pp. 7348–7359, Dec. 2015, doi: 10.1002/adfm.201502955.

[110] Q. Zhang, X. Qian, K. H. Thebo, H. M. Cheng, and W. Ren, "Controlling reduction degree of graphene oxide membranes for improved water permeance," Sci Bull (Beijing), vol. 63, no. 12, pp. 788–794, Jun. 2018, doi: 10.1016/J.SCIB.2018.05.015.

[111] G. Shi, Q. Meng, Z. Zhao, H.-C. Kuan, A. Michelmore, and J. Ma, "Facile fabrication of graphene membranes with readily tunable structures," ACS Publications, vol. 7, no. 25, pp. 13745–13757, Jul. 2015, doi: 10.1021/am5091287.

[112] C. A. Amadei, A. Montessori, J. P. Kadow, S. Succi, and C. D. Vecitis, "Role of Oxygen Functionalities in Graphene Oxide Architectural Laminate Subnanometer Spacing and Water Transport," Environ Sci Technol, vol. 51, no. 8, pp. 4280–4288, Apr. 2017, doi: 10.1021/ACS.EST.6B05711.

[113] Y. Li et al., "Mild annealing reduced graphene oxide membrane for nanofiltration," J Memb Sci, vol. 601, p. 117900, Mar. 2020, doi: 10.1016/J.MEMSCI.2020.117900.

[114] E. Yang, M. H. Ham, H. B. Park, C. M. Kim, J. ho Song, and I. S. Kim, "Tunable semi-permeability of graphene-based membranes by adjusting reduction degree of laminar graphene oxide layer," J Memb Sci, vol. 547, pp. 73–79, Feb. 2018, doi: 10.1016/J.MEMSCI.2017.10.039.

[115] Y. Li et al., "Thermally reduced nanoporous graphene oxide membrane for desalination," Environ Sci Technol, vol. 53, no. 14, pp. 8314–8323, Jul. 2019, doi: 10.1021/ACS.EST.9B01914/ASSET/IMAGES/LARGE/ES-2019-01914J_0006.JPEG.

[116] H. Liu, H. Wang, and X. Zhang, "Facile fabrication of freestanding ultrathin reduced graphene oxide membranes for water purification," Advanced Materials, vol. 27, no. 2, pp. 249–254, Jan. 2015, doi: 10.1002/ADMA.201404054.

Chapter 3

Graphene Oxide Membranes for High Salinity, Produced Water Separation by Pervaporation

3.1 Abstract

Oil and gas industries produce a huge amount of wastewater known as produced water, which contains diverse contaminants including salts, dissolved organics, dispersed oils, and solids making separation and purification challenging. The chemical and thermal stability of graphene oxide (GO) membranes make them promising for use in membrane pervaporation, which may provide a more economical route to purifying this water for disposal or re-use compared to other membrane-based separation techniques. In this study, we investigate the performance and stability of GO membranes cast onto polyethersulfone (PES) supports in the separation of simulated produced water containing high salinity brackish water (30 g/L NaCl) contaminated with phenol, cresol, naphthenic acid, and an oil-in-water emulsion. The GO/PES membranes achieve water flux as high as 47.8 L m^{-2} h^{-1} for NaCl solutions for membranes operated at 60 °C, while being able to reject 99.9% of the salt and upwards of 56% of the soluble organic components. The flux for membranes tested in pure water, salt, and simulated produced water was found to decrease over 72 h of testing but only to 50–60% of the initial flux in the worst-case scenario. This drop was concurrent with an increase in contact angle and C/O ratio indicating that the GO may become partially reduced during the separation process. Additionally, the pervaporation impact on the membrane crosslinker (Zn^{2+}) was investigated. It was found that the membrane crosslinker hydrolyzes overtime to $Zn(OH)_2$ with much of it being washed away during the long-term pervaporation.

3.2 Introduction and Literature Review

The extraction of oil and gas creates a significant volume of oily wastewater which is generally known as produced water. The amount of produced water from a given reservoir ranges from less than 1% to more than 80% of the amount of oil extracted depending on the nature of the oil reservoir and its age [1,2]. Furthermore, reports indicate that global oil and gas industries produce about 210 million barrels of produced water from oil processing per day—an amount that is almost three times the quantity of oil produced worldwide [3,4]. Developing methods capable of efficiently purifying this water for release or reuse are of significant economic and environmental concern [5].

The constituents of produced water rely significantly on the reservoir's geographic location and geologic formation [6]. Generally, the components of produced water include dispersed oil, dissolved organic compounds, treatment chemicals, bacteria, produced solids, metals, and salts that are often similar to those found in seawater with sodium chloride being dominant. These contaminants pose a high burden to the environment and local ecosystems unless processed and treated before disposal. However, the varied composition makes treatment challenging and costly.

Different oil/water separation technologies have been employed in the petroleum industries such as floatation, heating, gravity settling, and centrifugal separators. Additionally, membrane separation has seen growing use over the past decades and is replacing some conventional techniques [7,8]. More common membrane separation technologies include microfiltration (MF), ultrafiltration (UF), nanofiltration (NF), and reverse osmosis (RO). Reverse osmosis is the most dominant technology among other membrane separation technologies in the petroleum industry [8]. However, it is one of the most power consuming separations. It also suffers from fouling problems [9], and swelling-induced failure caused by oil and organic contaminants which are often soluble in polymeric membranes

[10,11]. These challenges require that significant pre-treatment steps be implemented prior to the produced water entering the membrane unit.

Nowadays, graphene oxide (GO) is emerging as an exciting membrane material due to its high selectivity and high flux of water transport [12,13]. GO is fundamentally a mono-layer-thick hexagonal honeycomb lattice that bears a large amount of oxygenated functional groups on its basal plane surface and edges which lead to high hydrophilicity and good fouling resistance [14–18]. Furthermore, the flow of selective permeants across a GO membrane occurs through interlayer gaps between the sheets, inter-edge spaces, wrinkles, and surface pores that are created by these functional groups [19]. While fouling can still occur on the hydrophobic regions of the GO basal plane [19], it is often restricted to the surface of the membrane making GO membranes more fouling resistant than polymeric membranes [20].

While GO membranes do not swell significantly in organics or oily dispersions, they do have the tendency to swell in aqueous solutions [21]. This swelling increases the width of the interlayer spaces resulting in poor selectivity and possible delamination and destruction of the membrane [22]. Thus, while GO membranes hold promise in applications such as reverse osmosis (RO), this poor selectivity due to swelling has slowed commercialization and has inspired a significant research effort [23]. For example, to reduce the swelling, engineering the d-spacing between the GO sheets has been accomplished by physical confinement, enabling control over membrane selectivity [24]. In this approach, stacked GO strips were encapsulated using an epoxy to produce physical confined graphene oxide (PCGO). PCGO membranes were then tested for five days and no d-space change was observed. However, a small reduction in permeation was noted that could be attributed to a partial clogging of the nanochannels. While promising, this method is not capable of producing large area membranes [23]. Various other treatments [22,24,25] for improving the selectivity of GO have been investigated

59

such as the use of crosslinkers with varying chain length, multi-valent cations, etc., but all of these adversely impact the flux and performance of the membrane [25].

One way to bypass this swelling problem is to avoid contacting the GO membrane with water on both sides. One of the oldest membrane technologies used to separate liquids with different volatilities is pervaporation. In pervaporation, a liquid mixture is passed on one side of the membrane and the volatile components are driven through the membrane by a partial pressure difference generated by a vacuum or sweep-gas on the permeate side of the membrane [26,27]. Desalination by pervaporation has recently gained traction as an alternative to RO and membrane distillation processes [28,29] and could provide a promising route to purification of produced water. Liang et al. were the first to demonstrate that unmodified GO membranes supported on polyacrylonitrile (PAN) could be used to effectively desalinate water with >99.8% rejection of salt and high flux (65.1 L m^{-2} h^{-1}) when operated at 90 °C, which suggests that swelling of GO is not as challenging in this application due to the presence of a gas phase on one side of the membrane.

Building upon this work, in this study, we probe the performance of GO membranes for pervaporative separation of a model produced water formulated based on contaminants found in the wastewater resulting from the steam-assisted gravity drainage (SAGD) oil extraction process. This study proposes the purification of a produced water model using membranes prepared by vacuum filtered GO sheets on PES films, cross-linked via Zn^{2+} to increase its stability during pervaporation as shown in Figure 3-1. In addition, we report a long-term study of 72 h of pervaporation. Moreover, a closer look at the membrane's cross-linker was investigated before and after usage.

60
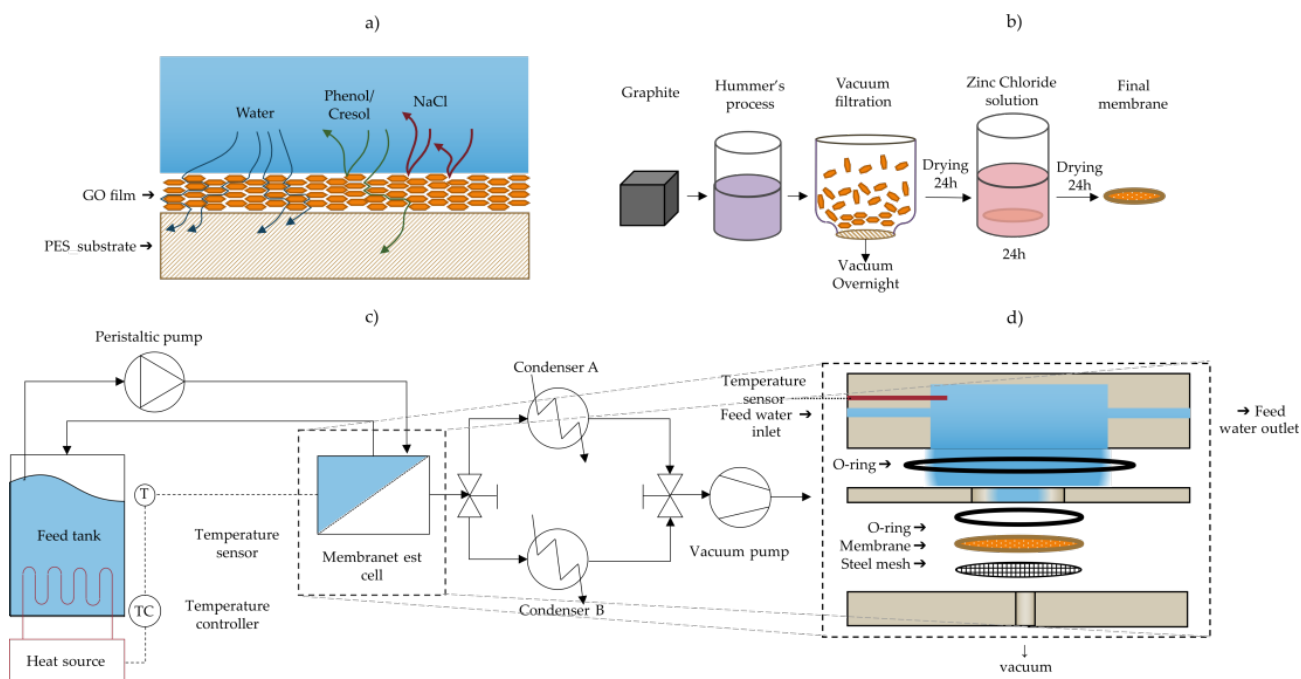
Figure 3-1: (a) Illustration of rejection of chemicals and purification of water via the use of GO membrane pervaporation; (b) method of production of GO membranes; (c) schematic diagram of the pervaporation separation apparatus; (d) schematic of the membrane test cell module showing the flow directions and permeate outlet.

3.3 Materials and Methods:

3.3.1 GO and Membrane Synthesis

GO was synthesized by a modified Hummer's method [30] as described by Marcano et al. [31]. Briefly, 1.5 g of graphite flakes (obtained from Alfa Aesar, Haverhill, MA, USA, -10 mesh, metal basis, 99.9%) were oxidized at 45 °C overnight via addition to a 9:1 mixture of H_2SO_4 (240 mL, Sigma Aldrich, St. Louis, MO, USA) and H_3PO_4 (20 mL, Sigma Aldrich) in which 9 g of $KMnO_4$ (Sigma Aldrich) was initially dissolved. Afterwards, the solution was transferred to approximately 200 mL of ice water and cooled down. Approximately 5 mL of 30% H_2O_2 (Sigma Aldrich) was slowly added while the solution

was stirred until a brilliant yellow dispersion was obtained. The resulting GO was then washed of residual acids, etc. by centrifugation (3300 rpm for 30 min, Fisher Scientific, Waltham, MA, USA— acuuSpin™ 3) and redispersion of the pellet twice with 10% HCl (Sigma Aldrich) and then three times with 95% ethanol (reagent alcohol grade, Sigma Aldrich). After the final ethanol centrifuge, the GO was redispersed in ethanol, and the resulting GO solution was kept in ethanol as a slurry, and its concentration was measured. The stock was stored prior to use. Fourier-transform infrared spectroscopy (FTIR- BRUKER) was carried out in order to ensure the successful synthesis of GO from 4000 to 400 cm^{-1} with a resolution of 4 cm^{-1} using a potassium bromide (KBr) disc. Additionally, atomic force microscopy (AFM) was carried out in contact mode (NP-STT10 tips, Nanoscope MultiMode AFM, Veeco) to investigate the exfoliation state of graphene oxide sheets. Dilute dispersions of GO were spun coat from n-butanol onto an ozone treated silicon wafer.

Membranes with three different thicknesses were made by vacuum filtration of varying volumes and concentrations of GO. Using a pipette, 62.7 µL, 89.6 µL, and 134.4 µL were taken from a 6 mg mL^{-1} GO in ethanol stock solution and dispersed in 50 mL of n-butanol (Sigma Aldrich) for each coating, the GO dispersion in n-butanol was tip sonicated at 50% amplitude (Biologics Inc., Manassas, VA, USA, Model: 150V/T). Afterwards, the entire dispersion was vacuum-filtered through a polyethersulfone (PES) filter (0.1 microns, Sterlitech Corporation, Kent, WA, USA) and was left covered (to prevent evaporation) over night. This led to membranes with areal mass loadings of 35 µg cm^{-2}, 50 µg cm^{-2}, and 75 µg cm^{-2}, respectively. The formed GO/PES membranes were dried in a dry air desiccator (Terra Universal, Series-100) at a relative humidity (RH) of 0.5% for at least 24 h.

The GO-coated PES membranes were then immersed in a solution of 100 mL of 0.1 M $ZnCl_2$ adjusted to a pH of approximately 5–6 for 24 h using a dilute HCl solution (<1%), in order to crosslink the GO sheets with the divalent Zn^{2+} and enhance the membrane stability in water [22]. Afterwards, the

membranes were kept in the dry air desiccator for at least 24 h before testing. The stability of the cross-linked GO was tested by submerging crosslinked and uncrosslinked GO/PES membranes in water under a high speed of mechanical stirring. Figure 3-1b summarizes the membrane preparation method.

3.3.2 Pervaporation and Membrane Performance

Pervaporation experiments were carried out for six types of solutions: 30,000 ppm (30 g L^{-1}) NaCl in DI water solution, single organic constituents (phenol, cresol mixture of isomers, or naphthenic acid) in water solution with a concentration as shown in Table 3-1 with no salt, a laboratory-made produced water model (PWM) solution, and its composition as shown in Table 3-1 [32], and a laboratory made solution of oil foulant mixed with a produced water model solution. Oil foulant solutions were synthesized by dissolving 50 ppm of sodium dodecyl sulfate (SDS, Sigma Aldrich) in DI water that contains 1500 ppm hexadecane (Sigma Aldrich), followed by mixing using a homogenizer (CAT, Model: X-120) for 2 h at 1500 rpm [33]. The resulting emulsion was a white milky dispersion and was stable for at least 24 h (long enough for membrane testing). Afterwards, the produced water model components shown in Table 3-1 were added to the prepared oil-in-water emulsion.

Table 3-1: Composition of produced water model solution, based on steam assisted gravity drainage (SAGD) process [32].

Component	Concentration (ppm)
Phenol	45
Cresol (mixture of isomers)	45
Naphthenic acid	10
Sodium chloride	30,000

Phenol and cresol have similar molecular structure. Phenol consists of phenyl ring bonded to hydroxyl group, while cresol consists of phenol with a methyl group added to it. Naphthenic acid composes of

cyclopentane with two ethyl groups and a carboxyl group. Table 3-2 shows the vapor pressure of the different components of the produced water, i.e., their volatility, compared to the water. Water has the highest volatility among the components and therefore, it is the most volatile one and separates easier when subjected to a vacuum pressure.

Table 3-2: Volatility of produced water model constituents.

Component	Vapor pressure (@ 405 K) (1 bar)
Phenol	0.207
Cresol (mixture of isomers)	0.104
Naphthenic acid	3.2 E-6 to 1.9 E-10
Sodium chloride	2.77

Pervaporation experiments were carried out using a customized test cell module made from stainless steel (grade 316). Figure 3-1 illustrates a process flow diagram of the pervaporation separation process used. A rendering of the test cell and flow channel are shown in Figure 3-1a and d. The feed solution held in a 500 mL flask was heated to either 30 °C or 60 °C using a hotplate. The temperature of the feed solution was controlled by a thermocouple submerged in the aqueous phase inside the test cell and connected to the hotplate, in order to maintain the temperature via the hotplates' feedback control system. This fluid was circulated to the test cell using a peristaltic pump at a rate of 75 mL min^{-1} (Fisher Scientific), and the retentate was recycled back to the stock feed solution. The effective membrane area exposed in the test cell is 5.07 cm^2. A vacuum pump (Edwards, Model: E2M-1.5) was used to generate a vacuum of approximately −0.1 MPa (gauge) and the resulting water vapor was collected in one of two glass condensers (Sigma Aldrich, inner cold surface area of 334 cm^2) cooled to approximately −35 °C with a dry ice/ethanol slurry. Switching between two such condensers with a 3-way valve allowed for continuous operation of the membrane setup and collecting water while measuring the

amount of water collected in the other condenser. The mass of the condenser was measured before and after collecting the condensate using a digital balance (OHAUS, Model: NV2101, repeatability = 0.1 g) to determine the permeation flux. The water permeation flux (J) through the membrane was calculated using Equation (1):

$$J = \frac{M}{A \cdot \Delta t}, \ (\text{L m}^{-2} \text{ h}^{-1}),$$ (1)

Where M is the amount of water collected, A is the effective membrane area, and Δt is the given time interval.

In short-term pervaporation experiments, three independent GO/PES membranes were tested. The feed was circulated through the system at 30 °C for 20 min in order for the test-cell to reach thermal equilibrium. Permeate was then collected for 2 h in approximately 20-min intervals. The temperature was then raised to 60 °C and left for 1 h to reach thermal equilibrium. Afterwards, permeate was collected for 2 h in approximately 20 min intervals. The average flux and rejection for each temperature or test solution was calculated and the error was approximated as ± the standard deviation.

In longer term studies, the various feed compositions were examined for 72 h of permeation using the 50 µg cm^{-2} GO/PES membrane. After the test cell reached thermal equilibrium (20 min), sample collection was carried out every 1 h.

The Nelson method was used to indicate outliers in permeate flux which were defined as data points more than three standard deviations away from the mean. Additionally, one-way ANOVA tests were performed to determine whether the differences in fluxes and rejections are statistically significant by figuring out its p-value.

Water samples collected in the condensers were analyzed for salt concentration and produced water model solutes, by measuring the conductivity and by using ultraviolet-visible spectroscopy (UV-Vis, Thermo Scientific Evolution 300), respectively, before and after separation runs. Permeate conductivity measurements were carried out using an OAKTON (PC700, Vernon Hills, IL, USA) conductivity meter. For UV/vis, a set of known solution concentrations were prepared to establish a concentration calibration curve with their respective intensities at wavelength of 269 nm for phenol and 271 cresol, in order to measure their respective concentrations in the collected samples. For naphthenic acid, PWM and produced water model with foulants solution, the absorption intensities of the feed, and collected samples were measured at 265 nm for naphthenic acid, and 270 nm for PWM and PWM with foulants' solutions. The resulting UV/vis curves were normalized in order to investigate any changes in the absorbed peaks and were compared to the starting feed intensity peaks. The solute rejection was calculated using Equation (2):

$$R = \left(1 - \frac{C_p}{C_f} \right) \times 100\%, (\%), \tag{2}$$

Where C_f and C_p are the initial feed and collected concentration, respectively.

The change in hydrophilicity of the membrane due to chemical changes or the adsorption of simulated produced water model foulants was carried out using the sessile drop method and a smart-phone camera carefully positioned normal to the substrate plane [34]. A drop of DI water was added vertically using a pipette to the surface of the membrane, and a photo was taken directly. The droplet was further analyzed using ImageJ software. The contact angle of three droplets placed on different areas of the same membrane were used to calculate the average contact angle and the standard deviation was used to approximate the error. All membranes tested for contact angle were left to dry for at least 24 h after the pervaporation test was done. Membranes of 50 μg cm^{-2} GO specific deposition were tested before

and after the long-term pervaporation experiment for all three of the tested solutions. Powder X-ray diffraction (XRD, Rigaku Miniflex II) was acquired using a range of 2θ between 5° to 65° using Cu kα radiation ($\lambda = 1.54059$ Å). A thermal emission scanning electron microscope (SEM) imaging was done by a TESCAN Vega instrument with voltage acceleration of 10 kV using a secondary electron detector. Samples were sputtered with gold for 139 s to render the surface of the membranes conductive for imaging. The thickness of the GO layer was estimated from a cross sectional image using several measurements by ImageJ software.

Elemental composition was carried out by XPS for unused (control) and used membranes for long periods of pervaporation (72 h). The XPS analysis was carried out using (Thermal Scientific KAlpha XPS spectrometer) operated in ultra-high vacuum (2×10^{-10} mbar) with acquisition time of 0.2 s. Survey spectra and high-resolution scans for C 1s, O 1s, and Zn 2p spectra were obtained. The distribution of the C and O groups at the membrane surface were identified by deconvolution of the spectra peaks using CASAxps software, and all the peaks were shifted based on the C-C peak (284.5 eV) and using a Shirley background removal.

3.4 Results and Discussion

3.4.1 GO Membrane Characterization

Figure 3-22a shows AFM images of the exfoliated GO sheets. The results show that most of the GO flakes are atomically flat, unwrinkled, and comprised of single layers with thickness of approximately 1 nm. A histogram of the lateral sheet size distribution is shown in Figure 3-2b illustrating that the majority are ~0.5 µm in size with a tail in the distribution showing some sheets as large as 1–10 µm. Figure 3-2c shows the FTIR spectrum of the synthesized graphene oxide. Several characteristic peaks for GO are observed including a broad peak between 3600 cm^{-1}–2400 cm^{-1}, which is attributed to

stretching vibrations of O–H groups, a sharp peak at 1740 cm^{-1} attributed to the C=O stretching vibration, a sharp peak at 1623 cm^{-1} due to unoxidized sp^3 C-C bond, a peak at 1415 cm^{-1} due to C–OH deformation, and 1227 cm^{-1} due to C–O–C vibrations [31,35]. An SEM image of the top surface and cross section of a GO/PES membrane is shown in Figure 3-2d. The GO layer thickness is estimated to be 466 ± 52 nm. This is thicker than what would be expected based on the loading and assumed full density of GO (~1.8 g cm^{-3}) which for 50 µg cm^{-2} would lead to a fully dense thickness of 278 nm. It is known that vacuum filtration yields somewhat disordered films compared to a technique like pressure assisted vacuum filtration. A more ordered film is likely to form early in the vacuum filtration process when the flow is high while evaporation of the solvent at the slower stage of filtration may cause the upper portion to become more disordered. For example, Tsou et al. [36] demonstrated a factor of 384 nm/231 nm = 1.66 difference between vacuum filtered GO films and nearly fully dense films prepared by pressure-assisted vacuum filtration, which is nearly the same ratio we observe above (1.67).
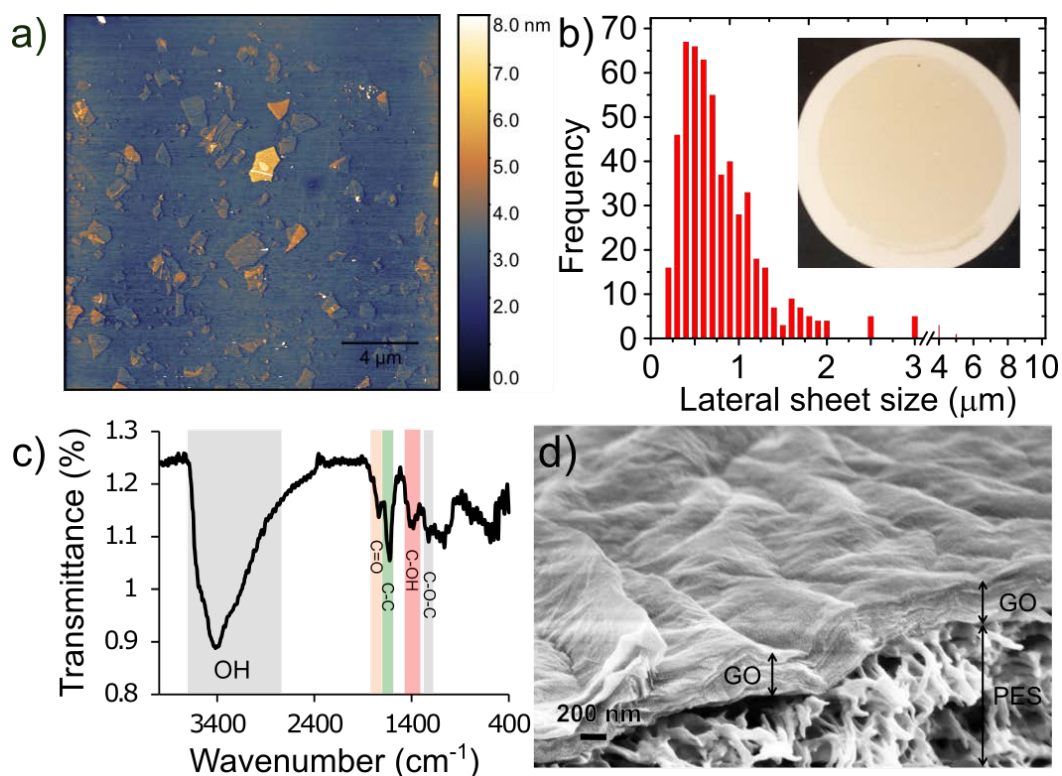
Figure 3-2. (a) AFM images of graphene oxide flakes spun coat onto Si wafer, (b) histogram of lateral sheet size distribution. The inset shows a photo of a 50 μg cm^{-2} GO/PES membrane prepared by vacuum filtration. (c) FTIR spectrum for GO sheets; and (d) cross-sectional SEM image showing surface topology and thickness of a 50 μg cm^{-2} GO membrane and the underlying PES support.

To improve the stability of the various GO membranes, the GO was cross-linked with Zn^{2+} by soaking the membranes in a solution of $ZnCl_2$. Figure 3-3 compares the stability of vacuum-filtered GO/PES membranes before and after cross-linking and after exposure to high-speed mechanical stirring of water. Without cross-linking, the GO began to flake off the substrate while the cross-linked GO remained intact. The good mechanical strength of cross-linked GO sheets was first reported by Yeh et al. [22], where they discovered that Al^{3+} originating from AAO filter discs was the cause of the mechanical property enhancement of vacuum cast films using this popular but non-scalable membrane support. In addition, the GO functional groups like hydroxyl and carboxyl groups can be used with different

69

metallic cross-linking agents to create a coordination bond, and thus it can be used to increase the membrane's stability and tune the d-spacing between GO sheets [25]. These metallic cross-linking agents include divalent cations like: Ni^{2+}, Mg^{2+}, and Ca^{2+}, or trivalent cations like: La^{3+}, Fe^{3+}, and Al^{3+} [25,37]. Moreover, Yu et al. [31] listed the ions' stability capabilities as follows: $Al^{3+} > Ca^{2+} > Mg^{2+} > Na^+$. This has since become a common method to enhance GO membranes for nanofiltration applications but has not been studied using pervaporation. Membranes that were not enhanced by Zn^{2+} crosslinking were found to be unstable and caused frequent leaks in our pervaporation cell. As shown in Figure 3-4, the rejection for all 30 g/L NaCl samples was higher than 99.31%.

Figure 3-3: Membrane stability enhancement by Zn^{2+} crosslinking: (a) vacuum filtered GO membrane immersed in water for 30 min; (b,c) squares of membrane exposed to high speed mechanical stirring with no zinc treatment: squares in (b) have no Zn^{2+} treatment while the membrane in (c) was soaked in the Zn^{2+} solution for 24 h.

3.4.2 Short-Term Membrane Performance

Figure 3-4a shows the average water permeation flux and salt rejection through the GO membrane for tests carried out at both 30 °C and 60 °C using membranes of different GO loadings (i.e., thickness). The flux for pure water through the 50 µg cm^{-2} membrane at 30 °C was 31.6 ± 1.3 L m^{-2} h^{-1}, which was slightly higher than the solution containing 30 g L^{-1} NaCl (26.5 ± 2.7 L m^{-2} h^{-1}). Our GO membranes outperform those reported by Liang et al. [38], who measured a flux at 30 °C only as high

as 14.3 L m^{-2} h^{-1} for 35 g L^{-1} NaCl with an even thinner membrane (1.8 µg cm^{-2}). This improvement might be attributed to differences in the GO synthesis method used or the fact that we use a Zn^{2+} cross-linker, which could increase the d-spacing. They also reported a decrease in flux with increasing salt concentration in the range of 2000–100,000 ppm but did not test under pure water. The drop in flux is likely due to a decrease in the concentration and activity of free water vs. water bound to the salt ions as a hydration shell. The flux was found to increase with temperature in all cases with a more significant increase for the NaCl cases vs. pure water. This also confirms the results of Liang et al. who illustrated a positive activation energy for water transport and the Arrhenius-like temperature dependence of permeance for their GO membranes. The flux was also found to be almost linearly dependent on decreasing membrane thickness. While thinner membranes could be fabricated, we found that the 35 µg cm^{-2} had a low failure rate compared to thinner ones. As shown in Figure 3-4b), the permeate flux and rejection remained relatively constant over the 2 h pervaporation run.
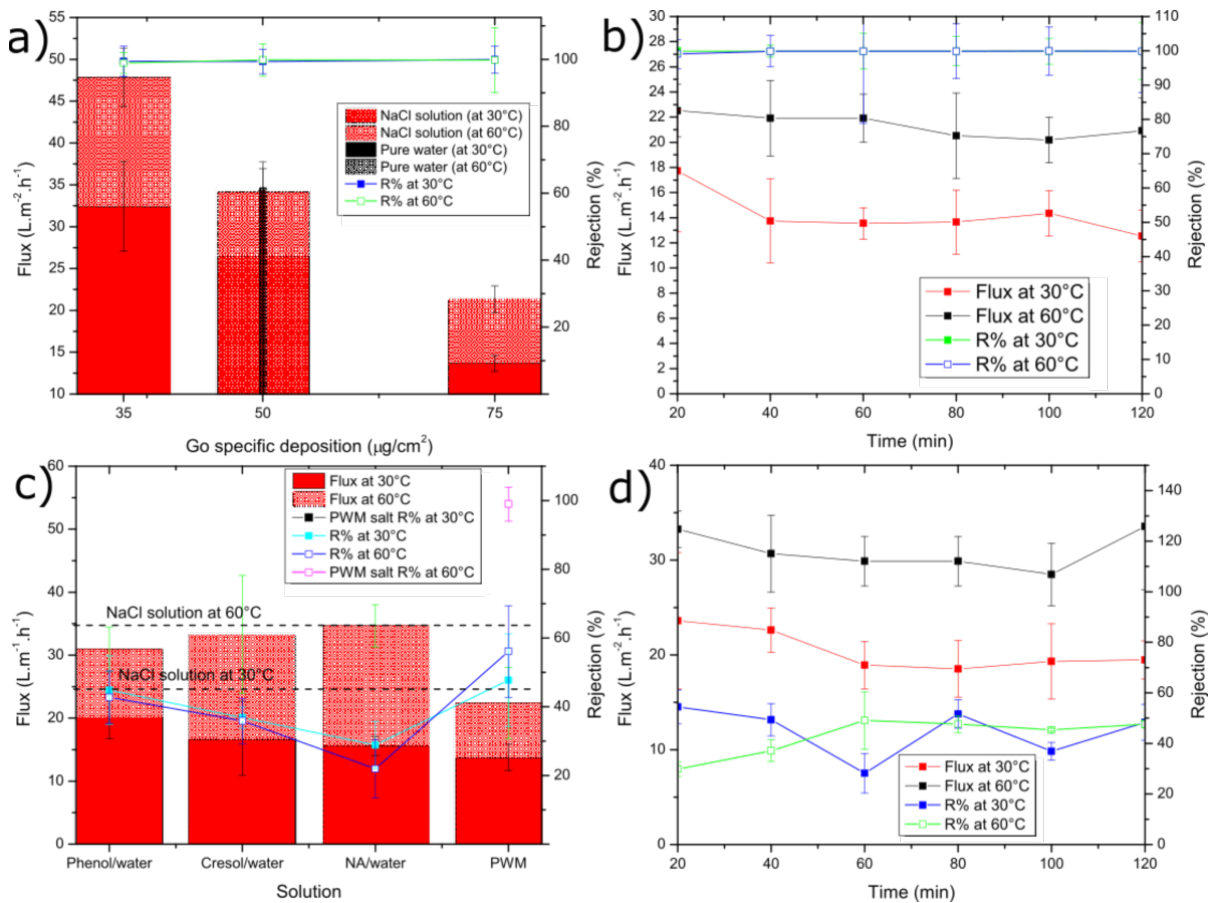
Figure 3-4. Average water flux and solute rejection for: (a) NaCl solution and pure water at different GO loading; (b) NaCl solution tested by 75 μg cm⁻² GO loading; (c) single organic and PWM solutions; (d) single organic (phenol solution). For (c,d), a 50 μg cm⁻² GO loading was used. The error bars were estimated as ± one standard deviation of three independent measurements.

Next, we introduce several of the model contaminants used in our PWM to study their impact on flux and the GO membrane's ability to reject these contaminants. As shown in Figure 3-4c), at both 30 °C and 60 °C, the flux through the membrane drops slightly compared to the NaCl only case. However, it is not found to change significantly (as determined by ANOVA with $p > 0.05$) as a function of either the single or mixed organic contaminants. The decreased flux can also be explained by the additional solutes added, which would act to decrease the activity on the feed side as discussed previously.

72

However, since the single organic solutions contain no salt and these mixtures have less dissolved solute, it is more likely that the contaminants may adsorb to the GO within the membrane and inhibit water transport. Figure 3-4c also shows that the rejection of each contaminant is similar within error (as determined by ANOVA with $p > 0.05$) and is ~40% irrespective of temperature. The reason for this could be the similar molecular structure. Phenol and cresol have a similar aromatic structure, except cresol has an extra methyl ($-CH_3$) group, and NA has a longer chain of repeated aromatic groups, but it was used at lower concentration. An example of a single organic component (phenol) flux vs. rejection is given as shown in Figure 3-4d. Both values were fairly constant over the 2 h run.

As also shown in Figure 3-4c, the water permeation flux of combined PWM through the GO membrane shows no significant difference in flux when compared to the single organic components at 30 °C as ANOVA testing reveals a value of $p > 0.05$. The flux is 13.8 ± 2.1 L m^{-2} h^{-1}, with a rejection of 47.7% $\pm 13.5\%$. However, there was a significant difference with the higher temperature tests at 60 °C, which exhibited slightly lower flux of 22.4 ± 5.7 L m^{-2} h^{-1} and rejection of 56.1% $\pm 13.3\%$ as ANOVA testing shows a $p < 0.05$. As shown in Figure 3-5, when all PWM contaminants were added together, the permeate collected had a nearly identical UV/vis plot but scaled down in intensity. Normalizing the plot reproduced the original mixture which suggests that all components were collected in the same proportion as in the feed but at a reduced concentration. Thus, the rejection in this case could be easily calculated from the overall UV/vis results without having to deconvolute contributions from the individual components. Thus, all contaminants whether present together or individually are rejected to a similar extent (~40–55%) by the GO membrane. These results demonstrate that, while being able to effectively desalinate the produced water, the membrane may also be used to purify produced water from residual soluble organic components with moderate selectivity.

73
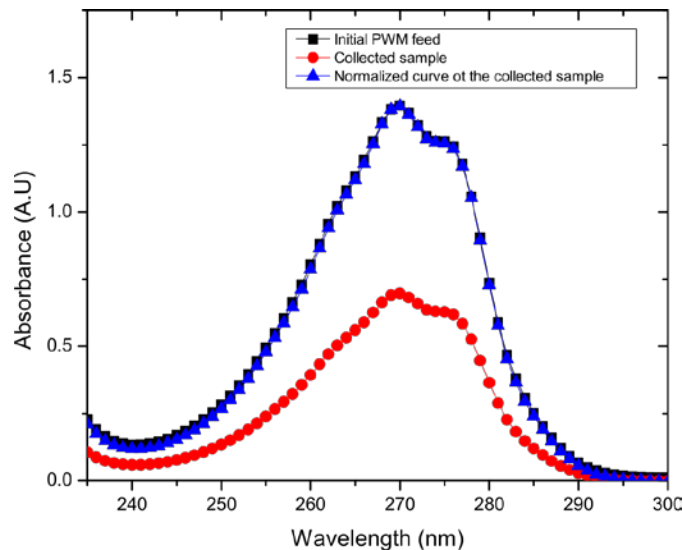
Figure 3-5: Example UV/vis spectra for one of the collected samples, and its normalized curve matching the initial PWM curve.

Moreover, the water permeation flux for PWM is generally lower than that of NaCl solution and single organic component solution and presented results with a higher standard deviation throughout the experiment. For example, the relative error for the NaCl only case is 10% and 8% for 30 °C and 60 °C, respectively, while, for the PWM, was 15% and 25% for 30 °C and 60 °C. The reason behind that is the continuous adsorption and desorption of the PWM solutes on the membrane surface which may act to block some of the nano-scale channels within the GO membrane's pores.

3.4.3 Long-Term Pervaporation Study

The GO membranes were also tested to investigate their performance over longer periods of time using the NaCl solution, PWM, and PWM with foulants along with the control solution of water as shown in Figure 3-6.

The water flux followed the same general trend as shown in Figure 3-4b. To better highlight the changes as a function of time, the flux normalized to the initial flux is plotted as in Figure 3-6a. In all cases,

74

there is a drop in flux over the 72 h period with the PWM and PWM with foulants exhibiting a larger drop of 50–60% of the initial while the pure water and NaCl solutions retain 70–80% of their initial flux. This is likely due to both the continuous build-up of foulants within the GO selective layer and concentration polarization near the membrane surface, which is more severe in the PWM cases. However, it could be due in part to the partial deoxygenation of the GO in water as will be discussed later. The rejection for solutions of the PWM and PWM with foulants slightly increased with time. This could be attributed to pore plugging by the foulants caused by the direct adsorption of contaminants onto the membrane surface.
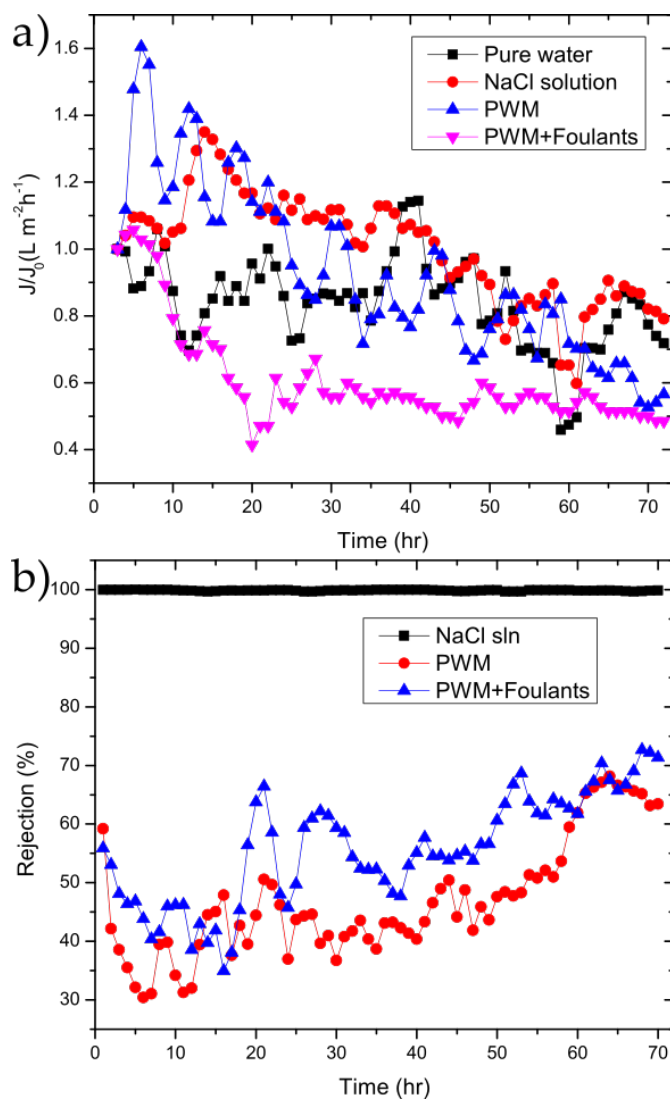
Figure 3-6: (a) flux/flux$_0$ (J/J$_0$); (b) and rejection vs. time for 50 μg cm^{-2} GO membrane for the tested solutions.

The membranes used in the longer-term PV tests were removed from the test cell and further characterized to determine any chemical and structural changes resulting in the decreased flux observed. To further understand the changes in flux over the 72 h pervaporation, we carried out XPS and measured the contact angle of water on the used membranes. Survey spectra and high-resolution C 1s, O 1s, and Zn 2p spectra were obtained. Figure 3-7 demonstrates the XPS scan spectrums obtained

along with the peaks' deconvolution analysis and the C/O ratio analysis. The binding energies for the carbon, oxygen, and zinc were identified, and their atomic percentages were calculated.

The deconvolution of C 1s revealed four individual peaks of C-C, C-O, C=O, and O-C=O and their relative percentages are shown in Table 3-2. This reveals a higher content of C-C bonding and lower C-O content for all of the used membranes compared to the unused control.

Table 3-3: Relative contribution (%) of the deconvoluted C 1s peaks for unused and used membranes corresponding to different bonding environments.

Peaks	Control	Pure Water	NaCl Solution	PWM	PWM + Foulants
C-C	38.67	49.2	39.08	53.73	72.94
C-O	42.72	38.66	30.08	13.8	17.58
C=O	14.1	7.54	22.27	9.6	5.31
O-C=O	4.51	4.6	8.57	22.87	4.17

The corresponding change in C/O ratio is illustrated in Figure 3-7b. The membrane that was used for pure water pervaporation has the highest C/O ratio after the 72 h run. Since there is no organic materials present in the feed, the increase must be due to the deoxygenation of GO upon exposure to water. It is well known that the chemical structure of GO can evolve upon exposure to water, which has been described by the Tour group's dynamic structural model (DSM) [39]. In this model, the structure of GO is not static and will continuously change when it reacts with water, introducing new oxygen containing functional groups and leaving the GO structure by different mechanisms. New protons (H_3O^+) are created from the acidic groups on GO, making the GO more negatively charged, and

stabilized by the resonance of the oxygen containing groups and by the formed electric double layer near the surface.

In the case of NaCl solution pervaporation, Na^+ ions will be loosely associated near the GO surface by coulombic forces and will compete with H_3O^+ ions. However, Dimiev et al. [39] found that the presence of NaCl will change the orientation of the water molecules to be away from the GO surface, and therefore less deoxygenation happens to the GO, which is also observed in Figure 3-7b by a less severe change in C/O ratio as with pure water. In the case of PWM and PWM with foulants, these solutions have the same concentration of NaCl, and, therefore, their higher C/O ratio when compared to NaCl solution is likely due to the deposition of the organic materials on the surface which increased the C-C content and blocked the pores from the water, causing further deoxygenation. Furthermore, the PWM shows a relatively higher content of O-C=O as shown in Table 3-2. This may be attributed to naphthenic acid that remains adsorbed to the GO. These findings are all in agreement with the contact angle measurements as shown in Figure 3-8.
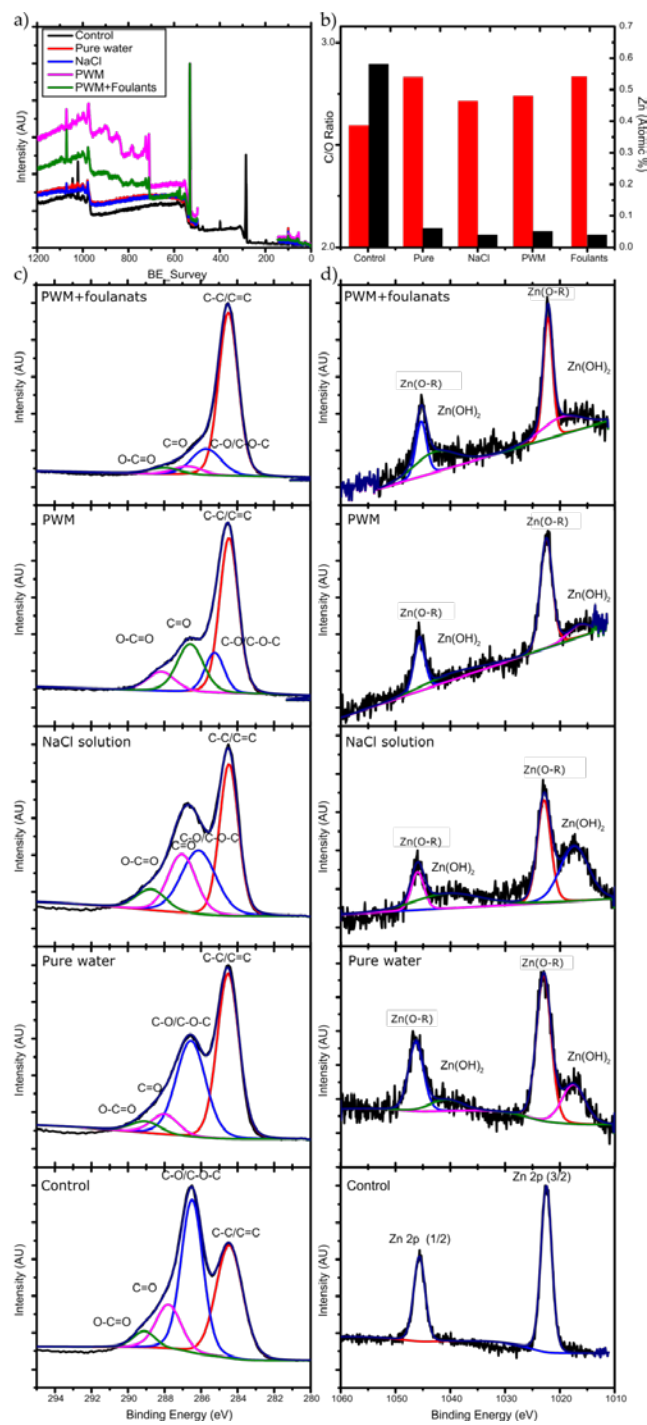
Figure 3-7: (a) XPS survey data; (b) C/O ratio (red bars) and Zn atomic % (black bars), high resolution XPS for (c) C 1s and (d) Zn 2p for the unused and used membranes for different solutions.
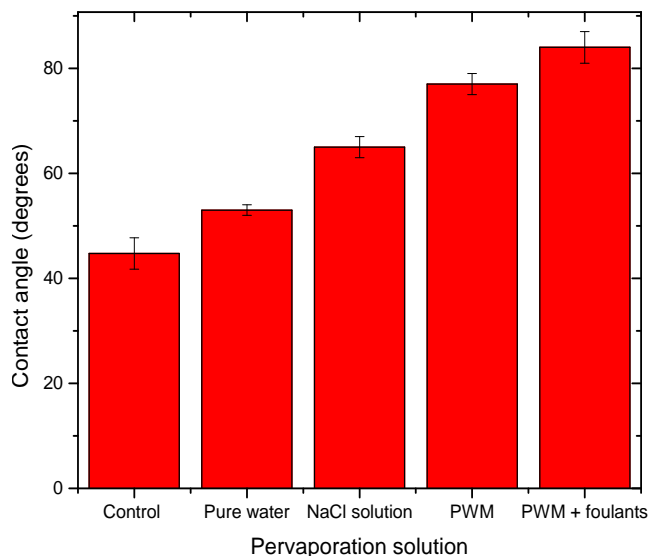
Figure 3-8: Average contact angle for unused and used GO/PES membranes tested for different solutions. The error bars were estimated as ± one standard deviation of three independent measurements.

Moreover, Figure 3-7b shows the deconvolution of the Zn 2p spectra. There are two strong peaks around 1021.3 and 1044.5 eV that are attributed to the binding energies of Zn $2p_{3/2}$ and Zn $2p_{1/2}$ of the Zn(O–R) interaction caused by the crosslinking between adjacent GO. After 72 h of pervaporation, these initial peaks each split into two broad peaks. The lower binding energy deconvoluted peaks represent the Zn^{2+} of the hydroxide (lower intensity), and the higher binding energy of the deconvoluted peaks represents the Zn(O–R) interaction (higher intensity) [40]. The Zn(OH)$_2$ was formed due to the hydrolysis of the Zn/GO organometallic complex during the pervaporation as illustrated in Equation (3) (reproduced from [41]).

$$\tag{3}$$
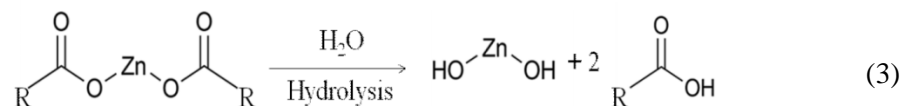
The amount of Zn present before and after membrane testing is shown in Table 3-3. A reduction of the Zn-crosslinker is observed after 72 h of pervaporation. XPS Zn 2p spectra suggests that more degradation happened to the Zn(O-R) cross-linker for the membranes used for pure water and NaCl solution due to a higher peak intensity of $Zn(OH)_2$ compared to Zn(O-R) peak intensity. This is likely due to the higher flux of these membranes which hydrolyzes more of the Zn to $Zn(OH)_2$, which may also act to reduce the membrane stability over longer time exposure to water.

In addition, different elements were observed from the survey spectra at the surface of the membrane; these elements include Na, Cl, and S. Table 3-3 shows the atomic percentage (%) on each tested membrane. In the pure water tested membrane, no Na or Cl elements were observed, since there were likely to be washed away from the surface after a long period of pervaporation. The high S content in the PWM with foulants membrane is likely coming from the SDS that was added to the solution as a foulant.

Table 3-4: Atomic% of Na, Cl, S, and Zn elements observed on the membrane surface.

Element	Control	Pure Water	NaCl Solution	PWM	PWM + Foulants
S	0.43	0.25	0.22	0	3.23
Na	1.69	0	1.01	2.3	1.79
Cl	0	0	0.44	0.86	1.22
Zn	0.56	0.06	0.04	0.05	0.05

TGA attempted to investigate the nature of foulants on the membrane, but the loading of the GO on the PES is too thin and its mass nor the mass of other adsorbed organics and foulants could be detected. The GO forms only around 0.7% of the overall weight of the membrane.

While produced water separation has not been studied by pervaporation with pure GO-based selective layers, it has been studied with several mixed-matrix membranes. In a work done by Alammar et al. [42], a high permeation flux (91.3 L m^{-2} h^{-1} bar^{-1}) and rejection (99.96%) were achieved using a thick GO/rGO and PBI matrix membrane for their simulated produced water model. Moreover, randomly arranged GO sheets in the GO membrane by vacuum filtration and cross-linked by polyethyleneimine (PEI) was used to for oil water separation by gravity filtration [43]. In their work, they achieved as high a permeation flux as 688 L m^{-2} h^{-1} of a simulated oil-in-water emulsion of water in hexane (99:1). Additionally, graphene/polyvinylidene fluoride (G/PVDF) used for produced water–air gap membrane distillation (AGMD) [44], and it showed a high permeation flux of (20.5 L m^2 h^{-1}) and salt rejection (99.99%) for optimal graphene loading of 0.5 wt%. Furthermore, the long-term study of 10 days showed that incorporating graphene in the PVDF membrane will enhance the robustness of the membrane and wetting resistance when compared to commercial PVDF. We can compare our results and stability to some recently published literature on desalination and produced water separation using other technologies. Recently, Liu et al. [45] used MXene-based membranes for pervaporation desalination and demonstrated fluxes as high as 120 L m^{-2}h^{-1} at 65 °C for their thinnest membranes. While this is slightly higher than what we report for the salt solution case, their long-term testing, also carried out at 30 °C, resulted in a permeance of < 3.5 L m^{-2} h^{-1}. Our membranes, even with the additional PWM contaminants, achieved a very similar level of performance. In even more recent work, impressive permeance and selectivity have been achieved with cross-linked polymer systems such as

cross-linked polyvinyl alcohol/PAN [46]. However, these polymer systems have not been tested with produced water and may foul quite rapidly.

3.5 Conclusions

In this study, graphene oxide (GO) membranes were prepared by vacuum filtration on polyethersulfone (PES) and cross-linked using divalent zinc cations to enhance their stability. The prepared membranes were tested for desalination and produced water separation using a simulated SAGD process model. Short- and long-term studies were carried out on three different GO loading membranes to investigate the permeation flux and solute rejection. The initial fluxes were significantly higher than those reported previous for GO membrane-based desalination, but the flux gradually reduced as increasing solutes and foulants were added to the water. While the rejection for salt was found to be ~99% in all cases, the rejection of soluble organic components (phenol, cresol, napthanic acid) was in the range of 40–50%. The flux and rejection slightly reduced over 72 h of membrane operation. The flux for the pure water, salt, and simulated process water gradually decreased to a steady state of 70%, 80%, and 50%, respectively. In addition, this study highlighted the degradation of the Zn^{2+} crosslinker used to hold the GO sheets together. After 72 h of pervaporation, the examined membranes showed a lower amount obtained for Zn^{2+} and a hydrolysis transformation to $Zn(OH)_2$. This is an important aspect to focus on in determining the membrane's stability over a longer period of usage. While this flux is in the same range as what has been reported for the best performing MXene membranes used for pervaporation-base desalination, future work will focus on stabilizing the high initial flux we observe in our GO membranes while reducing the thickness without compromising mechanical stability. We hope that these results shed light on the promise of using pervaporation and graphene oxide membranes as a tool for more economical produced water separations.

3.6 References

[1]   J. Lee, H.-R. Chae, Y. J. Won, K. Lee, C.-H. Lee, H. H. Lee, *et al.*, "Graphene oxide nanoplatelets composite membrane with hydrophilic and antifouling properties for wastewater treatment," *Journal of Membrane Science,* vol. 448, pp. 223-230, 2013.

[2]   E. Zangaeva, "Produced water challenges: influence of production chemicals on flocculation," University of Stavanger, Norway, 2010.

[3]   N. L. Le and S. P. Nunes, "Materials and membrane technologies for water and energy sustainability," *Sustainable Materials and Technologies,* vol. 7, pp. 1-28, 2016.

[4]   C. E. Clark and J. A. Veil, "Produced water volumes and management practices in the United States," Argonne National Lab.(ANL), Argonne, IL (United States)2009.

[5]   A. Fakhru'l-Razi, A. Pendashteh, L. C. Abdullah, D. R. A. Biak, S. S. Madaeni, and Z. Z. Abidin, "Review of technologies for oil and gas produced water treatment," *Journal of hazardous materials,* vol. 170, pp. 530-551, 2009.

[6]   J. Neff, K. Lee, and E. M. DeBlois, "Produced water: overview of composition, fates, and effects," *Produced water,* pp. 3-54, 2011.

[7]   M. A. B. Pauzan, M. Abd Rahman, and M. H. D. Othman, "Hydrocarbon Separation and Removal Using Membranes," in *Membrane Technology Enhancement for Environmental Protection and Sustainable Industrial Growth*, ed: Springer, 2021, pp. 73-90.

[8]   S. Alzahrani and A. W. Mohammad, "Challenges and trends in membrane technology implementation for produced water treatment: A review," *Journal of Water Process Engineering,* vol. 4, pp. 107-133, 2014.

[9]   X. Wei, S. Zhang, Y. Han, and F. A. Wolfe, "Treatment of petrochemical wastewater and produced water from oil and gas," *Water Environment Research,* vol. 91, pp. 1025-1033, 2019.

[10]   K. Rezzadori, F. M. Penha, M. C. Proner, G. Zin, J. C. C. Petrus, P. Prádanos*, et al.*, "Evaluation of reverse osmosis and nanofiltration membranes performance in the permeation of organic solvents," *Journal of Membrane Science,* vol. 492, pp. 478-489, 2015.

[11]   J. Chau, P. Basak, and K. K. Sirkar, "Reverse osmosis separation of particular organic solvent mixtures by a perfluorodioxole copolymer membrane," *Journal of Membrane Science,* vol. 563, pp. 541-551, 2018.

[12]   R. Joshi, P. Carbone, F.-C. Wang, V. G. Kravets, Y. Su, I. V. Grigorieva*, et al.*, "Precise and ultrafast molecular sieving through graphene oxide membranes," *science,* vol. 343, pp. 752-754, 2014.

[13]   J. Abraham, K. S. Vasu, C. D. Williams, K. Gopinadhan, Y. Su, C. T. Cherian*, et al.*, "Tunable sieving of ions using graphene oxide membranes," *Nature nanotechnology,* vol. 12, p. 546, 2017.

[14]   J. Wang, X. Gao, H. Yu, Q. Wang, Z. Ma, Z. Li*, et al.*, "Accessing of graphene oxide (GO) nanofiltration membranes for microbial and fouling resistance," *Separation and Purification Technology,* vol. 215, pp. 91-101, 2019.

[15]   D. An, L. Yang, T.-J. Wang, and B. Liu, "Separation performance of graphene oxide membrane in aqueous solution," *Industrial & Engineering Chemistry Research,* vol. 55, pp. 4803-4810, 2016.

[16]   M. Paulauskas, "Pervaporation using graphene oxide membranes," University of Leeds, 2015.

[17]   E. N. Wang and R. Karnik, "Graphene cleans up water," *Nature nanotechnology,* vol. 7, pp. 552-554, 2012.

[18]   T. Szabó, O. Berkesi, P. Forgó, K. Josepovits, Y. Sanakis, D. Petridis*, et al.*, "Evolution of surface functional groups in a series of progressively oxidized graphite oxides," *Chemistry of materials,* vol. 18, pp. 2740-2749, 2006.

[19]   M. Hu, S. Zheng, and B. Mi, "Organic fouling of graphene oxide membranes and its implications for membrane fouling control in engineered osmosis," *Environmental science & technology,* vol. 50, pp. 685-693, 2016.

[20]   S. Tiwari, A. Gogoi, and K. A. Reddy, "Effect of an ionic environment on membrane fouling: a molecular dynamics study," *Physical Chemistry Chemical Physics,* vol. 23, pp. 5001-5011, 2021.

[21]   S. Zheng, Q. Tu, J. J. Urban, S. Li, and B. Mi, "Swelling of graphene oxide membranes in aqueous solution: characterization of interlayer spacing and insight into water transport mechanisms," *ACS nano,* vol. 11, pp. 6440-6450, 2017.

[22]   C.-N. Yeh, K. Raidongia, J. Shao, Q.-H. Yang, and J. Huang, "On the origin of the stability of graphene oxide membranes in water," *Nature chemistry,* vol. 7, pp. 166-170, 2015.

[23]   S. Castelletto and A. Boretti, "Advantages, limitations, and future suggestions in studying graphene-based desalination membranes," *RSC Advances,* vol. 11, pp. 7981-8002, 2021.

[24]   S. Remanan, N. Padmavathy, S. Ghosh, S. Mondal, S. Bose, and N. C. Das, "Porous graphene-based membranes: preparation and properties of a unique two-dimensional nanomaterial membrane for water purification," *Separation & Purification Reviews,* pp. 1-21, 2020.

[25]   Z. Wang, F. He, J. Guo, S. Peng, X. Q. Cheng, Y. Zhang, *et al.*, "The stability of a graphene oxide (GO) nanofiltration (NF) membrane in an aqueous environment: progress and challenges," *Materials Advances,* vol. 1, pp. 554-568, 2020.

[26]   G. Jyoti, A. Keshav, and J. Anandkumar, "Review on pervaporation: theory, membrane performance, and application to intensification of esterification reaction," *Journal of Engineering,* vol. 2015, 2015.

[27]   X. Feng and R. Y. Huang, "Liquid separation by membrane pervaporation: a review," *Industrial & Engineering Chemistry Research,* vol. 36, pp. 1048-1066, 1997.

[28]   Q. Wang, N. Li, B. Bolto, M. Hoang, and Z. Xie, "Desalination by pervaporation: A review," *Desalination,* vol. 387, pp. 46-60, 2016.

[29]   W. Kaminski, J. Marszalek, and E. Tomczak, "Water desalination by pervaporation– Comparison of energy consumption," *Desalination,* vol. 433, pp. 89-93, 2018.

[30]   W. S. Hummers Jr and R. E. Offeman, "Preparation of graphitic oxide," *Journal of the american chemical society,* vol. 80, pp. 1339-1339, 1958.

[31]   D. C. Marcano, D. V. Kosynkin, J. M. Berlin, A. Sinitskii, Z. Sun, A. Slesarev, *et al.*, "Improved synthesis of graphene oxide," *ACS nano,* vol. 4, pp. 4806-4814, 2010.

[32]   D. Singh and K. K. Sirkar, "Desalination of brine and produced water by direct contact membrane distillation at high temperatures and pressures," *Journal of Membrane Science,* vol. 389, pp. 380-388, 2012.

[33]   Y. Huang, H. Li, L. Wang, Y. Qiao, C. Tang, C. Jung, *et al.*, "Ultrafiltration membranes with structure-optimized graphene-oxide coatings for antifouling oil/water separation," *Advanced materials interfaces,* vol. 2, p. 1400433, 2015.

[34]   H. Chen, J. L. Muros-Cobos, and A. Amirfazli, "Contact angle measurement with a smartphone," *Review of Scientific Instruments,* vol. 89, p. 035117, 2018.

[35]   S. Chaiyakun, N. Witit-Anun, N. Nuntawong, P. Chindaudom, S. Oaew, C. Kedkeaw*, et al.*, "Preparation and characterization of graphene oxide nanosheets," *Procedia Engineering,* vol. 32, pp. 759-764, 2012.

[36]   C.-H. Tsou, Q.-F. An, S.-C. Lo, M. De Guzman, W.-S. Hung, C.-C. Hu*, et al.*, "Effect of microstructure of graphene oxide fabricated through different self-assembly techniques on 1-butanol dehydration," *Journal of Membrane Science,* vol. 477, pp. 93-100, 2015.

[37]   L. Nie, K. Goh, Y. Wang, J. Lee, Y. Huang, H. E. Karahan*, et al.*, "Realizing small-flake graphene oxide membranes for ultrafast size-dependent organic solvent nanofiltration," *Science Advances,* vol. 6, p. eaaz9184, 2020.

[38]   B. Liang, W. Zhan, G. Qi, S. Lin, Q. Nan, Y. Liu*, et al.*, "High performance graphene oxide/polyacrylonitrile composite pervaporation membranes for desalination applications," *Journal of Materials Chemistry A,* vol. 3, pp. 5140-5147, 2015.

[39]   A. M. Dimiev, L. B. Alemany, and J. M. Tour, "Graphene oxide. Origin of acidity, its instability in water, and a new dynamic structural model," *ACS nano,* vol. 7, pp. 576-588, 2013.

[40]   M. Wang, L. Jiang, E. J. Kim, and S. H. Hahn, "Electronic structure and optical properties of Zn (OH) 2: LDA+ U calculations and intense yellow luminescence," *RSC advances,* vol. 5, pp. 87496-87503, 2015.

[41]   G. Iannaccone, A. Bernardi, R. Suriano, C. L. Bianchi, M. Levi, S. Turri*, et al.*, "The role of sol–gel chemistry in the low-temperature formation of ZnO buffer layers for polymer solar cells with improved performance," *RSC advances,* vol. 6, pp. 46915-46924, 2016.

[42] A. Alammar, S.-H. Park, C. J. Williams, B. Derby, and G. Szekely, "Oil-in-water separation with graphene-based nanocomposite membranes for produced water treatment," *Journal of Membrane Science,* vol. 603, p. 118007, 2020.

[43] T. Huang, L. Zhang, H. Chen, and C. Gao, "Sol–gel fabrication of a non-laminated graphene oxide membrane for oil/water separation," *Journal of Materials Chemistry A,* vol. 3, pp. 19517-19524, 2015.

[44] Y. C. Woo, Y. Kim, W.-G. Shim, L. D. Tijing, M. Yao, L. D. Nghiem*, et al.*, "Graphene/PVDF flat-sheet membrane for the treatment of RO brine from coal seam gas produced water by air gap membrane distillation," *Journal of Membrane Science,* vol. 513, pp. 74-84, 2016.

[45] G. Liu, J. Shen, Q. Liu, G. Liu, J. Xiong, J. Yang*, et al.*, "Ultrathin two-dimensional MXene membrane for pervaporation desalination," *Journal of membrane science,* vol. 548, pp. 548-558, 2018.

[46] Y. L. Xue, J. Huang, C. H. Lau, B. Cao, and P. Li, "Tailoring the molecular structure of crosslinked polymers for pervaporation desalination," *Nature communications,* vol. 11, pp. 1-9, 2020.

Chapter 4

Highly Stable, Metal Cation-Crosslinked Partially Reduced Graphene Oxide Membrane for High Salinity and Produced Water Treatment by Pervaporative Separation

4.1 Abstract

Produced water is the wastewater that is brought to the surface during the extraction of oil and gas in the petroleum fields. Petroleum industries generate extremely large volumes of produced water that is estimated to be up to 98% of the total amount extracted. Produced water consists of different organics, oily waste, salts, and suspended solids that form a burden on the environment and needs to be treated in economical and safe way. Recently, graphene-based (GO) membranes have drawn a lot of research attraction and they form a potential for produced water treatment, owning to its great properties of mechanical and chemical stability, flexibility and tunability, and hydrophilicity and antifouling activity. However, since GO membranes are not stable in water, it remains challenging to utilize in the industry. Consequently, in this study we propose a more stable GO membranes in aqueous phase, with high permeation and salt and organic solute rejection for a simulated produced water treatment by pervaporation. GO membranes were fabricated on polyethersulfone (PES) support by vacuum filtration, and further treated by vacuum reduction and metal cation crosslinking. Two different orders of fabrication were followed, either crosslinking the rGO, or reduced M^+–GO. Divalent (Zn^{2+}) and trivalent (Fe^{3+}) crosslinkers were used and the membranes were characterized and tested for their performances. Zn^{2+}–rGO and Fe^{3+}–rGO membranes had the highest permeation flux of 8.3 ±1.5 L m^{-2} h^{-1} and 7.0 ± 0.4 L m^{-2} h^{-1}, for saline water separation, respectively; and 7.5 ± 0.7 L m^{-2} h^{-1},

and 5.5 ± 0.3 L m^{-2} h^{-1} for produced water separation, respectively. All the membranes had a salt rejection higher than 99%. Fe^{3+} crosslinked membranes presented the highest organic solute rejections for produced water of 69%. Additionally, long term pervaporation testing was done for the Zn^{2+}–rGO membrane for 12 hours. The membrane showed a permeation flux drop of 6%, while Zn^{2+}–GO had a drop of 24%. Moreover, an abrasion test was conducted for the membranes to examine its mechanical integrity. Fe^{3+}–rGO membranes illustrated the highest mechanical abrasion resistance of 95% of non-reduced and non-crosslinked GO.

4.2 Introduction and Literature Review

Petroleum industries generate large volumes of wastewater that is associated as a byproduct with the crude oil and gas during the extraction and production in the fields that is known as the produced water. The amount of produced water generated is continuously increasing as the global demand on petroleum is successively growing. The quantity and quality of produced water depends primarily on the nature of the petroleum reservoir, in which the crude is extracted.

In fact, produced water is highest single volume of waste stream produced in the petroleum fields and it exhibits around 80% of the total waste generated in some fields [1], and that could reach to around 98% in nearly depleted oil reservoirs [2]. In addition, in a recent report in 2019 by Produced Water Society, produced water amount was projected to be around 300 million barrels per day [3], accounting for three times the volume of oil produced [4], however, reports reveal that these amounts are projected to escalate to 12 times the volume of oil produced by 2025 as a consequence of aging of current oil reservoirs [2].

Produced water typically consists of a mixture of variable constituents of organic and inorganic chemicals dissolved in water that contains salts, minerals and heavy metals, suspended solids, as well as bacteria [2], [5]–[7]. Accordingly, the growing oil and gas production activities have raised an environmental concern for produced water and its immensely added negative impact on the ecosystem degradation worldwide [8], [9]. Consequently, an effective and feasible method to treat produced water is crucial for its management. Produced water can be managed by reuse as potable water, irrigation, utilized in the rest of the processes in the processing plants, discharge to environment, and back reinjection to the well formation [10]–[12].

Various techniques have been developed for produce water treatment in the petroleum industries that include chemical (oxidation, activated sludge and aerated biological filters) and physical (adsorption, floatation, sand filtration) methods [13]. In the few past years, membrane separation technique was an emerging technology that offered an effective way for produced water separation. Membrane separation is relatively cheaper and more efficient technique than the conventional separation methods [14]. It primarily consists of a filter media between two phases with a specific pore rating that have the capability of passing the water through and selectively excluding the contaminants [15], [16]. Produced water membrane treatment techniques include ultrafiltration (UF), microfiltration (MF), nanofiltration (NF), and reverse osmosis (RO). UF and MF are the least efficient methods in salt removal are their effluents require further processing with NF or RO in order to meet the standard requirements [17], [18]. NF and RO on the other hand are more effective in saline water desalination and metal and organic removal. Reverse osmosis is the widely used technique in petroleum industry for water purification, however, RO consumes very high energy to overcome the osmotic pressure. In addition, RO membranes suffer from suspended particles build up and fouling deposition that result in pores clogging, which eventually cause a permeation flux reduction [19].

The pervaporation, on the other hand, is an alternate technology of RO that seems to be promising and started to gain much attention lately. Pervaporation consumes less energy, and reject organic solutes at a higher rate than RO. Moreover, less turn down periods needed for pervaporation membrane module for cleaning and maintenance purposes due to fouling and clogging [20]–[22].

The pervaporation separates liquid mixtures based on the difference of the component's volatility. The liquid mixture is fed to the membrane module, and the more volatile phase (higher partial pressure) is driven across the membrane to the permeate side, by the large capillary partial pressure difference generated from the nanochannels of the membrane using a vacuum pump or a sweep gas on the permeate side. The permeated phase is further captured in a low temperature condenser [23]–[26].

Furthermore, the selection of material for membrane separation technology has been broadly investigated. Membrane materials have an inherited properties that limit its usage by the trade-off between fouling resistivity, permeation flux, solute selectivity, power consumption, and life span [27], [28].

Recently, graphene oxide (GO) and its derivatives are considered as a prominent potential as a membrane material for water treatment by membrane separation technology and extensive number of research studies investigating its performance were conducted [29]–[31]. GO is a two-dimensional hexagonal structure nanosheet consisting of single flat layer of carbon atoms that is rich in oxygen-containing functional groups such as epoxy, carboxyl, and hydroxyl groups. These oxygen-containing functional groups are located asymmetrically at the edges and on the basal surface which provide it with high mass transportation rate, molecular sieving, and antifouling aspects [30]–[34].

Nevertheless, these large number of oxygen groups make the GO negatively charged upon hydration in aqueous phases, and therefore, GO nanosheets start to repel each other because of the electrostatic repulsion forces are increasing the interlayer d-spacing, and thus, GO will start swelling until they

overcome the attractive forces (hydrogen bonding and Van der Waals), in which the GO sheets will eventually disintegrate [35]–[37]. Consequently, the stability of GO membranes in water-based environments forms a critical point of concern in membrane water treatment application. Several attempts to enhance the GO membranes' stability had been conducted, such as crosslinking, physical restriction, and partial GO reduction.

In GO nanosheets crosslinking, different crosslinkers can be employed to hold the GO neighboring nanosheets together and inhibit the increase in d-spacing due to hydration, such as a polymer [38], organic molecules [39], low molecular weight molecules [40], and ions [41] by covalent and non-covalent interactions. Moreover, this modification method can also be used to precisely control the GO interlayer d-spacing to meet the solute rejection specifications via adding a spacer of specific molecular size [42]–[44]. Unlike polymeric and organic crosslinkers, metal cation crosslinkers show a higher precise control of the lamellar distance in GO, and therefore, a higher permeation and selectivity rate are achieved, as well as an increased stability in aqueous solutions [41].

Furthermore, in GO nanosheets reduction, the oxygen groups are partially reduced via chemical reaction or thermal treatment. However, there is a trade-off between the permeation flux, rejection, and stability of rGO membranes [45], [46].

Reducing GO results in introducing more of the pristine graphitic sp^2 regions, where there is less amount of oxygen functional groups in the basal plane, and therefore the water permeation through it has lower flow resistance that is created by the hindrance from the hydrogen bond interaction between water and oxygen. In fact, water permeation in lower oxidation degree GO membrane is ten times higher than that of high oxidation degree [47]–[49]. However, reducing GO can also result in decreasing the interlamellar d-spacing between the nanosheets, and thus decreasing the transportation channel volume size for the water to pass through significantly [46], [48]. Additionally, reducing GO will also

improve the membrane's stability by substantially improving the π–π interactions between the rGO sheets [50].

This paper presents a study conducted aiming for developing a more stable, highly permeable, and selective GO membrane for produced water treatment using the pervaporation technology by combining different strategies. The study proses a partial reduction and metal cation crosslinking of GO membranes after vacuum filtering the GO on a polyethersulfone (PES) paper. The GO membranes were fabricated by either metal cation crosslinking the rGO membranes (method I) or reducing the crosslinked GO membranes (method II). Metal cations of Zn^{2+} and Fe^{3+} were incorporated into the laminar structure of rGO as divalent and trivalent crosslinkers, respectively, to crosslink the nanosheets together. The prepared M^+–rGO were further tested by the pervaporation technique for produced water resulted from the steam-assisted gravity drainage (SAGD) in the petroleum industry. Additionally, an abrasion test was performed to assess the mechanical stability of the membrane.

4.3 Experimental Methods

4.3.1 GO Synthesis and Membrane Preparation:

A modified Hummer's method [51], [52] was used to synthesis GO. Graphite flakes of 1.5 g (Alfa Aesar, Haverhill, MA, USA, -10 mesh, metal basis, 99.9%) were measured and oxidized in a mixture of 9 g of $KMnO_4$ (Sigma Aldrich, St. Louis, MO, USA) dissolved in concentrated 240 mL of H_2SO_4 (Sigma Aldrich, St. Louis, MO, USA) and 20 mL of H_3PO_4 (Sigma Aldrich) and the reaction was kept at 45 °C for overnight. Subsequently, the solution was cooled down in around 200 mL of ice water in which about 5 mL of H_2O_2 (30%, Sigma Aldrich, St. Louis, MO, USA) was carefully added to the mix under continuous stirring until the solution turned into brilliant yellow color. Afterwards, washing the obtained GO dispersion of residual acids, etc. was done with two cycles using HCl (10%, Sigma

Aldrich) and three cycles using ethanol (95%, reagent alcohol grade, Sigma Aldrich, St. Louis, MO, USA) by centrifugation at 3500 rpm for 30 minutes (acuuSpin^{TM}3, Fisher Scientific, Waltham, MA, USA), and redispersing the pellet. Lastly, redispersion for the GO solution was done in ethanol and the resulted slurry stock was sealed and kept for future uses after measuring its concentration, and analyzing its functional groups to confirm that the GO was synthesized successfully using Fourier transform-infrared spectroscopy (FTIR, Thermo Nicolet, Madison, WI, USA). FTIR scanning was applied from 4000 to 400 cm^{-1} using a potassium bromide (KBr) disc.

GO membranes were fabricated by vacuum filtration technique. A volume of 89.6 μL was pipetted from 6 mg mL^{-1} GO in ethanol stock solution and dispersed in 50 mL of n-butanol (Sigma Aldrich, St. Louis, MO, USA). Afterwards, the solution was sonicated in an ice bath at 50% amplitude for 10 minutes using tip sonicator (Sonics, Vibra cell^{TM}, Tip model: CV334, CT, USA). Subsequently, the solution was vacuum filtered through a filter substrate of polyethersulfone (PES) (pore size of 0.1 microns, diameter of 47mm, Sterlitech Corporation, Kent, WA, USA) and was kept covered overnight. All fabricated membranes were dried for at least 24 h in a dry air desiccator at 0.5% relative humidity (Series-100, Terra Universal).

4.3.2 Preparation of Zn-rGO and Fe-rGO:

The prepared membranes were further treated by either of the two different treatment methods as shown in Figure 4-1. The first path is by partially reducing the membrane for different time periods, and then followed by crosslinking. The second path is by crosslinking the membrane in different crosslinking solutions concentrations, and then partially reduced.
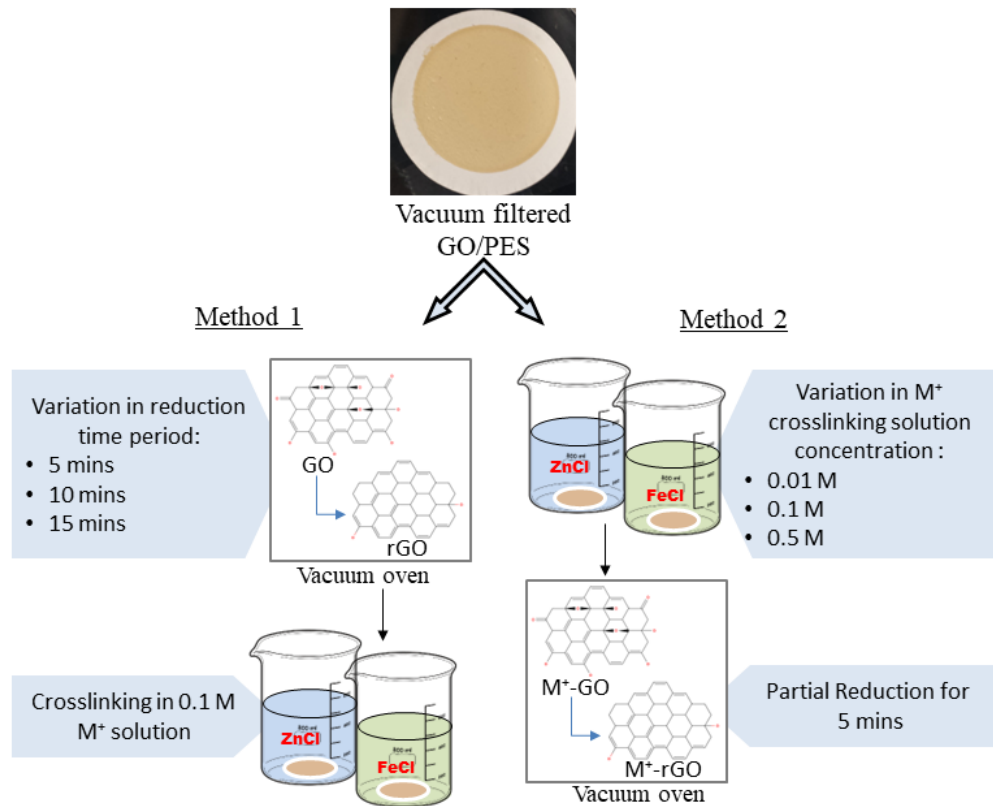
Figure 4-1: Methods of treatments for vacuum filtered membranes

In the first method, the prepared GO/PES membranes were reduced in a vacuum oven (Isotemp, Thermo Fisher Scientific, Marietta, OH, USA) at 200 °C for 5, 10, or 15 minutes. The rGO membranes were then left to cool down to room temperature in a dry air desiccator before immersing in the crosslinking solutions for 24 h. Two types of solutions of 100 mL of 0.1 M were prepared by dissolving $ZnCl_2$ (Sigma Aldrich, St. Louis, MO, USA) and $FeCl_3$ (Sigma Aldrich, St. Louis, MO, USA) in DI-water, and adjusting their pH to approximately 5-6 using dilute HCl solution (<1%, Sigma Aldrich, St. Louis, MO, USA). Afterwards, the membranes were left to dry in the dry air desiccators for a minimum of 24 hours prior to any characterization or pervaporation testing.

In the second method, the prepared GO/PES membranes were crosslinked in solutions of 0.01 M, 0.1 M, and 0.5 M of Zn^{2+} and Fe^{3+} ions as prepared above, followed by drying. Afterwards, the crosslinked membranes were reduced under vacuum in the vacuum oven at 200 °C for 5 minutes, and then kept in the dry air desiccator before characterization or pervaporation testing.

4.3.3 Membrane Characterization:

The prepared membranes were characterized using different techniques. the degree of reduction and metal cation crosslinker loading on the membrane were measured using an energy dispersive X-ray spectroscopy (EDS, Oxford Instruments, model: INCA X-act) fitted on a thermal emission scanning electron microscope (SEM, TESCAN Vega). Membrane samples were gold sputter-coated for 139 s before the analysis so as to increase their electric conductivity. Moreover, cross-sectional imaging was carried out for the GO/PES membrane using 10 kV acceleration voltage and using a secondary electron detector. The thickness of the membrane was further estimated using ImageJ software.

The change in the interlayer d-spacing between GO sheets was detected via powder X-ray diffraction (XRD, Rigaku Miniflex II), by measuring 2θ over a range between 5° to 65° using radiation of Cu kα (λ= 1.54059 Å). Samples were kept sealed away from humidity until they were tested. The intensities of the measured peaks were corrected to the internal PES reference peak. Further, the change in membranes' hydrophilicity was evaluated by a laboratory made sessile drop technique and a smart phone camera [53]. ImageJ software was used to measure the contact angle of a DI-water droplet pipetted on the surface of the membrane. The analysis was repeated three times using different locations on the membrane.

4.3.4 Membrane Performance Testing by Pervaporation:

Membranes separation performance was evaluated in a laboratory designed pervaporation filtration model as outlined in Figure 4-2. Two types of solutions were used for testing: saline water, and a laboratory made produced water model based on produced water originating from the steam assisted gravity drainage (SAGD) process [54]. The saline water solution was prepared by dissolving 30,000 ppm (30 g L^{-1}) of NaCl in DI water. The produced water model was prepared by adding 45 ppm of phenol, 45 ppm of cresol, and 10 ppm of naphthenic acid (mixture of isomers) to the saline water solution. The solutions were fed to the laboratory made customized pervaporation test cell module via a peristaltic pump (Fisher Scientific), at a rate of 75 mL min^{-1}, and the temperature inside the test cell was maintained at 30 °C by a thermocouple measuring the instant solution temperature and connected to the hotplate's feedback controller. The pervaporation experiment was run for 2 h and samples were collected every 20 min from the condensers (Sigma Aldrich, inner condensation surface area of 334 cm^2) that are cooled to about -35 °C using a slurry of dry ice in ethanol. Each membrane sample was examined for three runs using a new sample on each run.
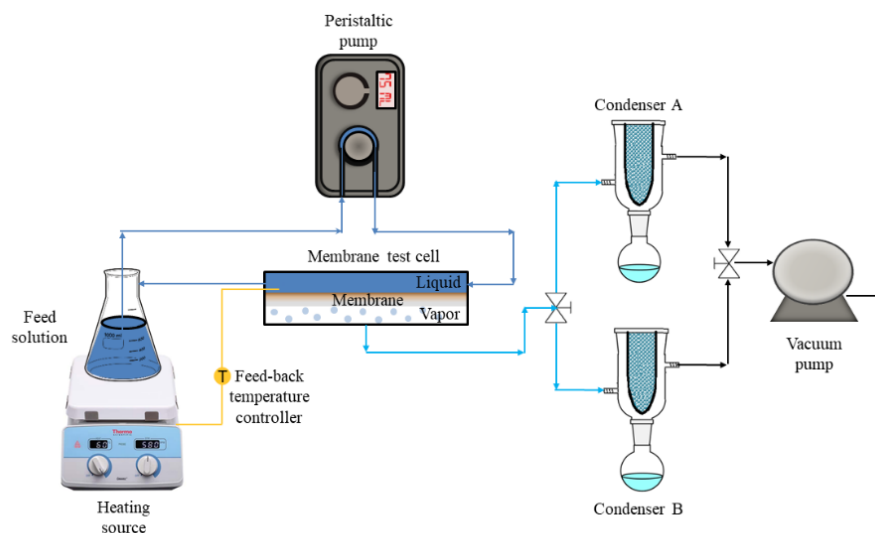
Figure 4-2: Membrane pervaporation separation apparatus outline.

99

Long term pervaporation tests were carried out for Zn-rGO membrane prepared by the second method of crosslinking GO/PES in 0.1 M of Zn^{2+} solution. The membrane was tested for pervaporation using PWM mixed with oil foulants solution. The solution was prepared by mixing 50 ppm of sodium dodecyl sulfate (SDS, Sigma Aldrich, St. Louis, MO, USA) and 1500 ppm hexadecane (Sigma Aldrich, St. Louis, MO, USA) in 500 ml DI water using a homogenizer (CAT, Model: X-120, Staufen, Germany) at 1,500 rpm for 2 h [55]. Subsequently, the PWM solutes were added to the resulting white milky emulsion, and the pervaporation was run at 30 ℃ for 12 h and samples were collected every 60 min.

The water permeation flux was figured by measuring the mass of the condensers before and after each cycle by a digital balance (OHAUS, Model: NV2101, repeatability = 0.1 g). calculations for the The permeation flux (J) through the membrane was figured out using equation (1):

$$J = \frac{M}{A \cdot \Delta t} \, , (\mathrm{L} \, m^{-2} \, \mathrm{h}^{-1}) \tag{1}$$

where M is the mass of the collected water, A is the effective membrane area and Δt is the collection time period. In order to identify the permeation flux outliers for collected samples, Nelson's rule was used which points out the samples that are greater than three standard deviations from the average flux.

Further analysis for the collected permeated water samples was done to determine their salt content and produced water model components concentration by measuring the conductivity (OAKTON PC700, Vernon Hills, IL, USA), and using the ultraviolet visible analysis (UV-Vis, Thermo Scientific Evolution 300). The solute rejection was calculated using equation (2):

$$R = \left(1 - \frac{C_p}{C_f}\right) \times 100\% \, , (\%) \tag{2}$$

where C_p and C_f are the collected permeate and the initial feed solute concentrations, respectively.

4.3.5 Mechanical Abrasion Testing:

Membrane stability and mechanical integrity was tested using an abrasion resistance assessment. The setup consists of an abrasive rotary wheel that is connected to a PC and controlled by Allpath software. In this method, the membranes were dipped in water for around 1 sec and placed flat at the sample holder, and the wheel (Material: canton flannel buffs, diameter= 15 cm, McMaster-Carr, USA) was rotated at a speed of 1 rpm for 10 seconds. The total area of the GO layer on the substrate was determined before and after the abrasion by analyzing photographs for abraded vs. non-abraded areas using ImageJ software.

4.4 Results and Discussion

4.4.1 Membrane Characterization:

FTIR spectrum of the synthesized GO nanosheets used in fabricating the membranes is shown in Figure 4-3a. Detected characteristic peaks shows the GO was successfully synthesized with ample oxygen containing functional groups presented for crosslinking the nanosheets together. FTIR spectrum Characteristic peaks include a broad peak at 3600 cm^{-1} – 2500 cm^{-1} due to the O–H groups stretching vibration, a sharp peak at 1735 cm^{-1} attained due to the stretching vibration of C=O groups, a sharp peak at 1623 cm^{-1} corresponds to unoxidized sp^3 C–C bonding, a peak at 1380 cm^{-1} attributed due to the bending deformation of C–OH groups, and a peak at 1226 cm^{-1} due to the vibration of C–O–C groups

[52], [56]. The obtained membranes by vacuum filtration are defect free and uniform as shown in Figure 4-3b.
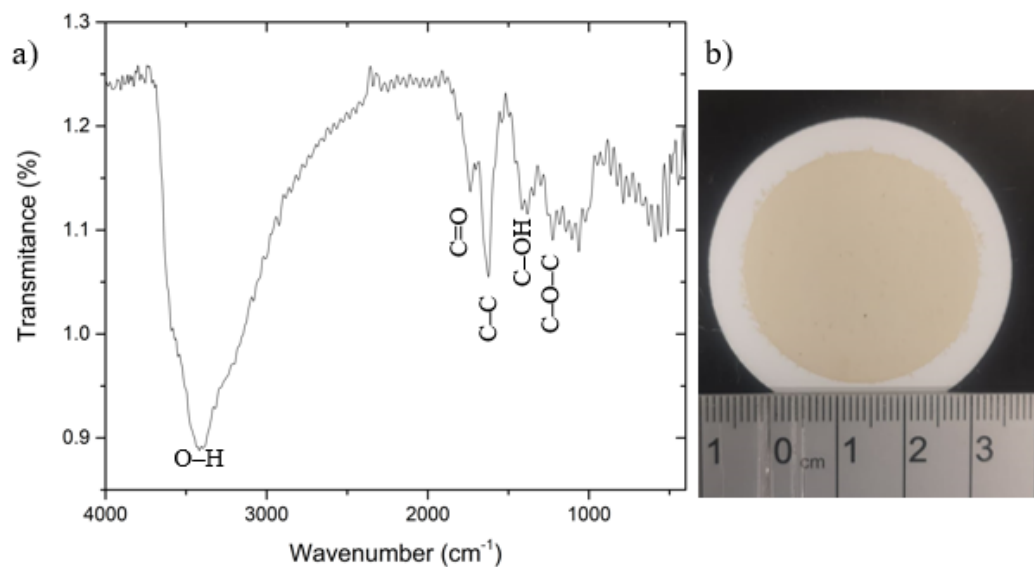
Figure 4-3: a) FTIR spectrum of the synthesized GO sheets, b) a photo of GO/PES vacuum filtered membrane.

In order to verify the reduction and the crosslinking of the prepared GO membranes and measure their degrees, EDS was carried out for membrane samples before and after reduction and crosslinking treatments. Figure 4-4 shows the C/O ratio and the metal cation crosslinker content in the membrane.
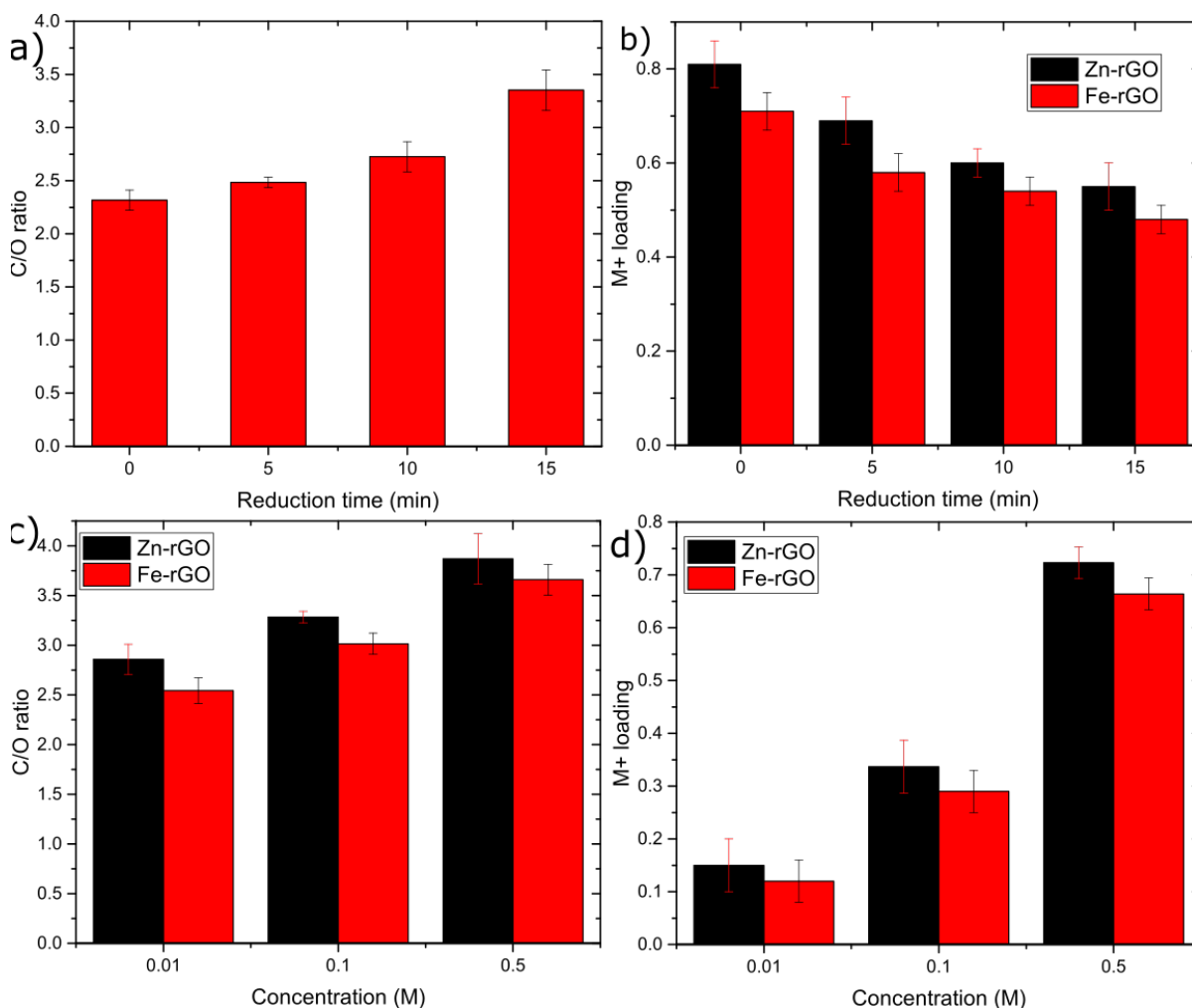
Figure 4-4: C/O ratio and their metal cation crosslinkers loading percentage for GO membranes prepared via a, b) first method (reduced then crosslinked), respectively, c, d) second method (crosslinked then reduced), respectively, measured by EDAX. The error bars represent one standard deviation of three independent measurements.

For the membranes that are prepared by the first method, which is a partial GO reduction followed by metal cation crosslinking, the results show an increase in their C/O ratio (2.48 ± 0.05 to 3.35 ± 0.19) compared to the control one of 2.32 ± 0.10 (0 min reduction and 0.1 M^+), and as the reduction time increases, the higher the reduction degree is attained as shown in Figure 4-4a. Moreover, the metal

cation crosslinker loading in these membranes decreases as the reduction time increases, due to the lower amount of the O-groups present for crosslinking as shown in Figure 4-4b. Zn^{2+} metal cations make 4 and 6 coordination bonds with the O-groups in GO while the coordination number for Fe^{3+} is 6 [57], [58]; and therefore, it is expected that Zn^{2+} cations loading in GO membranes is higher due to the lower number of O-groups needed for Zn^{2+}–O bonding.

Membranes prepared by the second method of crosslinking the GO sheets by Zn^{2+} and Fe^{3+} at different concentrations followed by a partial GO reduction, show a C/O ratio ranging between 2.86 ± 0.09 to 3.87 ± 0.27, and 2.54 ± 0.09 to 3.66 ± 0.09, respectively. M^{+}–rGO membranes prepared by the second method have higher C/O ratio than those prepared by the first method, as shown in Figure 4-4c (by comparing the membranes of 5 mins reduction followed by 0.1 M M^{+}, with 0.1 M M^{+} followed by 5 mins reduction). Since the presence of metal cations in GO improve the order of the laminar structure, in which they increase the thermal conductivity of GO membranes, achieving faster reduction rate than non-crosslinked membranes [59]. Consequently, this also explains the higher reduction rate of membranes crosslinked in higher metal cation concentration solutions.

Additionally, the membranes immersed in higher crosslinker concentration solutions achieved higher M^{+} loadings as illustrated in Figure 4-4d. In addition, membranes crosslinked with Zn^{2+} achieved higher loading in the membranes compared to Fe^{3+} due to the lower number of O-groups needed for bonding as mentioned above.

Contact angle measurements were performed for the treated membranes as well as a control membrane of GO/PES (non-crosslinked and non-reduced), as shown in Figure 4-5a. The degree of hydrophilicity decreases as the C/O ratio increases due to the high amount of carbon present that lowered the degree of water droplet adsorption. Additionally, membranes that are crosslinked with Fe^{3+} cations are more

hydrophilic than those crosslinked with Zn^{2+} cations despite their higher loading, since Fe^{3+} cations are more electronegative and can attract water at a higher rate [60], [61].

The interlayer d-spacing of the lamellar stacked GO sheets in the membrane decreases after crosslinking and reduction treatments, as shown by the XRD analyses in Figure 4-5b. The partial loss of oxygen containing groups in GO that causes the repulsion between the sheets, and the presence of M^+–π interaction after crosslinking overcomes the low remaining repulsive forces by oxygen containing groups in the GO, leading to narrower interlayer spaces between the GO sheets [48], [62]. By comparing the two controls of M^+–rGO membranes (membranes prepared by 5 mins reduction followed by 0.1 M M^+, and 0.1 M M^+ followed by 5 min reduction); it can be shown that Zn-rGO membranes show lower d-spacing than Fe-rGO, due to the higher loading of Zn^{2+} cations, as illustrated by the EDS results, and hence more attraction forces exist resulting in smaller interlayer d-spacings, despite the smaller size of Fe^{3+} ion (radius= 0.60 Å) compared to Zn^{2+} ion size (radius= 0.74 Å) [63].
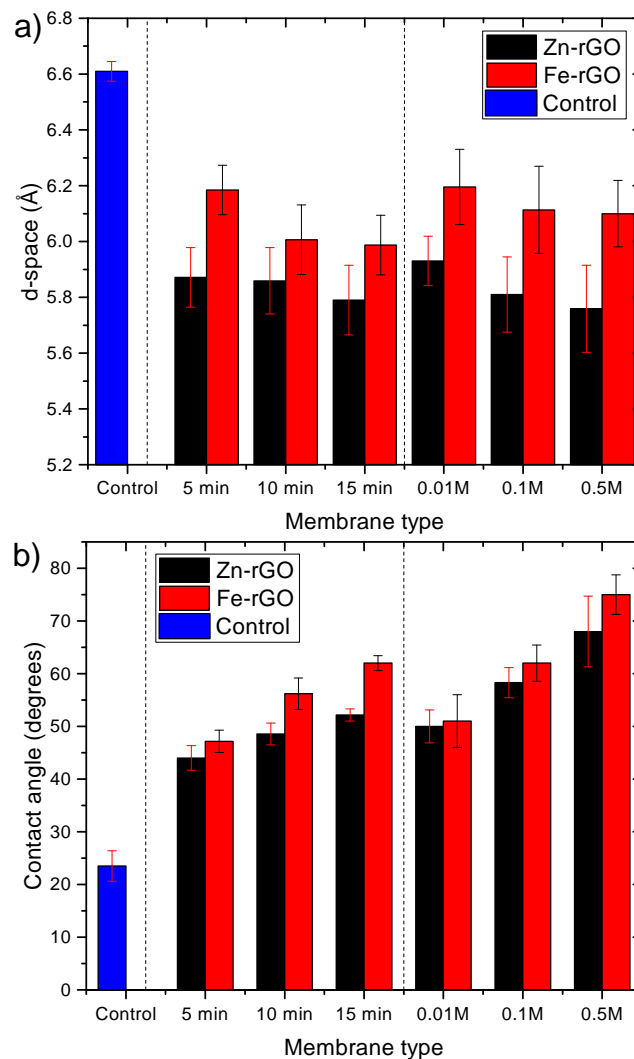
Figure 4-5: a) Contact angle measurements and b) XRD analysis for the membranes prepared via two methods, control sample is non-reduced and non-crosslinked GO/PES membrane. The error bars are one standard deviation of three independent measurements.

4.4.2 Membranes Performance:

The pervaporation performances of the synthesized membranes of different crosslinking concentration, reduction time and preparation order, were evaluated by determining their water flux and salt and

organic solutes rate of rejection as shown in Figure 4-6. Generally, the results show that the higher the reduction rate of a membrane in the second method resulted in a lower permeation flux of water passes through when comparing the control membranes of both methods (5 minutes partial reduction followed by crosslinking in 0.1 M M^+, or, crosslinking in 0.01 M M^+ followed by a partial reduction for 5 minutes) in testing saline water and PWM. Since the higher reduction rate of the membrane resulted in lowering the interlayer d-spacing between the GO sheets, the volume size of pathway channels for water to flow through were reduced and hence the permeation flux decreased [46], [48]. Moreover, reducing the graphene oxide membranes will increase the tortuosity for the flowing water, because the membranes' porosity was decreased by losing the oxygen functional groups that form bigger pores at the edges of the GO sheets.

Additionally, the water permeation flux of Zn^{2+}–rGO membranes is higher, since it was reduced at a higher rate than Fe^{3+}–rGO, and thus, more unoxidized regions present in Zn^{2+}–rGO, allowing lower flux friction of water molecules with Oxygen containing groups by forming H-bonding interaction [47]–[49].

Saline water pervaporation separation by membranes prepared by both methods shows > 99% of salt rejection for all membranes and a pure water flux of 3.6 ± 1.6 L $m^{-2} h^{-1}$ to 8.3 ± 1.5 L $m^{-2} h^{-1}$ as shown in Figure 4-6a. The highest permeation flux of 10.5 ± 1.8 L $m^{-2}h^{-1}$ was attained for non-reduced GO membranes since they have the highest interlayer spacing, whereas the flux decreased as reduction rate for GO increases. Additionally, the repulsive forces between the salt and the crosslinking cations of Zn^{2+} and Fe^{3+} prevented the salt from passing through the membrane. Upon the hydration of the M^+–GO membranes, the interlayer d-spacing can precisely be controlled by the cation–π interactions generated from the cations and the aromatic rings, which can selectively induce molecular permeation through the M^+–GO membranes [41], [64].

107

PWM pervaporation separation flux shows a similar trend to the saline water separation with lower a flux permeation rate of 3.1 ± 1.1 L m^{-2} h^{-1} to 7.5 ± 0.7 L m^{-2} h^{-1} as shown in Figure 4-6b. The solute component rejection rate increases by both the decrease of the interlayer d-spacing and metal cation loading on the membrane. Additionally, Fe^{3+} crosslinked membranes show higher solute rejections rate than Zn^{2+} in general. The higher electronegative ion of Fe^{3+} formed higher repulsive interaction forces with the polar solutes in PWM that resulted in a higher rejection rate than Zn^{2+} crosslinked membranes.

The highest PWM solute rejection rate was around 69% for the membranes that were prepared by crosslinking in 0.5 M Fe^{3+} solution followed by 5 minutes reduction, in which they obtained the lowest water permeation flux. This shows the trade-off between permeation flux and solute rejection, as reported in many other membranes fabricated with different materials which has always been the drawback in membrane desalination [65]–[68].
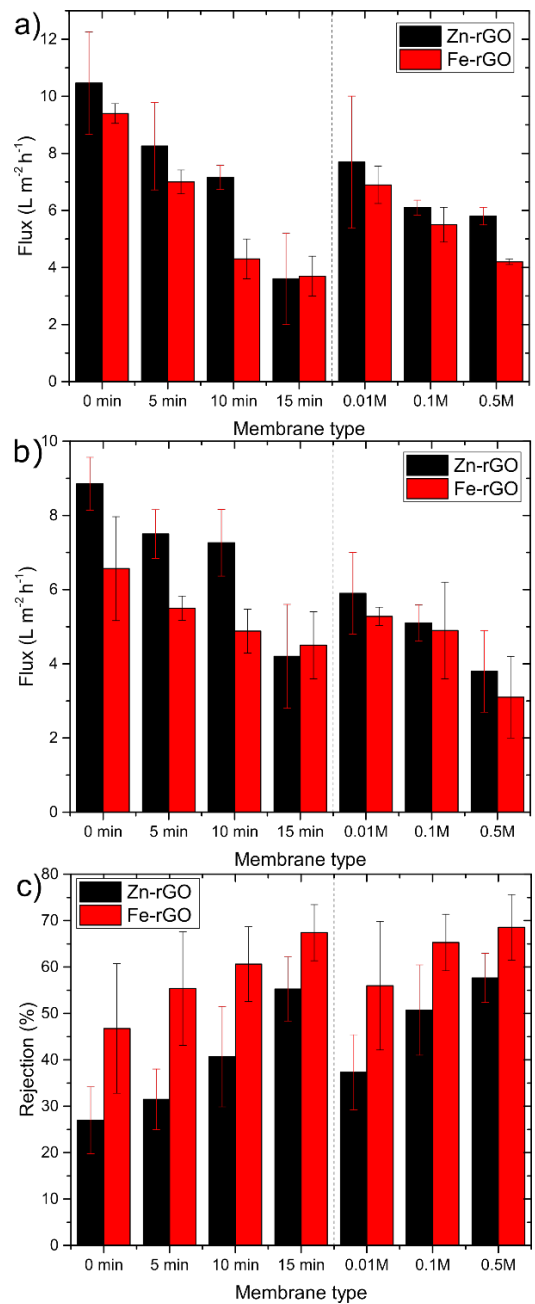
Figure 4-6: Water permeation flux for different types of membranes prepared by the two methods used in a) NaCl solution, and b) PWM; c) rejection rate of organic solutes of PWM. Control sample is 0 minutes reduction and 0.1 M M$^+$ loading. The error bars represent one standard deviation of three independent measurements.

Furthermore, membranes' rejection towards the PWM solutes is nonselective, because of the fact that simulated PWM solutes have the same chemical structure and functional groups. This was proven by the curves of UV-Vis as shown in Figure 4-7. The figure shows that the shape of the plotted UV-Vis curves is identical for both of the collected sample curve when normalized and the initial PWM feed curve.
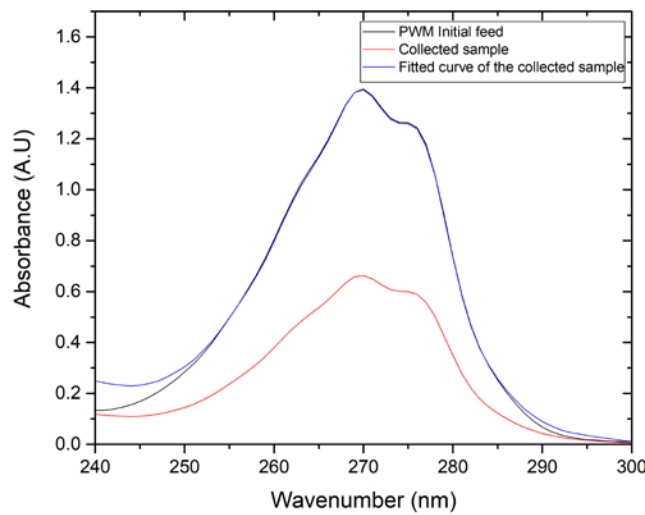
Figure 4-7: UV-vis spectra example of one of the collected permeate samples from PWM separation, and its normalized curve that matches its initial feed solution spectra.

4.4.3 Long Term Pervaporation Performance:

Long term pervaporation separation was carried out to examine the membranes' performance over an extended period of time of 12 hours using a solution of PWM with foulants. The membrane sample used was a reduced GO after crosslinking in 0.1 M Zn^{2+} solution and the pervaporation experiment was repeated three times with independent samples. The permeation flux was compared with non-reduced Zn-GO membrane that was treated in 0.1 M $ZnCl_2$ solution for 24 hours from our previous work [69].

110

In order to show its performance with the experiment progress in a clearer way, the measured flux at each hour was normalized with respect to the initial flux as shown in Figure 4-8. The Zn-rGO membrane shows a drop of 6% from the initial flow with a slight increase in solute rejection for PWM with foulants as shown in Figure 4-8; whereas, Zn-GO membranes shows a drop in flux of 24% and a large increase in solute rejection over time [69]. The drop in the permeation flux is mostly a result of the concentration polarization and foulants build up near the GO surface which appear to be more severe in the non-reduced GO membranes because of their high functionality. Moreover, the increase in PWM and foulant rejection is due to the adsorption of some of the foulant molecules onto the surface. Additionally, The NaCl rejection for both tested membranes were > 99% throughout the experiment. Additionally, water permeation through rGO membranes portrays a more stable and consistent flow throughout the pervaporation experiment than non-reduced GO membranes. This is likely due to the less interaction between water molecules and the rGO sheets in the membrane compared to the non-reduced GO membranes that has abundant functional groups, and consequently, more uniform flow and less amount of water is being trapped within the rGO membrane at any certain time which makes the flow of water more constant.
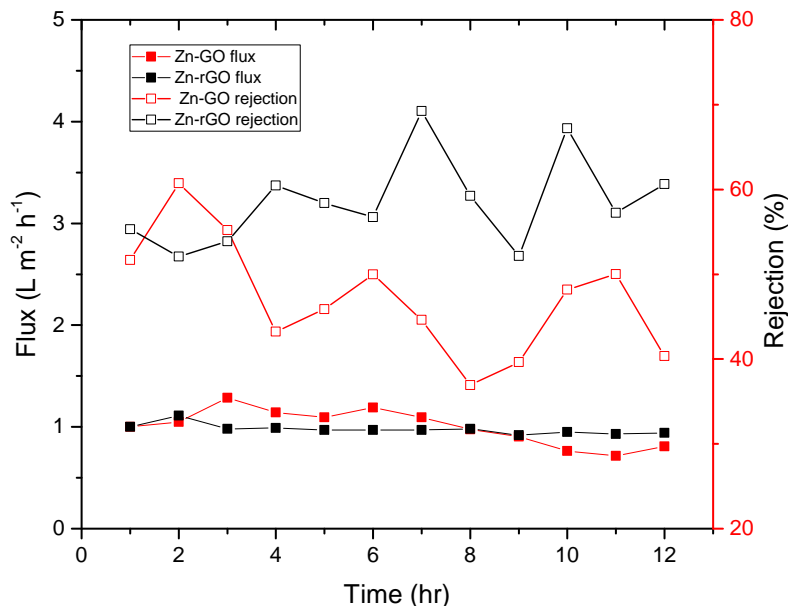
Figure 4-8: Flux/flux0 (J/J$_0$), and PWM organic solutes rejection vs. time by Zn–rGO and Zn–GO membranes.

4.4.4 Stability Testing:

The mechanical integrity of the prepared M$^+$–rGO membranes were examined by an abrasion method. Figure 4-9a demonstrates how resistive the membranes are by showing its abraded area when subjected to abrasion by a rotating wheel abrader. The higher the abraded area percentage, the least mechanically stable the membrane is. Membranes that were prepared by the second method in 0.5 M M$^+$ solution show the highest abrasion resistance. Fe^{3+}–rGO and Zn^{2+}–rGO Show an area abraded of 3.7% and 25.1%, respectively. This indicates an improvement of 95%, and 67% in resistance to abrasion by comparing it to the area abraded of control GO/PES membrane for both Fe^{3+} and Zn^{2+} crosslinkers, respectively. In general, membranes' resistivity towards abrasion is higher for the membranes that have a higher C/O ratio. The reason is that GO sheets with low functionality have less interlayer repulsion

112

forces and are more intact together after wetting. In addition, membranes that are cross-linked with Fe^{3+} cations show higher resistance towards abrasion, this shows that Fe^{3+} bonding to GO is stronger, probably because Fe^{3+} has higher electronegativity than Zn^{2+}, and therefore, it forms more stronger bonds with the oxygen in the GO membranes.

Figure 4-9: a) Abraded area of the membrane by a wheel abrader for the prepared membranes. (control membrane is non-reduced and non-crosslinked GO/PES membrane), b) the abraded area of the membrane before and after the second treatment step.

Moreover, Figure 4-9b shows the effect of the second step of crosslinking rGO or reducing M^+-GO, for both methods in strengthening the membrane resistance to abrasion. Membranes that are crosslinked with Zn^{2+} got more reinforced in the second step treatment in both methods, because of their higher loading in the membranes.

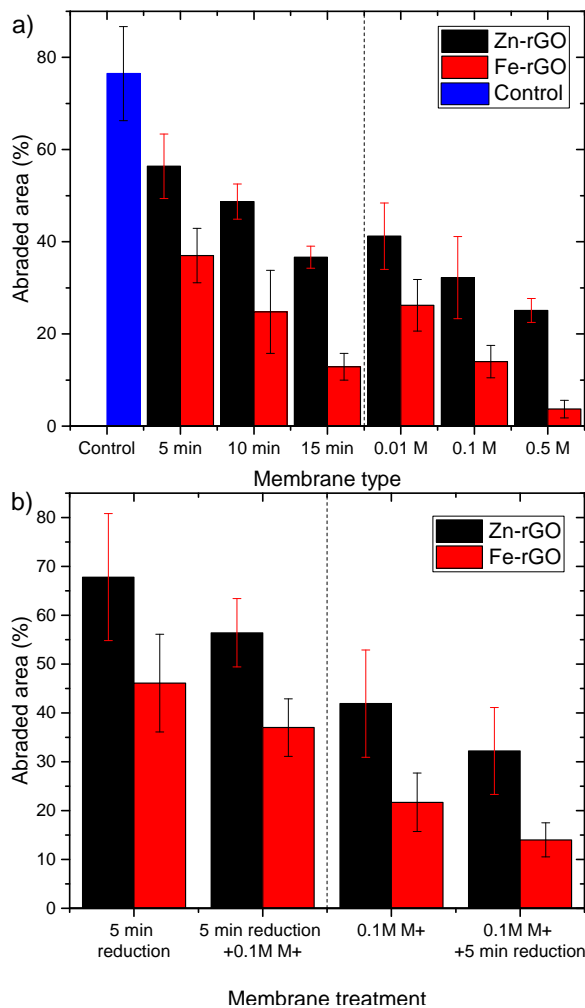Furthermore, the stability testing conducted further illustrates the nature tradeoff of graphene-based membranes between their permeation flux, selectivity, and stability in water. It can be realized, as expected, that the highly stable membranes have the lower interlayer spacing and higher C/O ratio, and thus, they have higher organic solute rejections and lower water flux. The crosslinking agents not only enhanced the membranes stability in aqueous solutions, but also improved the organic solute rejections from passing through the membrane. While water treatment using graphene-based membranes been widely studied, their performances remain under the theoretical limit up to date [70]. Nevertheless, produced water separation was not studied broadly by pervaporation technique, and few studies have been conducted. GO modified Al_2O_3 membranes were used for commercial ceramic microfiltration [71]. Their GO modified membrane was tested in a crossflow membrane module under a pressure of 0.1 MPa. It revealed a flux of 667 L $h^{-1}m^{-2}$ which is 27.8% higher flux than the unmodified membrane. The oil rejection achieved was 98.7%, however, the system was not tested for salt rejections. In another work, graphene on a polyvinylidene difluoride (PVDF) was prepared by phase inversion and tested for RO brine resulted from coal seam gas produced water using air gap membrane distillation (AGMD) [72]. Their membrane achieved a permeation flux of 20.5 L m^{-2} h^{-1} with a salt rejection of 99.99%. However, their system was not tested for organic solutes rejection and AGMD was used as a second step after RO, which implies more energy required for the multi-step process. Furthermore, in a more recent study, amine-GO incorporated on a polysulfone (PSF) substrate was synthesized by interfacial polymerization and utilized for shale gas produced water purification using a nanofiltration method

114

with a pressure of 0.1 MPa to 0.5 MPa [73]. The highest flux obtained was 49.30 L m^{-2} h^{-1}, and the salt and organic solute (glucose) rejection of around only 60% to 95%, and 47%, respectively. In addition, a recent study showed a produced water purification by nanofiltration using GO/β-cyclodextrin on porous substrates of PSf membrane [74]. The optimal performance membrane showed a flux of 107 L m^{-2} h^{-1} and 103.5 L m^{-2} h^{-1} for testing salt water and oil solution permeability. In addition, an excellent rejection of hydrocarbons of 100%, however, the rejection of the monovalent and divalent salts was only about 89% and 74%, respectively, for a very low concentrated solutions of 1000 ppm each. Additionally, a high pressure of 0.6 MPa was used to drive the membrane separation.

Furthermore, in a very recent and similar study conducted for produced water separation by GO/PES and TiO_2 nanoribbons/PES prepared by phase inversion. In this study, produced water obtained from an oil field, and tested by a nanofiltration at a pressure of 0.3 MPa [75]. The best optimal membrane was the GO/PES membrane that had a flux of 85 L m^{-2} h^{-1} and the highest salt rejection rate of 81% only for the chloride ion constituent that was fed to the system at a very low concentration of 10,220 ppm; and oil rejection of 88%.

In addition, similar recent research was carried out to investigate saline water separation utilizing a crosslinked rGO with monovalent metal cation of K^+ [70]. The membrane was tested in dead end test cell under 0.6 MPa. In addition, the highest permeation flux obtained was 0.1 L m^{-2} h^{-1} with NaCl rejection of 91%. Additionally, contrary to the findings of their study, the M^+–rGO membranes prepared in our study by reducing the crosslinked GO membranes (method II) have a strong stability than crosslinking the rGO. Further, it is noteworthy that the K^+ cation crosslinkers used in the study is a weak ion compared to most of other ions present in salts, and therefore, K^+ is expected to tend to leak out of the GO lattice, because of the presence of other competing ions which have stronger interactions with GO, which eventually affect the stability and selectivity of the membrane [76]. Whereas the

115

crosslinkers presented in our study (Zn^{2+} and Fe^{3+}), have a higher interaction rate with the GO, thus, their cation–π interactions keep the GO nanosheets intact for longer time.

4.5 Conclusions

In conclusion, the performance and stability of graphene oxide (GO) membranes were improved by the strategies of physical reduction and crosslinking. GO membranes were synthesized and prepared by vacuum filtration technique on polyethersulfone (PES) substrates. Afterwards, it was further treated by either reducing the GO membranes followed by crosslinking; or, reducing a crosslinked GO membrane. GO reduction was carried out under a vacuum at 200°C for different periods of time. The GO nanosheets were crosslinked utilizing divalent (Zn^{2+}) and trivalent (Fe^{3+}) metal cations with different concentrations. The membranes prepared by the two pathways were further characterized and tested for their performances. The obtained M^+–rGO membranes were used for produced water treatment of simulated water of SAGD process, by a pervaporation separation technique.

M^+–rGO membranes were characterized first for their degree of reduction. Membranes that bear a higher C/O ratio showed a lower interlayer d-spacing between the GO nanosheets, and hence, a higher separation sieving for the organic solutes of the produced water. Also, the higher C/O ratio membranes suffered from a lower water permeation flux through its nanochannels. The highest permeation flux of M^+–rGO membrane obtained was for Zn^{2+} cation crosslinker of 8.3 ± 1.5 L m^{-2} h^{-1} for saline water separation, and 7.5 ± 0.7 L m^{-2} h^{-1} for PWM separation. The salt rejection was > 99% for all the membranes, and the highest organic solute rejection was 69%. On the other side, these membranes exhibited the highest resistivity against the mechanical abrasion due to the increased cation–π interactions between the metal cation and basal rGO structure.

In addition, Zn^{2+}–rGO membrane was tested for long term produced water pervaporation separation. The results were compared with non-reduced Zn^{2+}–GO form our previous study. The Zn^{2+}–rGO membranes showed a more consistent water flow through the membrane, and a smaller drop of 6%, in the permeation flux than the non-reduced Zn^{2+}–GO membrane (drop in flux = 24%), as well as a higher organic solutes rejection. Additionally, Fe^{3+} modified rGO membranes prepared by the second method showed a higher abrasion resistance of 95% compared to 67% for Zn^{2+} modified rGO membranes.

While the flux and salt rejection of our membrane is higher than the recent similar reported study of monovalent crosslinked K^+–rGO, the future direction of this research will focus on enhancing the water permeation flux without compromising the selectivity and mechanical integrity of the graphene-based membrane. We wish that these obtained findings will enrich the knowledge of produced water separation by the technique of pervaporation using GO membranes.

4.6 References

[1]   T. D. Kusworo, N. Aryanti, Qudratun, and D. P. Utomo, "Oilfield produced water treatment to clean water using integrated activated carbon-bentonite adsorbent and double stages membrane process," *Chemical Engineering Journal*, vol. 347, pp. 462–471, Sep. 2018, doi: 10.1016/J.CEJ.2018.04.136.

[2]   P. J. McCabe, "Oil and Natural Gas: Global Resources," in *Fossil Energy*, New York, NY: Springer New York, 2013, pp. 7–23. doi: 10.1007/978-1-4614-5722-0_2.

[3]   N. Sönnichsen, "Daily demand for crude oil worldwide from 2006 to 2020." 2020.

[4]   C. Clark and J. Veil, "Produced water volumes and management practices in the United States.," 2009, Accessed: Sep. 29, 2022. [Online]. Available: https://www.osti.gov/biblio/1007397

[5]   R. T. Duraisamy, A. H. Beni, A. Henni, R. T. Duraisamy, A. H. Beni, and A. Henni, "State of the Art Treatment of Produced Water," *Water Treatment*, Jan. 2013, doi: 10.5772/53478.

[6]   J. Neff, T. C. Sauer, and A. D. Hart, "Bioaccumulation of Hydrocarbons from Produced Water Discharged to Offshore Waters of the US Gulf of Mexico," *Produced Water*, pp. 441–477, 2011, doi: 10.1007/978-1-4614-0046-2_24.

[7]   P. J. C. Tibbetts, I. T. Buchanan, L. J. Gawel, and R. Large, "A Comprehensive Determination of Produced Water Composition," *Produced Water*, pp. 97–112, 1992, doi: 10.1007/978-1-4615-2902-6_9.

[8]   Y. Liu *et al.*, "A review of treatment technologies for produced water in offshore oil and gas fields," *Science of The Total Environment*, vol. 775, p. 145485, Jun. 2021, doi: 10.1016/J.SCITOTENV.2021.145485.

[9]   K. O.-H. Gijutsu and undefined 2019, "US energy information administration (EIA): 2019 edition US annual energy outlook report (AEO2019)," *inis.iaea.org*, Accessed: Oct. 02, 2022. [Online]. Available: https://inis.iaea.org/search/search.aspx?orig_q=RN:50064205

[10]   M. Nasiri and I. Jafari, "Produced water from oil-gas plants: A short review on challenges and opportunities," *Periodica Polytechnica Chemical Engineering*, vol. 61, no. 2, pp. 73–81, 2017, doi: 10.3311/PPch.8786.

[11]   T. Bora and J. Dutta, "Applications of Nanotechnology in Wastewater Treatment—A Review," *J Nanosci Nanotechnol*, vol. 14, no. 1, pp. 613–626, Jan. 2014, doi: 10.1166/JNN.2014.8898.

[12]   F. C. Dolan, T. Y. Cath, and T. S. Hogue, "Assessing the feasibility of using produced water for irrigation in Colorado," *Science of The Total Environment*, vol. 640–641, pp. 619–628, Nov. 2018, doi: 10.1016/J.SCITOTENV.2018.05.200.

[13]   N. Zhang *et al.*, "Review on structural control and modification of graphene oxide-based membranes in water treatment: From separation performance to robust operation," *Chin J Chem Eng*, vol. 27, no. 6, pp. 1348–1360, Jun. 2019, doi: 10.1016/J.CJCHE.2019.01.001.

[14]   P. Y. Apel *et al.*, "Prospects of Membrane Science Development," *Membranes and Membrane Technologies 2019 1:2*, vol. 1, no. 2, pp. 45–63, May 2019, doi: 10.1134/S2517751619020021.

[15]   P. Xu, J. D.-S. and P. Technology, and undefined 2006, "Viability of nanofiltration and ultra-low pressure reverse osmosis membranes for multi-beneficial use of methane produced water,"

Elsevier, Accessed: Oct. 04, 2022. [Online]. Available: https://www.sciencedirect.com/science/article/pii/S1383586606001109

[16] J. Li, H. Wang, X. Yuan, J. Zhang, and J. W. Chew, "Metal-organic framework membranes for wastewater treatment and water regeneration," *Coord Chem Rev*, vol. 404, p. 213116, Feb. 2020, doi: 10.1016/J.CCR.2019.213116.

[17] E. Igunnu, G. C.-I. journal of low-carbon, and undefined 2014, "Produced water treatment technologies," *academic.oup.com*, Accessed: Oct. 04, 2022. [Online]. Available: https://academic.oup.com/ijlct/article-abstract/9/3/157/807670

[18] N. Zhang *et al.*, "Review on structural control and modification of graphene oxide-based membranes in water treatment: From separation performance to robust operation," *Chin J Chem Eng*, vol. 27, no. 6, pp. 1348–1360, Jun. 2019, doi: 10.1016/J.CJCHE.2019.01.001.

[19] H. Chang, T. Li, B. Liu, R. D. Vidic, M. Elimelech, and J. C. Crittenden, "Potential and implemented membrane-based technologies for the treatment and reuse of flowback and produced water from shale gas and oil plays: A review," *Desalination*, vol. 455, pp. 34–57, Apr. 2019, doi: 10.1016/J.DESAL.2019.01.001.

[20] M. Sagehashi, T. Nomura, H. Shishido, and A. Sakoda, "Separation of phenols and furfural by pervaporation and reverse osmosis membranes from biomass – superheated steam pyrolysis-derived aqueous solution," *Bioresour Technol*, vol. 98, no. 10, pp. 2018–2026, Jul. 2007, doi: 10.1016/J.BIORTECH.2006.08.022.

[21] B. Liang *et al.*, "High performance graphene oxide/polyacrylonitrile composite pervaporation membranes for desalination applications," *pubs.rsc.org*, vol. 00, pp. 1–3, 2013, doi: 10.1039/x0xx00000x.

[22]   G. Liu *et al.*, "Ultrathin two-dimensional MXene membrane for pervaporation desalination," *J Memb Sci*, vol. 548, pp. 548–558, Feb. 2018, doi: 10.1016/J.MEMSCI.2017.11.065.

[23]   G. Jyoti, A. Keshav, and J. Anandkumar, "Review on Pervaporation: Theory, Membrane Performance, and Application to Intensification of Esterification Reaction," *Journal of Engineering (United Kingdom)*, vol. 2015, 2015, doi: 10.1155/2015/927068.

[24]   W. Kaminski, J. Marszalek, and E. Tomczak, "Water desalination by pervaporation – Comparison of energy consumption," *Desalination*, vol. 433, pp. 89–93, May 2018, doi: 10.1016/J.DESAL.2018.01.014.

[25]   X. Qian, N. Li, Q. Wang, and S. Ji, "Chitosan/graphene oxide mixed matrix membrane with enhanced water permeability for high-salinity water desalination by pervaporation," *Desalination*, vol. 438, pp. 83–96, Jul. 2018, doi: 10.1016/J.DESAL.2018.03.031.

[26]   D. Wu, A. Gao, H. Zhao, and X. Feng, "Pervaporative desalination of high-salinity water," *Chemical Engineering Research and Design*, vol. 136, pp. 154–164, Aug. 2018, doi: 10.1016/J.CHERD.2018.05.010.

[27]   P. Goh, T. Matsuura, A. Ismail, N. H.- Desalination, and undefined 2016, "Recent trends in membranes and membrane processes for desalination," *Elsevier*, Accessed: Oct. 04, 2022. [Online]. Available: https://www.sciencedirect.com/science/article/pii/S0011916415301508

[28]   W. Kaminski, J. Marszalek, E. T.- Desalination, and undefined 2018, "Water desalination by pervaporation–Comparison of energy consumption," *Elsevier*, Accessed: Oct. 04, 2022. [Online]. Available: https://www.sciencedirect.com/science/article/pii/S0011916417313772

[29] A. Morelos-Gomez *et al.*, "Effective NaCl and dye rejection of hybrid graphene oxide/graphene layered membranes," *Nature Nanotechnology 2017 12:11*, vol. 12, no. 11, pp. 1083–1088, Aug. 2017, doi: 10.1038/nnano.2017.160.

[30] B. Mi, "Graphene oxide membranes for ionic and molecular sieving," *Science (1979)*, vol. 343, no. 6172, pp. 740–742, 2014, doi: 10.1126/SCIENCE.1250247.

[31] R. K. Joshi *et al.*, "Precise and ultrafast molecular sieving through graphene oxide membranes," *Science (1979)*, vol. 343, no. 6172, pp. 752–754, 2014, doi: 10.1126/SCIENCE.1245711.

[32] K. Huang, G. Liu, Y. Lou, Z. Dong, J. Shen, and W. Jin, "A Graphene Oxide Membrane with Highly Selective Molecular Separation of Aqueous Organic Solution," *Angewandte Chemie International Edition*, vol. 53, no. 27, pp. 6929–6932, Jul. 2014, doi: 10.1002/ANIE.201401061.

[33] P. Sun *et al.*, "Selective ion penetration of graphene oxide membranes," *ACS Nano*, vol. 7, no. 1, pp. 428–437, Jan. 2013, doi: 10.1021/NN304471W/SUPPL_FILE/NN304471W_SI_001.PDF.

[34] C. Tsou, Q. An, S. Lo, … M. D. G.-J. of M., and undefined 2015, "Effect of microstructure of graphene oxide fabricated through different self-assembly techniques on 1-butanol dehydration," *Elsevier*, Accessed: Oct. 11, 2022. [Online]. Available: https://www.sciencedirect.com/science/article/pii/S0376738814009429

[35] S. Zheng, Q. Tu, J. J. Urban, S. Li, and B. Mi, "Swelling of Graphene Oxide Membranes in Aqueous Solution: Characterization of Interlayer Spacing and Insight into Water Transport Mechanisms," *ACS Nano*, vol. 11, p. 52, 2017, doi: 10.1021/acsnano.7b02999.

[36]   J. Ma, Y. He, H. Shi, Y. Fan, H. Yu, and Y. Li, "Stable graphene oxide-based composite membranes intercalated with montmorillonite nanoplatelets for water purification," *J Mater Sci*, vol. 54, no. 3, pp. 2241–2255, Feb. 2019, doi: 10.1007/S10853-018-2997-6.

[37]   Y.-H. Xi *et al.*, "Graphene oxide membranes with strong stability in aqueous solutions and controllable lamellar spacing," *ACS Publications*, vol. 8, no. 24, pp. 15557–15566, Jun. 2016, doi: 10.1021/acsami.6b00928.

[38]   M. L. Liu *et al.*, "One-step enhancement of solvent transport, stability and photocatalytic properties of graphene oxide/polyimide membranes with multifunctional cross-linkers," *J Mater Chem A Mater*, vol. 7, no. 7, pp. 3170–3178, Feb. 2019, doi: 10.1039/C8TA11372F.

[39]   W. S. Hung *et al.*, "Cross-linking with diamine monomers to prepare composite graphene oxide-framework membranes with varying d-spacing," *Chemistry of Materials*, vol. 26, no. 9, pp. 2983–2990, May 2014, doi: 10.1021/CM5007873/ASSET/IMAGES/LARGE/CM-2014-007873_0008.JPEG.

[40]   K. H. Thebo, X. Qian, Q. Zhang, L. Chen, H. M. Cheng, and W. Ren, "Highly stable graphene-oxide-based membranes with superior permeability," *Nature Communications 2018 9:1*, vol. 9, no. 1, pp. 1–8, Apr. 2018, doi: 10.1038/s41467-018-03919-0.

[41]   L. Chen *et al.*, "Ion sieving in graphene oxide membranes via cationic control of interlayer spacing," *Nature 2017 550:7676*, vol. 550, no. 7676, pp. 380–383, Oct. 2017, doi: 10.1038/nature24044.

[42]   J. Abraham *et al.*, "Tunable sieving of ions using graphene oxide membranes," *Nature Nanotechnology 2017 12:6*, vol. 12, no. 6, pp. 546–550, Apr. 2017, doi: 10.1038/nnano.2017.21.

[43]   S. Xia, M. Ni, T. Zhu, Y. Zhao, N. L.- Desalination, and undefined 2015, "Ultrathin graphene oxide nanosheet membranes with various d-spacing assembled using the pressure-assisted filtration method for removing natural organic," *Elsevier*, Accessed: Oct. 10, 2022. [Online]. Available: https://www.sciencedirect.com/science/article/pii/S001191641500363X

[44]   W. S. Hung *et al.*, "Cross-linking with diamine monomers to prepare composite graphene oxide-framework membranes with varying d-spacing," *Chemistry of Materials*, vol. 26, no. 9, pp. 2983–2990, May 2014, doi: 10.1021/CM5007873.

[45]   H. H. Huang, R. K. Joshi, K. K. H. de Silva, R. Badam, and M. Yoshimura, "Fabrication of reduced graphene oxide membranes for water desalination," *J Memb Sci*, vol. 572, pp. 12–19, Feb. 2019, doi: 10.1016/J.MEMSCI.2018.10.085.

[46]   Q. Zhang, X. Qian, K. H. Thebo, H. M. Cheng, and W. Ren, "Controlling reduction degree of graphene oxide membranes for improved water permeance," *Sci Bull (Beijing)*, vol. 63, no. 12, pp. 788–794, Jun. 2018, doi: 10.1016/J.SCIB.2018.05.015.

[47]   G. Shi, Q. Meng, Z. Zhao, H.-C. Kuan, A. Michelmore, and J. Ma, "Facile fabrication of graphene membranes with readily tunable structures," *ACS Publications*, vol. 7, no. 25, pp. 13745–13757, Jul. 2015, doi: 10.1021/am5091287.

[48]   C. A. Amadei, A. Montessori, J. P. Kadow, S. Succi, and C. D. Vecitis, "Role of Oxygen Functionalities in Graphene Oxide Architectural Laminate Subnanometer Spacing and Water Transport," *Environ Sci Technol*, vol. 51, no. 8, pp. 4280–4288, Apr. 2017, doi: 10.1021/ACS.EST.6B05711.

[49]   Y. Li *et al.*, "Mild annealing reduced graphene oxide membrane for nanofiltration," *J Memb Sci*, vol. 601, p. 117900, Mar. 2020, doi: 10.1016/J.MEMSCI.2020.117900.

[50] K. Goh, W. Jiang, H. Karahan, … S. Z.-A. F., and undefined 2015, "All-carbon nanoarchitectures as high-performance separation membranes with superior stability," *Wiley Online Library*, vol. 25, no. 47, pp. 7348–7359, Dec. 2015, doi: 10.1002/adfm.201502955.

[51] W. S. Hummers and R. E. Offeman, "Preparation of Graphitic Oxide," *J Am Chem Soc*, vol. 80, no. 6, pp. 1339–1339, Mar. 1958, doi: 10.1021/ja01539a017.

[52] D. C. Marcano *et al.*, "Improved Synthesis of Graphene Oxide," *ACS Nano*, vol. 4, no. 8, pp. 4806–4814, Aug. 2010, doi: 10.1021/nn1006368.

[53] H. Chen, J. L. Muros-Cobos, and A. Amirfazli, "Contact angle measurement with a smartphone," *Review of Scientific Instruments*, vol. 89, no. 3, p. 035117, Mar. 2018, doi: 10.1063/1.5022370.

[54] D. Singh, K. S.-J. of M. Science, and undefined 2012, "Desalination of brine and produced water by direct contact membrane distillation at high temperatures and pressures," *Elsevier*, Accessed: Oct. 14, 2022. [Online]. Available: https://www.sciencedirect.com/science/article/pii/S0376738811008106

[55] Y. Huang *et al.*, "Ultrafiltration Membranes with Structure-Optimized Graphene-Oxide Coatings for Antifouling Oil/Water Separation," *Adv Mater Interfaces*, vol. 2, no. 2, p. 1400433, Jan. 2015, doi: 10.1002/admi.201400433.

[56] Rattana *et al.*, "Preparation and characterization of graphene oxide nanosheets," *Procedia Eng*, vol. 32, pp. 759–764, 2012, doi: 10.1016/j.proeng.2012.02.009.

[57] T. Dudev and C. Lim, "Tetrahedral vs Octahedral Zinc Complexes with Ligands of Biological Interest: A DFT/CDM Study," *J Am Chem Soc*, vol. 122, no. 45, pp. 11146–11153, Nov. 2000, doi: 10.1021/ja0010296.

[58]   I. L. Laure, S. v. Tkachev, E. Yu. Buslaeva, E. v. Fatushina, and S. P. Gubin, "The coordination chemistry of graphene oxide: Interactions with metal ions in water," *Russian Journal of Coordination Chemistry*, vol. 39, no. 7, pp. 487–492, Jul. 2013, doi: 10.1134/S1070328413070038.

[59]   H. Malekpour *et al.*, "Thermal conductivity of graphene laminate," *Nano Lett*, vol. 14, no. 9, pp. 5155–5161, Sep. 2014, doi: 10.1021/NL501996V/SUPPL_FILE/NL501996V_SI_001.PDF.

[60]   S. Shaik, D. Danovich, B. Braida, W. Wu, and P. C. Hiberty, "New landscape of electron-pair bonding: Covalent, ionic, and charge-shift bonds," *Struct Bond*, vol. 170, pp. 169–212, 2016, doi: 10.1007/430_2015_179.

[61]   J. Duan *et al.*, "Coordination ability determined transition metal ions substitution of Tb in Tb-Asp fluorescent nanocrystals and a facile ions-detection approach," *pubs.rsc.org*, Accessed: Sep. 25, 2022. [Online]. Available: https://pubs.rsc.org/en/content/articlehtml/2018/nr/c7nr09267a

[62]   X. bin Lv *et al.*, "A Novel Strategy to Fabricate Cation-Cross-linked Graphene Oxide Membrane with High Aqueous Stability and High Separation Performance," *ACS Appl Mater Interfaces*, vol. 12, no. 50, pp. 56269–56280, Dec. 2020, doi: 10.1021/ACSAMI.0C15178/ASSET/IMAGES/LARGE/AM0C15178_0012.JPEG.

[63]   E. R. Nightingale, "Phenomenological Theory of Ion Solvation. Effective Radii of Hydrated Ions," *J Phys Chem*, vol. 63, no. 9, pp. 1381–1387, Sep. 1959, doi: 10.1021/j150579a011.

[64]   Y. Yuan *et al.*, "Enhanced desalination performance of carboxyl functionalized graphene oxide nanofiltration membranes," *Desalination*, vol. 405, pp. 29–39, Mar. 2017, doi: 10.1016/J.DESAL.2016.11.024.

[65]   W. Kaminski, J. Marszalek, and E. Tomczak, "Water desalination by pervaporation – Comparison of energy consumption," *Desalination*, vol. 433, pp. 89–93, May 2018, doi: 10.1016/J.DESAL.2018.01.014.

[66]   Y. Kang, Y. Xia, H. Wang, and X. Zhang, "2D Laminar Membranes for Selective Water and Ion Transport," *Adv Funct Mater*, vol. 29, no. 29, p. 1902014, Jul. 2019, doi: 10.1002/ADFM.201902014.

[67]   G. Liu, W. Jin, and N. Xu, "Two-Dimensional-Material Membranes: A New Family of High-Performance Separation Membranes," *Angewandte Chemie International Edition*, vol. 55, no. 43, pp. 13384–13397, Oct. 2016, doi: 10.1002/ANIE.201600438.

[68]   P. Goh, A. I.- Desalination, and undefined 2018, "A review on inorganic membranes for desalination and wastewater treatment," *Elsevier*, Accessed: Sep. 21, 2022. [Online]. Available: https://www.sciencedirect.com/science/article/pii/S0011916417309219

[69]   K. Almarzooqi, M. Ashrafi, T. Kanthan, A. Elkamel, and M. A. Pope, "Graphene Oxide Membranes for High Salinity, Produced Water Separation by Pervaporation," *Membranes (Basel)*, vol. 11, no. 7, p. 475, Jun. 2021, doi: 10.3390/membranes11070475.

[70]   S. Yuan, Y. Li, Y. Xia, C. Selomulya, X. Z.-J. of M. Science, and undefined 2021, "Stable cation-controlled reduced graphene oxide membranes for improved NaCl rejection," *Elsevier*, Accessed: Oct. 13, 2022. [Online]. Available: https://www.sciencedirect.com/science/article/pii/S0376738820315684

[71]   X. Hu *et al.*, "The improved oil/water separation performance of graphene oxide modified Al2O3 microfiltration membrane," *J Memb Sci*, vol. 476, pp. 200–204, Feb. 2015, doi: 10.1016/J.MEMSCI.2014.11.043.

[72]   Y. C. Woo *et al.*, "Graphene/PVDF flat-sheet membrane for the treatment of RO brine from coal seam gas produced water by air gap membrane distillation," *J Memb Sci*, vol. 513, pp. 74–84, Sep. 2016, doi: 10.1016/J.MEMSCI.2016.04.014.

[73]   F. xin Kong, Z. Y. Yang, L. P. Yue, J. fu Chen, and C. mei Guo, "Nanofiltration membrane with substrate incorporated amine-functionalized graphene oxide for enhanced petrochemical wastewater and shale gas produced water desalination," *Desalination*, vol. 517, p. 115246, Dec. 2021, doi: 10.1016/J.DESAL.2021.115246.

[74]   A. Q. Al-Gamal, T. A. Saleh, and F. I. Alghunaimi, "Nanofiltration membrane with high flux and oil rejection using graphene oxide/β-cyclodextrin for produced water reuse," *Mater Today Commun*, vol. 31, p. 103438, Jun. 2022, doi: 10.1016/J.MTCOMM.2022.103438.

[75]   T. Ashraf, N. Alfryyan, M. Nasr, S. A. Ahmed, and M. Shaban, "Removal of Scale-Forming Ions and Oil Traces from Oil Field Produced Water Using Graphene Oxide/Polyethersulfone and TiO2 Nanoribbons/Polyethersulfone Nanofiltration Membranes," *Polymers 2022, Vol. 14, Page 2572*, vol. 14, no. 13, p. 2572, Jun. 2022, doi: 10.3390/POLYM14132572.

[76]   Y. Ying *et al.*, "Development of a stable cation modified graphene oxide membrane for water treatment," *2d Mater*, vol. 4, no. 4, p. 045006, Aug. 2017, doi: 10.1088/2053-1583/AA814C.

Chapter 5
Conclusion and Future Work:

In conclusion, the first study of the thesis examined the potential and feasibility of separating highly saline water and produced water separation by the pervaporation technique using a vacuum filtered graphene oxide (GO) membranes. The performance of GO membranes with different GO-loadings on polyethersulfone (PES) were assessed for short and long term for six types of solutions: brackish water (30,000 ppm NaCl/DI-water), single organic solute of simulated produced water: 45 ppm of phenol, 45 ppm of cresol, and 10 ppm of naphthenic acid, and a produced water model (PWM) solution simulated from SAGD process, which contains the mixture of the organic solutes and salt. In additions, the membranes were also tested for a laboratory simulated oil foulants containing 50 ppm of sodium dodecyl sulfate and 1,500 ppm of hexadecane. GO membranes were crosslinked with Zn^{2+} to hold the nanosheets together, and the experiment was run in a laboratory custom made test cell at different temperatures. The initial water permeation fluxes were substantially higher than those stated in literature for the GO membrane-based treatment. However, the flux gradually decreases when the organic constituents and foulants are introduced to the solution. The salt rejection was around 99% in for all the tested membranes, and the organic solute rejections were non-selective, and they are around 40–50%. In long term pervaporation experiments, the membranes were tested for 72 hours using 50 μg cm^{-1} GO membranes over the operation time, the flux and rejection were reduced. Moreover, in depth elemental analysis investigation of the long term GO membranes revealed that Zn^{2+} crosslinker goes under a hydrolysis transformation to $Zn(OH)_2$.

The second study of this project focused on improving the permeation flux and molecular sieving of the GO membranes as well as their stability for the pervaporation separation. Two techniques of

physical reduction and a multivalent cationic crosslinking were used in two different treatment methods. The first method is crosslinking a graphene oxide membrane that has been reduced for different periods of time in a vacuum oven, while the second method is reducing a metal cation crosslinked GO membrane that has been crosslinked using different solution concentrations. Divalent and trivalent metal cation crosslinkers of Zn^{2+} and Fe^{3+}, respectively, were used to link the graphene nanosheets together and decrease the swelling effect upon hydration. The prepared M^+–rGO/PES membranes were characterized for its chemical and physical properties,

and their performances were tested for high salinity water, PWM, and PWM with oil foulants pervaporation separation. The membranes showed a salt rejection higher than 99%. The water permeation flux rate studied in this project had lower flux than the first study due to the decrease in the interlayer d-spacing by reduction, however, they showed higher organic solute rejection, as well as more mechanical stability upon hydration. In addition, a stability testing by rotating wheel abrasion was carried out for the prepared membranes to examine their resistance when abraded in wet environment.

Moreover, long term pervaporation separation test was performed for 12 hours for Zn–rGO membrane for PWM with foulants. It showed higher and more stable performance and mechanical integrity than the membrane prepared in the first study. It achieved a lower permeation flux drop and lower organic solute rejection drop, than the membranes from the first study. Additionally, it showed higher mechanical integrity when subjected to the wheel abrader.

As it was illustrated in this research in the first study, GO exhibits a considerable membrane material potential for saline water and oil field produced water separation. Nevertheless, it has an inherited trade-off between its permeation flux, molecular sieving, fouling deposition, as well as stability and they can not be increased at the same time, which limit their usage capabilities as shown in the second study.

The future work aspects of this project include increasing the permeation flux through the membrane without affecting the high selectivity, improving the solute rejection, and enhancing the stability in water.

One of the effective methods to increase the flux can be achieved by reducing the tortuosity of the water transportation diffusion path. This can be done by synthesizing small graphene oxide flakes [1], [2]. Small lateral size of GO nanosheets membranes prepared by pressure assisted filtration can achieve an ultrafast organic permeation by around 10 folds higher when tested on a nanofiltration apparatus [1]. In another study investigated the effect of varying the GO lateral size of a mixed composite of GO on a PSF membrane, on its performance by forward osmosis desalination. Different sizes of GO nanosheets were varied using different sonication tip and sonication time of the synthesized GO dispersions. The study revealed that the smallest GO flakes showed 51% higher water flux [3].

In addition, another method of decreasing the tortuosity is to increase the number of pores in the GO lamellar structure by etching treatment. Etching introduces more nanopores, and can be performed by a chemical or physical etching of GO. In a very recent study, chemical etching was carried out by reacting H_2O_2 to GO solution to form holey GO, before further mixing it with a polymer and depositing it onto a substrate [4]. The resulted membrane had higher water and salt permeation with improved dye retention in a crossflow filtration.

Furthermore, one of the methods to enhance the solute rejection has been introduced in the membrane separation field, yet has not been extensively developed. It operates by inducing an electric current to the membrane surface in order to electrostatically attract or repel the undesired components in ion-exchange membrane separation technique [5], [6]. In a water desalination study, a mixed matrix membrane of sulfonated-PES incorporating GO was tested in a lab made electrodialysis system equipped with DC current. The membrane performance was investigated for power consumption and

current efficiency, and water permeation and salt rejection. The study revealed that incorporating GO in the polymeric membrane will decrease the power consumption by 20% and a more stable membrane [7]. The membranes in our study have been synthesized and crosslinked with cations of Zn^{2+} and Fe^{3+} which make them good electric conductors and have the potential for ion exchange membrane separation.

In addition, other future studies aspects of this project include different parameters that affect the performance of the membrane as following:

- Membrane crosslinking variation using different metal cation crosslinkers.
- In depth post-separation analysis for the membrane used at different process parameters such as: feed temperature, applied pressure, stock solution pH, and introducing different biofouling components to the feed stock.
- Test the performance of the membrane using real produced water obtained from the petroleum industry.

Moreover, the system that have been developed in this study shall require further study for real life processing plants scale by simulating the system and building a model for it using a simulation software and a computing tool for optimizing the best operational parameters.

Furthermore, the long-term future plans shall focus on synthesizing GO membranes on large, commercialized scale and testing their efficiencies for longer terms like 6 – 12 months using a real produced water that consists of different salts, scales, dissolved organic chemicals and foulants.

5.1 References

[1]   W. Hirunpinyopas, P. Iamprasertkun, M. A. Bissett, and R. A. W. Dryfe, "Tunable charge/size selective ion sieving with ultrahigh water permeance through laminar graphene membranes," *Carbon N Y*, vol. 156, pp. 119–129, Jan. 2020, doi: 10.1016/J.CARBON.2019.09.030.

[2]   L. Nie *et al.*, "Realizing small-flake graphene oxide membranes for ultrafast size-dependent organic solvent nanofiltration," *Sci Adv*, vol. 6, no. 17, Apr. 2020, doi: 10.1126/SCIADV.AAZ9184.

[3]   N. Akther *et al.*, "Influence of graphene oxide lateral size on the properties and performances of forward osmosis membrane," *Desalination*, vol. 484, p. 114421, Jun. 2020, doi: 10.1016/J.DESAL.2020.114421.

[4]   X. Chen *et al.*, "Engineering hierarchical nanochannels in graphene oxide membranes by etching and polydopamine intercalation for highly efficient dye recovery," *Chemical Engineering Journal*, vol. 433, p. 133593, Apr. 2022, doi: 10.1016/J.CEJ.2021.133593.

[5]   H. Strathmann, *Ion-exchange membrane separation processes*. 2004. Accessed: Oct. 27, 2022. [Online].   Available: https://books.google.com/books?hl=en&lr=&id=pcNF7HWbFPIC&oi=fnd&pg=PP1&dq=Ion-
Exchange+Membrane+Separation+Processes+By+H+Strathmann&ots=SMY5U4Yx4x&sig=CMgQvYpFsZ7b-7ru63Hgtrc1NOk

[6]   P. Goel, P. Mandal, E. Bhuvanesh, V. K. Shahi, and S. Chattopadhyay, "Temperature resistant cross-linked brominated poly phenylene oxide-functionalized graphene oxide nanocomposite

anion exchange membrane for desalination," *Sep Purif Technol*, vol. 255, p. 117730, Jan. 2021, doi: 10.1016/J.SEPPUR.2020.117730.

[7]   S. Gahlot, P. P. Sharma, H. Gupta, V. Kulshrestha, and P. K. Jha, "Preparation of graphene oxide nano-composite ion-exchange membranes for desalination application," *RSC Adv*, vol. 4, no. 47, pp. 24662–24670, Jun. 2014, doi: 10.1039/C4RA02216E.